UNIVERSIDAD NACIONAL AUTÓNOMA DE MEXICO

PROGRAMA DE MAESTRÍA Y DOCTORADO EN CIENCIAS MATEMÁTICAS Y DE LA ESPECIALIZACIÓN EN ESTADÍSTICA APLICADA

CONTINUOUS MODELS FOR BACTERIAL AGGREGATION WITH CHEMOTAXIS AND NON-LINEAR DEGENERATE DIFFUSION: MODELING, NUMERICAL SIMULATIONS AND ANALYSIS OF TRAVELING FRONTS.

TESIS
QUE PARA OPTAR POR EL GRADO DE:
DOCTOR EN CIENCIAS

PRESENTA:
JUAN FRANCISCO LEYVA BONILLA

TUTOR PRINCIPAL
DR. RAMÓN GABRIEL PLAZA VILLEGAS
INSTITUTO DE INVESTIGACIONES EN MATEMÁTICAS APLICADAS Y EN SISTEMAS - UNAM

MIEMBROS DEL COMITÉ TUTOR
DR. CARLOS MÁLAGA IGUIÑIZ
FACULTAD DE CIENCIAS - UNAM

DR. ANTONIO CAPELLA KORT
INSTITUTO DE MATEMÁTICAS - UNAM

CIUDAD DE MÉXICO, SEPTIEMBRE 2017

Acknowledgments

I would like to thank my PhD advisor, Professor Ramón G. Plaza Villegas, whose knowledge, guidance, enthusiasms, continuous support and patience led me to the culmination of this thesis.

I would like to thank Professor Carlos Málaga Iguiñiz for all his knowledge, support and advice during my doctoral studies.

I would like to thank Professor Antonio Capella Kort for all his support and useful discussions.

I would like to thank Professor Catherine García Reimbert for all her kindness, support and encouragement.

I would like to thank CONACYT for funding my doctoral work through a scholarship, grant no. 220865. Likewise, my work was partially supported by DGAPA-UNAM, program PAPIIT, grant IN-104814; and by DGAPA-UNAM, program PAPIME, grant PE-104116.

I would like to thank Professor Manuel Jesús Falconi Magaña and Professor Faustino Sánchez Garduño for their commentaries to improve this thesis.

I would like to thank to my friends at IIMAS whose support and encouragement was very important to me. Especially Salvador for his support and useful discussions.

Finally, but must important, I thank the people I love the most and I dedicate this thesis to them. To my wife Susana for her unconditionally love, support and encouragement. To my parents, Juan Francisco and Georgina, and my brother Jorge, for their love and support.

Contents

Introducción

Para muchas especies la movilidad es un rasgo fundamental que les permite sobrevivir. Es a través de diferentes estrategias y mecanismos que los microorganismos celulares se enfrentan a las condiciones ambientales adversas y maximizan las posibilidades de sobrevivencia de sus especies.

Se ha observado que muchas cepas bacterianas como por ejemplo *Escherichia coli, Salmonela typhimurium, Bacillus subtilis*, entre otras, desarrollan espectaculares patrones morfológicos cuando crecen en cajas de Petri (sobre agar), bajo condiciones adversas [20, 23, 29, 111, 138, 163]. Dichos patrones, también conocidos como patrones de agregación, son el resultado de un comportamiento gregario de las células que ha sido entendido como una respuesta de adaptación a un medio dinámico, y que involucra la generación cooperativa de información y señales para la formación de patrones espacio-temporales que incrementan la probabilidad de supervivencia de la especie. Uno de los mecanismos básicos de movilidad y señalización es la quimiotaxis, esto es, el movimiento en respuesta a una sustancia química. Es fundamental entender los mecanismos que participan en la agregación de microorganismos para poder comprender el desarrollo de organismos más complejos.

En esta tesis estamos interesados en los patrones de agregación de la bacteria *B. subtilis* [111], y nos concentramos en analizar los mecanismos básicos que intervienen en el desarrollo de estos patrones, por ejemplo, la quimiotaxis bacteriana en respuesta a las sustancias atrayentes. La cepa *B. subtilis* tiene una vasta morfología y los patrones de colonias observados, dependiendo en la dureza de la superficie (agar) y el nivel de nutriente, han sido clasificados en morfología fractal, de tipo Eden, de anillos concéntricos, de discos homogéneos y densamente ramificada (ver Fig. 3.1 en el Capítulo 3). La respuesta colectiva a nivel poblacional hacia los atrayentes (nutrientes) juega un papel clave en la formación de estos patrones [20].

En particular, en esta tesis estamos interesados en los patrones que corresponden a las morfologías de discos homogéneos y densamente ramificadas. Las observaciones experimentales de los patrones de *B. subtilis* muestran que el borde o frente de las colonias crece en la dirección externa, y que las bacterias que se

encuentran en el frente son las que dirigen la dinámica de las colonias y la formación de los patrones. Este tipo de comportamiento ha sido previamente identificado como ondas biológicas o frentes biológicos de invasión [141].

La descripción matemática continua determinista de los patrones de agregación bacteriana ha sido previamente hecha usando sistemas de ecuaciones diferenciales de reacción difusión, los cuales están incluidos en el marco teórico de las ecuaciones diferenciales parciales parabólicas cuasi lineales [20, 55, 73, 105, 106]. Estos modelos toman en cuenta los procesos básicos que están presentes en el desarrollo de las colonias tales como el movimiento bacteriano, la proliferación y la interacción entre las células individuales.

Nosotros seguimos este enfoque, y proponemos un nuevo modelo de reacción difusión quimiotaxis para los patrones de agregación bacteriana, el cual está basado en el modelo de Kawasaki *et al.* [73].

Esta tesis está organizada en cinco capítulos. En el Capítulo 2, empezamos dando una breve exposición de los antecedentes biológicos y de la modelación matemática de la quimiotaxis.

En el Capítulo 3 presentamos un resumen de los patrones morfológicos de la bacteria *B. subtilis*. Además, revisamos el modelo original de Kawasaki *et al.* [73]. Después, discutimos el papel que tiene la quimiotaxis inducida por nutrientes en el desarrollo de patrones bacterianos. Luego, proponemos un término quimiotáctico adecuado que está motivado por observaciones biológicas [55] y lo agregamos al modelo original de Kawasaki. Exploramos los efectos del nuevo término quimiotáctico en los patrones de agregación realizando simulaciones numéricas de alta resolución del nuevo modelo usando tarjetas de procesamiento gráfico (o GPU's por sus siglas en inglés) y técnicas de cómputo en paralelo.

En el Capítulo 4 continuamos explorando el impacto del término de quimiotaxis en los patrones de agregación, y nos concentramos en analizar los efectos en el frente envolvente de la colonia, ya que esta región es la que dirige el crecimiento de los patrones. De esta manera, exploramos los efectos que el término quimiotáctico tiene en la velocidad de propagación del frente envolvente de la colonia. Estimamos numéricamente la velocidad del frente, y haciendo ciertas suposiciones, aproximamos asintóticamente la velocidad de propagación. Mostramos que la velocidad es una función creciente del nivel de nutriente y de la sensibilidad quimiotáctica.

Las observaciones del comportamiento del frente de la colonia como una onda biológica viajera, y la deducción de una ecuación escalar aproximada para la densidad bacteriana nos motivó para estudiar las soluciones de tipo onda viajera de dicha ecuación. Específicamente, en el Capítulo 5 estudiamos la estabilidad, en espacios exponencialmente pesados, de ciertos subconjuntos del espectro correspondiente al operador linealizado alrededor de ondas viajeras suaves monótonas y

degeneradas de ecuaciones de reacción difusión de tipo Fisher-KPP con coeficiente de difusión no lineal degenerado.

Finalmente, en el Capítulo 6 presentamos algunas observaciones y conclusiones.

Chapter 1

Introduction

Motility is a fundamental trait for many organisms in order to survive. It is through different strategies and mechanisms that cellular microorganisms deal with adverse environmental conditions to maximize the chances of their species.

It has been observed that many bacterial strains such as *Escherichia coli, Salmonela typhimurium, Bacillus subtilis*, among others, develop spectacular morphologic patterns when they grow on agar plates under adverse conditions [20, 23, 29, 111, 138, 163]. Such patterns, also known as *aggregation patterns*, are the result of a gregarious cellular behavior that has been understood as an adaptation response to a dynamic environment, and involves the cooperative generation of information and signaling for the formation of spatio-temporal patterns that improve the chance of survivability of the species. One of the basic signaling and motility mechanisms is *chemotaxis*, that is, the movement in response to a chemical queue. It is fundamental to understand the mechanisms that are involved in the aggregation of microorganisms, in order to understand the dynamics in the development of higher organisms.

In this thesis we are interested in the aggregation patterns of the bacterium *B. subtilis* [111], and we focus on analyzing the basic mechanisms involved in the development of theses patterns, for instance, the bacterial chemotaxis response to attractants. The strain *B. subtilis* has a rich morphology and the observed colony patterns, depending on the hardness of the surface (agar) and the nutrient level, have been classified in fractal, Eden, concentric rings, homogeneous disks and densely ramified morphologies (see Fig. 3.1 in Chapter 3). The collective response at the populations level to attractants (nutrients) play a key role in the formation of these patterns [20].

In particular, in this thesis we are interested in the patterns pertaining to the homogeneous disks and densely ramified morphologies. The experimental observations of *B. subtilis* patterns show that the edge or front of the colony grows in the outward direction, being the bacteria at the front the ones that lead the

colony dynamics and the formation of the patterns. This type of behavior has been identified as biological waves or biological fronts of invasion [141].

The continuous-deterministic mathematical description of bacterial aggregation patterns has been previously done using reaction-diffusion systems of equations, which are included in theoretical framework of quasilinear parabolic partial differential equations [20, 55, 73, 105, 106]. These models consider the basic processes that take part in the colonial development such as bacterial movement, proliferation and interaction between individual cells.

We followed this continuous approach and we propose a new reaction-diffusion-chemotaxis model for bacterial aggregation patterns, which is based on the model by Kawasaki *et al.* [73].

The thesis is organized in five chapters. In Chapter 2, we begin by giving a brief account of the biological background and mathematical modeling of chemotaxis.

In Chapter 3 we give a summary of the morphological patterns of *B. subtilis*. In addition, we review the original model by Kawasaki *et al.* [73]. Afterwards, we discuss the role of the chemotaxis produced by nutrients in the development of bacterial patterns. Then, we propose a suitable chemotactic term that is motivated by biological observations [55] and add it to the original Kawasaki's model. We explore the effects of the new chemotactic term in the aggregation patterns by doing high resolution numerical simulations of the new model using Graphic Processing Units and parallel computation techniques.

In Chapter 4 we continue exploring the impact of the chemotaxis term on the aggregation patterns, and we focus on analyzing the effects at the colony envelope front, since this region is the one leading the growth of the patterns. In this fashion, we explore the effects that the chemotactic term has on the propagation velocity of the colony envelope front. We estimate numerically the velocity of the front, and under certain simplifying assumptions we approximate asymptotically the propagation velocity. We show that the velocity is an increasing function nutrient level and chemotactic sensitivity.

Motivated by the observations on the behavior of the colony front as a traveling biological wave, and the derivation of an approximated scalar equation for the bacterial density we then analyze the traveling wave solutions of such an equation. In particular, in Chapter 5 we study the stability in exponentially weighted spaces of certain subsets of the spectrum corresponding to the linearized operator around smooth-monotone-degenerate traveling waves supported by reaction-diffusion equations of Fisher-KPP type with non-linear degenerate diffusion coefficient.

Finally, in Chapter 6 we present some concluding remarks.

Chapter 2

Biological background and mathematical modeling

Complex biological phenomena are ubiquitous in nature and their mathematical description consists of the development of models that shed some light on the understanding of these phenomena. One reason for using mathematics as a tool in biological sciences is to guide intuition derived from experience (experimentation), as well as to provide a theoretical framework to draw conclusions. Mathematical models should be designed carefully, based on biological facts, and they often represent a simplification of phenomena under consideration. The complexity involved in biochemical phenomena force mathematical modeling to make models of models, being this a vital step of the process: the exercise of effective simplification. For this, we should identify the most important factors involved in a biological situation. The analysis of a mathematical model should provide additional information (both qualitative and quantitative) of the biological system under consideration and, in the best scenario, it should serve as basis for new experiments or draw concluding arguments. It is worth noting that a model could motivate new hypotheses and the design of experimental programs in a more efficient manner. Mathematical models applied to biological/chemical systems are often too complicated to be analyzed using standard analytic techniques, and thus, it is common to conduct numerical simulations. The interpretation of these simulations should be carefully made, and in certain cases may lead to further improvements of the model.

Mathematical models can take different forms, for example, differential equations, dynamical systems, stochastic models, among others. One example of a type of model are the reaction-diffusion (R-D) systems that are contained in the framework of partial differential equations of parabolic type.

R-D systems describe the concentration of one or more substances by means of two mechanisms: the local transformation of the constituents into each other according to a certain process, and the transport into space by diffusion. These

systems have been applied naturally in chemistry, but also there are examples of applications to others fields such as biology, ecology, medicine, etc. In general, R-D systems are often applicable to ecosystems with diffusing populations [112].

The mechanism of R-D systems was proposed by Turing [151] to establish the chemical basis of morphogenesis, and has served as base model for theoretical biology. More recent works [105, 106] have explained the coat patterns found in zebras, leopards, butterflies, and others.

In the field of medicine, great effort has been made to understand diseases such as cancer, and the flexibility of R-D models has allowed to consider elements of the complex process of tumoral angiogenesis, which is the development of new blood vessels. For instance, Anderson and Chaplain [9] developed a hybrid model, discrete and continuous, to explain the formation of capillary networks due to a tumoral chemical stimulus. For a review on the mathematical modeling of vasculogenesis and angiogenesis, see [133].

Migration of populations in biology is a multiple-scales phenomenon that has been studied thoroughly because of its impact on human society. Examples of migrating animals (mammals and birds), insects and plants have been observed as biological invasions that give rise to expansion patterns also known as biological waves (see [141]). At smaller scale, examples of traveling cell populations can be found in (biological) processes such as wound healing [45], inflammatory response of the immune system [88], and growth patterns in bacterial cultures [20].

The deterministic continuous approach to model migrating populations is based on R-D systems, which describe the time evolution of the population density according to interactions among the individuals, such as birth, death, competition, cooperation, and dispersal in space. In the following section we make a heuristical derivation of R-D equations from simple ideas involving conservation laws.

2.1 Formal derivation of equations

Reaction-diffusion equations arise in a natural way in the process of mathematical modeling of spatio-temporal phenomena that involve a general conservation law. We describe their derivation as follows.

In the continuous approach to model the migrating behavior of populations (e.g. cells or animals), the distribution of interacting individuals is described through density functions.

The individuals are contained within a region, which we denote V, and we assume that it is an open subset, $V \subset \mathbb{R}^n$, $n \geq 1$, with a smooth boundary $S = \partial V$. In particular, we are interested in the cases $n = 1, 2$ and 3.

Let $u(x,t) : V \times \mathbb{R}^+ \to \mathbb{R}$, be the density function that represents the concentration of matter or biomass (e.g. population density). The general conservation

equation says that the rate change of the amount of matter in V is equal to the rate flow of matter across S into V plus the matter created in V.

Hence

$$\frac{\partial}{\partial t}\int_V u(x,t)dv = -\int_S J\cdot\hat{n}dS + \int_V f dv,$$

where $\hat{n}$ is the unit exterior normal vector to the boundary S, J is the matter flux and f is the source or interaction term among individuals that could depend on u, x and t. Using the divergence theorem we get

$$\int_V \left(\frac{\partial u}{\partial t} + \nabla\cdot J - f(u,x,t)\right) dv = 0.$$

Since the volume V is arbitrary, the integrand must be zero. Thus, we obtain the balance equation

$$\frac{\partial u}{\partial t} = -\nabla\cdot J + f(u,x,t). \tag{2.1.1}$$

For an specific model, the terms f and J must be supplied. The general flux term J must be specified in each situation which population migration is conveyed by diffusion, advection or other directional movement mechanisms such as *chemotaxis*. For example, considering Fick's Law [112], $J = -D\nabla u$, we get the general reaction-diffusion system

$$\frac{\partial u}{\partial t} = \nabla\cdot(D\nabla u) + f(u,x,t), \tag{2.1.2}$$

where D is the constant of diffusivity.

In a more general situation, we can consider various interacting populations, each one with population density $u_i(x,t)$, for $i = 1, ..., m$. Then, $U(x,t) = (u_1(x,t), ..., u_m(x,t)) \in \mathbb{R}^m$, represents a vector of densities of interacting species. Thus, equation (2.1.2) is generalized to the R-D system of m equations

$$\frac{\partial U}{\partial t} = \nabla\cdot(D\nabla U) + F(U,x,t), \tag{2.1.3}$$

where now D is the matrix of diffusivities and F denotes the vector of reaction among all the populations, and could depend on x and t as well. Observe that the term $D\nabla U$ is a matrix, and hence $\nabla\cdot(D\nabla U)$ is a vector. When the matrix D is diagonal, there are no terms of cross diffusion.

For example, consider two populations with density functions $u_1(x,t)$ and $u_2(x,t)$, and diffusion constants D_{11} and D_{22}, respectively. This species interact among themselves through the reaction function $F(U) = (f_1(u_1,u_2), f_2(u_1,u_2))$, which is, in general, non-linear. Suppose that $D = (D_{ij})$, for $1 \le i,j \le 2$, is a general matrix of diffusivities. Hence, in this case system (2.1.3) has the form

$$\begin{pmatrix} \partial_t u_1 \\ \partial_t u_2 \end{pmatrix} = \begin{pmatrix} D_{11}\Delta u_1 + D_{12}\Delta u_2 \\ D_{21}\Delta u_1 + D_{22}\Delta u_2 \end{pmatrix} + \begin{pmatrix} f_1(u_1,u_2) \\ f_2(u_1,u_2) \end{pmatrix}.$$

The terms of cross-diffusion arise when $D_{12}, D_{21} \neq 0$.

Equation (2.1.2) and system (2.1.3) belong to the semi-linear parabolic equation type. The monograph of Fife [48] is an excellent reference for the fundamentals on the mathematical theory of these equations, (see also [146] and [57]).

In the sequel, let us consider the case of a single species, that is, $m = 1$. In the case that we consider Fick's Law, with $D > 0$, and no reaction term, $f \equiv 0$, we obtain the well known linear diffusion or heat equation

$$\frac{\partial u}{\partial t} = D\Delta u.$$

The heat equation may be derived in alternative way such as random walk models [105, 112] or Brownian motion [32].

The canonical example of a R-D model is based on the seminal work of Fisher [50] and Kolmogorov, Petrovsky and Piskunov (KPP) [81]. In 1937, Fisher proposed the non-linear scalar R-D equation

$$\frac{\partial u}{\partial t} = D\Delta u + ru\left(1 - \frac{u}{K}\right), \tag{2.1.4}$$

as model for the propagation of and advantageous gene in a population. He considered that the increased in the gene frequency should propagate as a wave of stationary form advancing with constant speed. He used an heuristic reasoning to obtain the propagation speed of the wave. On the other hand, Kolmogorov *et al.* obtained the first analytic results on existence and stability of solutions.

Equation (2.1.4) is known as Fisher-KPP equation in the literature, but as was pointed out by Murray [105] (see also [142]), it was Luther [89] the first one who proposed this equation and performed a traveling wave analysis in the context of chemical reactions.

The non-linearity comes from the reaction term $f(u) = ru(1-u/K)$, also known as logistic growth law and was first proposed by Verhulst [153]. The parameter $r > 0$ is called the intrinsic reproduction rate, and $K > 0$ is called the carrying capacity of the environment.

Specifically, the logistic growth term is based on the assumption that an increase in population density leads to a decrease in birth rate and increase death rate. But, this assumption may not always be valid, as observed by Allee [5], for some species a higher density is better, regarding to cooperative hunting or defense. Hence for these species, their population may proliferate at higher densities, while at lower densities it may decline. This phenomenon is known as an *Allee effect* [105], and has been mathematically modeled by a density dependent growth function $f(u)$, that is negative at small positive values for u. An example of such a function is

$$f(u) = ru\left(1 - \frac{u}{K}\right)(u - a),$$

where the parameters r, K are positive and $a \in (0, K)$. The parameter a is the critical threshold density value, with the feature that density populations starting above this level will grow to the maximum level allowed by the carrying capacity K. Populations with density bellow a will decrease to zero. The R-D diffusion equation considering Fick's Law and the Allee effect has the following form

$$\frac{\partial u}{\partial t} = D\Delta u + ru\left(1 - \frac{u}{K}\right)(u - a),$$

and is sometimes refered as reduced Nagumo equation [105].

Skellam [144] considered the random walk model and various modes of population growth to explain in a systematic way the dispersal of animals (muskrats). The work of Skellam has served as a basis for the understanding of migration and dispersal of populations. Nevertheless, this model assumes that individuals make complete random paths, and predicts that an organism will move at infinite velocity (see [64]). In a subsequent work, Skellam [145] considered a generalized random walk, where if an organism move along a line it may have a biased movement, i.e., the probability of taking a step to the right or left is not equal and may depend on the space. This supposition accounts for the fact that an organism do not move completely random and respond to the environmental stimuli.

More realistic models of population diffusion have been derived considering further observable situations, for instance, population pressure. This is the effect by which the dispersal of a population is enhanced as its density increases, and was discussed first by Morisita in 1950 (cf. [101]), as he observed this phenomenon in a natural population of water striders.

Rather than consider the random motility of individuals, Gurtin and MacCamy [60] supposed that, in some biological situations, dispersal of population is promoted by densely inhabited regions; hence individuals avoid overcrowding. The authors proposed a non-linear degenerate R-D equation, where the diffusivity is density-dependent. The authors also proposed that the constitutive equation for the population flux must be non-linear.

The flux can be written as

$$J = -D(u)\nabla u, \tag{2.1.5}$$

where diffusion coefficient $D(u)$ now depends on the population density. For example, the authors in [60] took $D(u) = ku^{n-1}$, with $n \geq 2$, and derived the following equation

$$\frac{\partial u}{\partial t} = k\Delta(u^{n-1}\nabla u) + f(u), \tag{2.1.6}$$

that combines the mechanisms of the *porous medium* equation [13,152] and the interaction of individuals. We note that equation (2.1.6) degenerates at points where

$u = 0$, that is, where there is no individuals and the diffusion coefficient vanishes. The degeneracy has an important mathematical feature: a population which is initially confined to a bounded region spreads out with finite speed. This contrasts with the constant diffusion case, where all disturbance propagate from rest with infinite speed. A similar model was derived from probabilistic considerations by Gurney and Nisbet [58]; see also [12].

As we have mentioned, R-D equations are used as a model to describe the migration of populations. One particular migration situation is the invasion of species, that usually takes place as the propagation of an invading population front. Therefore, we will be interested in the solutions that have a *traveling wave* behavior. Hence we introduce the following

Definition 1. Let us consider the R-D equation

$$u_t = (D(u)u_x)_x + f(u), \quad (x,t) \in \mathbb{R} \times \mathbb{R}_+, \tag{2.1.7}$$

where $u = u(x,t)$, $f(u)$ is the reaction term and $D(u)$ is a general diffusion coefficient that could be constant, $D = D_0 > 0$, for linear diffusion or non-linear. A *traveling wave solution* (TWS) of *front* type is a solution that do not change its profile in time and travels with constant velocity. Hence, traveling fronts are of the form

$$u(x,t) = \varphi(x - ct) = \varphi(\xi),$$

where $c \in \mathbb{R}$ is the velocity of the front and $\varphi : \mathbb{R} \to \mathbb{R}$ is the profile function of the wave. In an unbounded domain, the propagation of a traveling front corresponds to the following conditions at infinity

$$u_- = \lim_{\xi \to -\infty} \varphi(\xi), \quad u_+ = \lim_{\xi \to +\infty} \varphi(\xi),$$

and we say that the front connects the equilibria u_- and u_+. The asymptotic limits are equilibrium points of the reaction function in consideration, that is, $f(u_\pm) = 0$.

In case that we consider a degenerate density-dependent diffusion coefficient, $D(u)$, equation (2.1.7) will support a TWS of *sharp* type, $\varphi(\xi)$, for which there will be a finite point $\xi_* \in (-\infty, +\infty)$ where its derivative is discontinuous. For a rigorous definition of sharp front see [126].

Sometimes TWS of front type are called smooth TWS, in contrast with the sharp ones, since its derivative is continuous at every point.

As mentioned earlier, the population flux function J must be specified for each migration situation. One of these specific situations is the bacterial chemotaxis, and we shall review some of its the basic biological aspects.

2.2 Chemotaxis

The response of an organism to a external stimulus is called "taxis". When the organism movement is response to a chemical substances is called *chemotaxis*. Horstmann [66] defines chemotaxis as "...the influence of chemical substances in the environment on the movement of mobile species."

If the organism moves towards the source of the chemical substance we say that the chemotaxis is positive, and the chemical substance is called a *chemoattractor*. A movement in the direction toward lower concentration areas is called negative chemotaxis, and the substance is a *chemorepellent.*

Chemotaxis is a phenomena present in many biological and physiological systems, such as the human immune system. Neutrophils (a type of white blood cells), are guided to the sites of bacterial infection through a system of chemotactic receptors which detect certain types of amino acids produced by bacteria [70].

Bacterial chemotaxis is an example of migration of cells and it was discovered more than a century ago by Engelmann [42] and Pfeffer [123, 124]. This phenomenon has become one of the most studied and well documented systems in biology, serving as a model for higher organisms.

The biochemical processes involved in chemotaxis were first studied in the pioneer works by Adler [1, 2] on the bacterium *Escherichia coli*. This strain has served as a model organism to further investigate this phenomenon in many other bacterial species, e.g., *Salmonella typhimurium* [91] and *Bacillus subtilis* [114].

Bacteria move using flagella, whip-like appendages randomly located in their membrane. The number and position of flagella varies between species, and as a consequence bacteria have developed different types of motility. Swimming and tumbling are two of the most common motility strategies that depend on flagella. See [40] for a list of flagella distribution and motility mechanism; see also [20, 55].

In the absence of stimuli bacteria move in a random walk, as result of a sequence of swimming and tumbling movements. *E. coli* alternates between 1.0 second swims and 0.1 second tumbles [68].

In non homogeneous environments, external stimuli (positive or negative) induces a random walk biased towards chemoattractants or avoiding chemorepellents [40]. The movement of bacteria cells is produced by rotation of the flagellar motor. Hence, bacteria move in random walks composed of (long) swims, due to a counterclockwise (CCW) rotation of the motor, and (short) tumbles, due to a clockwise (CW) rotation. CCW rotation makes the flagella come together into a bundle propelling the cell forward, meanwhile CW rotation disrupts the flagellar bundle causing the cell to randomly reorientate in a new direction [157]. Therefore, movement of bacteria across a gradient of attractant produces less CW rotations, decreasing cell reorientation, and favors CCW rotations resulting in longer swims into the "right" direction.

Therefore, the bias of the movement is controlled by chemical sensing of positive or negative signals. The core mechanism of chemotaxis lies in the signal transduction pathway, which is a complex intracellular system that change the direction of flagellar rotation upon detection of chemical concentration, in their immediate surroundings, using dedicate transmembrane receptors [40, 82, 157].

Being so small, bacteria can not sense chemical gradients spatially, instead, they rely on temporal sensing of chemical concentrations [82], and compare between sequential registers of their occupied chemoreceptors [40]. Bacteria dynamically adapt to respond to higher concentrations of attractant; this has been previously explained through Weber's law [98], that states that the minimum detectable difference on the intensity of a stimulus is proportional to the previous stimulus intensity.

The dynamic response, also known as adaptation, is a feedback system that encompasses different time scales, a fast excitatory response upon binding of chemoeffector, and a slow reset of chemoreceptors to a prestimulus state [84]. This mechanism, present in bacteria, has been conceptualized as "short-term memory", proposed for the first time by Macnab and Koshlad [91]. More recent works, have established that memory length, the time needed by bacteria to return its chemotaxis pathway to its steady state, is not fixed and depend, among other factors, on the gradient steepness of the stimulus [156]. Furthermore, in order to maintain adaptation, the memory length should match the time scale of long swims [82].

2.3 Chemotaxis modeling

Chemotaxis is a multi-scale phenomenon that is present at the individual (single cell) to the population scale, and its study comprehends the work from several disciplines (e.g. biology, chemistry, biophysics, mathematics and others).

At the single-cell scale, there have been studied specific chemotactic processes such as signal detection, adaptation response to chemical gradients, intra-cellular signal transduction, and the cell swimming mechanism [150]. At macroscopic level, the objective is to understand the dynamics and the behavior of chemotactic cell populations taking into account the chemotactic mechanisms from the individual scale. The mathematical modeling of chemotaxis it has been done from different approaches, e.g. stochastic, discrete and continuous deterministic. In the latter case, macroscopic models take the form of systems of PDE's that are based on phenomenological assumptions as well as on the microscopic description of the chemotactic processes.

The mathematical modeling of chemotaxis goes back to the pioneer works by Patlak in 1953 [121], Keller and Segel in the 70s decade [75–77], and more recently Alt [6]. Considered as one of the seminal works on the mathematical

modeling of chemotaxis, the Keller-Segel model has prevailed as mathematical tool to understand the gregarious behavior of certain chemotactic cell populations, in biological systems.

The generalized Keller-Segel model [63] has the following form:

$$\begin{aligned} u_t &= \nabla \cdot (D(u,v)\nabla u) + f(u,v) - \nabla \cdot (\chi(u,v)\nabla v), \\ v_t &= D_v \Delta v + g(u,v) - h(u,v)v, \end{aligned} \tag{2.3.1}$$

where $u = u(x,t)$ and $v = v(x,t)$ denote the populations density and the concentration of the chemo-attractor, respectively, in a space point x and time t. The coefficient $D(u,v)$ represents the diffusivity of the population, while $\chi(u,v)$ is the chemotactic sensitivity function; both functions might depend on u, v or both. The reaction term $f(u,v)$ denotes the population growth, and $g(u,v), h(u,v)$ are the production and the degradation of the chemical signal, respectively. $D_v \geq 0$ is the constant diffusion coefficient of the chemo-attractor. The system (2.3.1) is solved for initial distributions $u(x,0) = u_0(x)$ and $v(x,0) = v_0(x)$ of cells and chemical respectively, and appropriate boundary conditions.

2.3.1 Derivation of chemotaxis equations

Under favorable food conditions, cells of the slime mold *Dictystelium discoideum* forage independently; while under starvation the population aggregates into a motile slug, and then differentiate into a fruiting body which scatters spores into environment to search for better conditions. During the aggregation process, single amoebas migrate as a response to a chemo-attractor called cyclic-AMP (cAMP) which is produced by the amoebas themselves [105]. It has been shown that the amoebas also secrete an extracellular enzyme, phosphodiesterase, which reacts with the cAMP into a neutral waste complex.

The Keller-Segel (KS) model [75] was introduced to explain the aggregation process of the slime mold *D. discoideum* and is based on phenomenological assumptions of how cells respond to the external cAMP signal. The authors in [75] originally introduced a system of four parabolic R-D equations strongly coupled, for modeling the population migration due to the attractor cAMP, and which reacts with an extra cellular enzyme. Under certain assumptions, Keller and Segel, simplified the biochemical reactions between cAMP and the enzyme, and proposed a reduced model of two non-linear coupled parabolic equations. Following [75], we give a heuristic derivation based on phenomenological assumptions and general balance equations, of the two-equation reduced model, also known as the classical Keller-Segel model.

Consider an arbitrary fixed region A in the plane, with smooth boundary $S = \partial A$. Denote the amoeba density by the continuous function $a(x,y,t)$ at the point

$(x, y) \in A$ and time t. The concentration of the chemo-attractor is denoted by $\rho(x, y, t)$.

The general balance equation for the amoeba mass is

$$\frac{\partial}{\partial t} \iint_A a dx dy = \iint_A f dx dy - \int_S J_a \cdot \hat{n} dS, \tag{2.3.2}$$

where $f(a)$ is the growth term of the amoebas per unit area per unit time, $J_a(x, y, t)$ is the biomass flux, and $\hat{n}$ is the unit exterior normal to the boundary S. Applying the divergence theorem to (2.3.2) and in conjunction with the arbitrary choice of A, we have

$$\frac{\partial a}{\partial t} = f(a) - \nabla \cdot J_a. \tag{2.3.3}$$

Analogous equation holds for ρ, namely

$$\frac{\partial \rho}{\partial t} = g(a, \rho) - \nabla \cdot J_\rho, \tag{2.3.4}$$

where $g(a, \rho)$ is the source/degradation term for the attractor.

The flux function for the amoebas J_a has two components, one due to the random motion of cells and other due to chemotaxis. Thus, the flux function has the following form

$$J_a = J_{\text{Diff}} + J_{\text{Chem}}. \tag{2.3.5}$$

The diffusion contribution is given by Fick's Law

$$J_{\text{Diffusion}} = -D_a(\rho) \nabla a, \tag{2.3.6}$$

where $D_a(\rho)$ is the diffusion coefficient of the amoebas, possibly dependent on the attractant concentration. The chemotactic flux, J_{Chem}, is proportional to the gradient of the concentration, and the flux of amoebas will increase in proportion with the density of cells. Hence, we may write the chemotactic flux as

$$J_{\text{Chem}} = a\chi(\rho) \nabla \rho, \tag{2.3.7}$$

where $\chi(\rho) > 0$ denotes the response of amoeba to the attractant gradient. In this case, the chemotaxis is considered as positive, since the biased movement is towards the direction of $\nabla \rho$, amoebas move from lower to higher concentrations of the attractant ρ. The proliferation of amoebas is negligible during the aggregation phase, thus we consider the growth term $f(a) = 0$. In addition, is assumed that the diffusion coefficient for amoebas, $D_a(\rho) = D_a$, is constant. Combining equations (2.3.3), (2.3.5), (2.3.6) and (2.3.7) we obtain the basic chemotaxis equation

$$\frac{\partial a}{\partial t} = \nabla \cdot (D_a \nabla a - a\chi(\rho) \nabla \rho). \tag{2.3.8}$$

On the other hand, we suppose that the attractor flux is given by simple diffusion, $J_\rho = -D_\rho \nabla \rho$. Hence, we supplement equation (2.3.8) with the reaction-diffusion for ρ

$$\frac{\partial \rho}{\partial t} = \nabla \cdot D_\rho \nabla \rho + g(a, \rho), \tag{2.3.9}$$

where D_ρ is the constant of diffusivity of ρ. The system of equations (2.3.8)–(2.3.9) is known the classical Keller-Segel model for chemotaxis [75–77].

Keller and Segel [75] obtained a simpler model based on the following assumptions. The chemotactic sensitivity function is, $\chi(\rho) = \chi_0 > 0$, a positive constant. Also, they proposed $g(a, \rho) = f(\rho)a - k(\rho)\rho$, the net source/degradation of attractant. The term $f(\rho)a$ is the production rate by cells; while $-k(\rho)\rho$ is the rate at which attractant decays. Here, $f(\rho)$ is the secretion rate per cell.

In their classical paper of 1971 [77], Keller and Segel used the chemotaxis system (2.3.8)–(2.3.9) and sought for one dimensional traveling wave solutions to explain the motility of bands of *E. coli* which had been observed by Adler [1]. The authors assumed $g(a, \rho) = -k(\rho)\rho = -k_0\rho$, with $k_0 > 0$. Furthermore, they proposed the following singular chemotactic sensitivity

$$\chi(\rho) = \frac{\chi_0}{\rho},$$

where $\chi_0 > 0$ is constant and which is known as logarithmic sensitivity [105]. Such a choice for the sensitivity function turns out to be necessary for the existence of traveling waves [77]. Keller [74] discussed the validity of the above assumptions on the functions $\chi(\rho), k(\rho)$ and $D_a(\rho)$, as well as the implications on the mathematical modeling of the mobility behavior of chemotactic organism.

Another chemotactic sensitivity function previously considered is the receptor law [83]:

$$\chi(\rho) = \frac{\chi_0}{(K + \rho)^2},$$

which we will discuss in detail below (see Chapter 2).

Microscopic derivations

Segel and Jackson [136] used the continuous deterministic approach to develop a K-S model type to explain the experimental observations reported by Dalquist *et al.* [37] of the chemotactic response of bacteria *Salmonela typhimurium*. The authors discussed the scope of the former approach since they observed that, assuming that each member of the population responds in a similar way to the external stimuli, a variation of the results arises. They concluded that is important to consider the microscopic response of the individual cells into the macroscopic description of the population dynamics, because the assumption that the coefficients of the model

(e.g. diffusion and chemotaxis coefficients) are constant, is valid only when the population is homogeneous.

Several authors have been interested in considering the individual bacterial behavior in the process of the derivation of the macroscopic equations of bacterial migration and justify the phenomenological assumptions on the chemotaxis flux (equation (2.3.5) was postulated as constitutive law in [75]). We briefly mention some of the works where the authors gave alternative derivations of the classical chemotaxis equation by means of different techniques, assuming certain microscopic features of bacteria (e.g. intracellular kinetics) or taking into account the microscopic description of the movement of cells.

Segel [134] included the attractant-receptor kinetics to explain the bacterial chemotactic behavior, and justified the constitutive expression for the chemotactic flux (2.3.5). Specifically, he considered the binding process of the enzymes located at the receptors to the attractant molecules (sometimes called ligand). This process elicits the starting reaction of chemotaxis. The author proposed a model of enzyme-ligand interaction of four configuration states: enzyme can take the states open or bent; and the ligand can be bounded or unbounded. Likewise, he considered that bacteria move in one dimension, either to right or left; and bacteria change direction with certain probability, called reversal probability, that in turn depends on the configuration of receptors. Ignoring both the attractor uptake and the birth/death of bacterias and with the assumption that the attractant gradient is small, Segel found that the density of bacteria b is governed by the conservation equation $b_t = -J_x$ and the flux of cells is given by

$$J = -D(s)\frac{\partial b}{\partial x} + \chi(s)b\frac{\partial s}{\partial x},$$

as in the classical Keller-Segel model [75, 76]. Segel found explicit expressions for the diffusion coefficient $D(s)$ and the chemotaxis sensibility $\chi(s)$ in terms of microscopic variables, that in turn depend on the concentration of the attractant s.

Othmer, Dunbar and Alt [117] introduced a theoretical framework to study the dispersion of organism considering two characteristic modes for motility: one, that is called space jump processes and considers that organisms follow a sequence of jumps and pauses; and the second, that is called velocity jump processes that consist of a series of alternating characteristic motions: a linear motion at approximately constant speed called runs, followed by reorientations during which a new direction and velocity is chosen. The changes in direction are discontinuous and velocity is chose randomly by a Poisson process. The former processes are adequate to describe the movement of "large" organism (e.g. kangaroos or grasshoppers), where as the latter fit better to describe the cellular movement of bacteria (e.g. *E. coli*).

The velocity jump processes were used in [62,118] to derive the classical chemotaxis equation. The authors considered the diffusion-limit of transport equations, and allowed the turning kernel to be dependent on an external bias signal. Using perturbation analysis, they showed that the classical chemotaxis arises only if the external signal is small.

As noted by Erban and Othmer [43], Patlak [121] was the first to derive the chemotaxis sensitivity function from a velocity jump processes. The authors in [43] developed a multi-scale model for bacterial chemotaxis, describing the individual cells movement through velocity jump process, and each cell is considered to have an internal state, determined by the excitation and adaptation response of the cell, that evolve according to a linear ODE system. The turning rate of individuals depend linearly on the internal state, which in turn it depends on the external signal. Using moment-closure techniques in one dimension and appropriate scalings they derived both a second order hyperbolic equation for the population density and the classical chemotaxis equation. Erban and Othmer [44] generalized their results to higher dimensions and discussed some aspects regarding to modeling of the internal dynamics of bacteria, such as signal transduction. More recent works generalize the results in [43, 44]; for instance, in [166] it is allowed that the turning rate depends non-linearly on the internal state; and in [165], it is included a detailed model of bio-chemestry of intracellular signaling, which is in general, nonlinear. Both of this works, showed that under the assumption that the gradient of the external signal is small, the evolution of bacterial density can be approximated by the classical chemotaxis equation with signal-dependent chemotactic sensitivity.

Further approaches to derivate the classical chemotaxis equations from microscopic assumptions are based on reinforced random walks [119] and interacting stochastic many-particle system [148].

To finish this section we cite some review articles related to the mathematical theory of chemotaxis, in particular to the Keller-Segel models and its variations. The mathematical properties of these models such as existence of solutions, blow-up, traveling wave solutions and asymptotic behavior have been summarized in [16, 63, 66, 160]. Regarding to mathematical modeling of bacterial chemotaxis we mention two articles: (i) [150] where is given an overview of the modeling of chemotaxis at the single-cell level, and (ii) [149] where the authors review the mathematical modeling of bacterial chemotaxis at macroscopic cell population level.

2.4 Applications of the KS systems

We shall describe some of the applications where the mathematical modeling have been done by using a Keller-Segel type system. The most of the fields where K-S

models have been applied are related to biology, medicine or ecology due to the ability of the model to capture the biased movement of organism involved in the dispersion of species or the aggregation of cells populations [120].

Anderson and Chaplain [9] proposed a hybrid model, continuous and discrete, of the process of tumor induced angiogenesis. A solid avascular tumor, when reaches certain cell density (approx. 10^6 cells), have its growth limited to the diffusion of nutrients. Thus, to further growth, the tumor induces the development of new capillary network by "recruiting" the blood vessels in the periphery. The angiogenesis process starts when tumor cells segregate the tumor angiogenic factor (TAF), that diffuses in the surrounding tissue and forms a concentration gradient. The endothelial cells of the pre-existing vasculature migrate towards the tumor in a chemotactic response to TAF. In addition, the endothelial cells interact with the fibronectin, a macromolecule present in the extracellular matrix, that promotes the cell migration up a concentration gradient. This interaction is known as haptotaxis. The model by Anderson and Chaplain is composed of two parts, one uses the continuous deterministic approach (reaction-diffusion-chemotaxis equations) to describe the concentrations of TAF and fibronectin; and the second it considers an automata-like model based on a biased random walk model to describe the migration of endothelial cells.

Alt and Lauffenburger [7] proposed a K-S system to explain the leukocyte chemotaxis on a inflammatory response to bacterial invassion on tissue. They formulated a system of three reaction-diffusion-chemotaxis equations for the leukocyte and bacterial densities, and a chemotactic attractant concentration that mediates the migration response of leukocyte to the affected area. The authors above mentioned applied this model to explain observed clinical behavior of chemotaxis defects in leukocytes. These defects were correlated to severe bacterial infections on surgical patients, but not to the density level of leukocytes found in the affected area. Alt and Lauffenburger concluded that the diminished effect of the inflammatory response was due to a deficiency of the leukocytes to found the bacteria on the inflamed tissue.

Most of the times, microbial infections on the human body are not produced by a sole microorganism species, but by a more harmful entities called biofilms. Biofilms are complex ecosystems of microorganisms (e.g. bacteria, fungi, among others) contained in a protective extracellular matrix of self-secreted polysaccharide that adheres to a surface, either biotic or abiotic [35]. There is evidence that biofilms are responsible for many of the infectious diseases in the body including respiratory infections, caries and infections associated with indwelling medical devices (e.g. catheters, implants and valves) [90]. Infections due to biofilms are commonly acute and recurrent, since the coating from the extracellular matrix facilitates the avoidance of the immune system response and resistance antibiotics.

In addition, the matrix provides mechanisms that promote horizontal gene transfer that propagate the antibiotic resistance [36, 161]. The process of formation of biofilms involves several mechanisms of growth, differentiation, communication and movement, and from the modeling point of view, it represents a unique challenge.

The aggregation patterns exhibited by many bacterial strains in in-vitro experiments are examples of simpler biofilms [20, 23, 29, 111, 138, 163]. Ben-Jacob and coworkers [19], have shown experimental evidence that the bacterial aggregation patterns undergo morphological changes under antibiotic stress, in such a way that these changes optimize the survival of the colony. The authors discussed the mechanism used by bacterial colonies to adapt to the hostile conditions, being the chemotactic signaling the key strategy for their survival.

On the other hand, recent studies [113, 116] have put forward evidence that shows that the antimicrobial and antibiotic resistance has become a global health threat. It has been estimated that about 700,000 people die every year from drug-resistance infections, and if the tendency is not reverted for 2050 the death toll will be about 10 million people per year (cf. [113]).

This motivate us to use mathematical modeling as a tool for understanding the underlying processes of development of patterns, such as communication and movement. Ultimately, the level of knowledge that we can achieve by studying bacterial patterns will contribute to the process of understanding of biofilms development, and hopefully, in the future this will represent the right approach to the increasing problem of antibiotic resistance.

In the following chapter we introduce a continuous reaction-diffusion-chemotaxis model for *B. subtilis* colony patterns, and we carry out numerical studies to explore the underlying effects that chemotaxis signals have on the development of aggregation structures of this specific bacterial strain.

Chapter 3

Chemotaxis model - Numerical simulations

In this chapter we propose a new R-D system for bacterial aggregation patterns that considers nutrient chemotaxis and we explore the effects that the chemotactic signal has over the development of the bacterial colony.

We begin by giving, in Section 3.1, a summary of the morphological patterns of the bacterium *Bacillus subtilis* observed during in-vitro experiments. In Section 3.2 we review the original model by Kawasaki *et al.* [73] for growth patterns of *B. subtilis*. Section 3.2.1 is concerned with the modeling of chemotaxis and the role it has on the development of patterns. In Section 3.3, we introduce the new chemotactic term into the original model. The resulting system is normalized in Section 3.4, to reduce the number of free parameters. In Sections 3.5 and 3.6 contain the results of our numerical simulations. We compare the new emerging chemotactic patterns to those without chemotaxis.

3.1 Bacterial pattern formation

Bacteria have developed highly complex strategies to cope with adverse environmental conditions. These strategies include differentiation of cells, sophisticated biochemical communications capabilities and even programmed cell death [137]. All these features show that individual cells cooperate to achieve a multicellular organism behavior, which has been identified as characteristic bacterial trait [138]. The multicellular behavior is envisioned as communicating and decision-making capabilities that allow bacteria to optimize the population survival. It has been observed that, in some bacterial species, this survival behavior favors the spatial self-organization of the colony, and through high adaptability of individual cells, they form spatio-temporal patterns with very diverse morphologies.

Bacteria do not store all the necessary information to create every morphology; rather, additional information is cooperatively generated [22]. The pattern that emerges depends on the bacterial strain and the environmental conditions. Systematic studies of the morphological aggregation patterns exhibited by several bacterial strains, such as *Escherichia coli, Salmonela typhimurium, Bacillus subtilis*, among others, have been carried out by means of variations in the nutrient level and agar concentration, during in-vitro experiments [23, 29, 111, 138, 163]. In this section we give a summary of the experimental observations of colony patterns in *B. subtilis*.

3.1.1 *B. subtilis* colony patterns

B. subtilis is a gram-positive bacterium which is found in soil and gastrointestinal tract of some species of mammals, including humans. This bacterium strain has been extensively studied at the physiological level, in genetic essays and is taken as model organism for cell differentiation [147]. In addition, has been studied for its stimulating effects over the immune activity including activation of secretion of specific antibodies [33], and its antitumoral effects related to an augmented cytotoxicity of NK cells when used as immunotherapeutic agent [143].

It is known that *B. subtilis* colonies exhibit a fractal morphology when inoculated on solid agar with low levels of nutrient, which resemble diffusion-limited aggregation (DLA) (see [24,25,93,115]). DLA fractal morphology occurs when the mobility of bacteria is very limited and growth process is controlled by nutrient diffusion alone [24]. In the limit of low nutrient an underlying screening effect is present, that is, the most advanced parts of the colony consume the nutrient and the parts getting behind do not have access to enough nutrient to grow [154]. Keeping the agar concentration high and increasing the nutrient level, the screening effect is diminished and compact colonies with a rough (self-affine) interface emerge; these aggregation structures are known as "Eden-like" patterns [26, 155]. When inoculated on semi-solid surface (intermediate agar concentration) with poor nutrient level, bacterial colonies assume a dense branching morphology (DBM) with a smooth round envelope that propagates outward [23, 111].

DLA and DBM-like patterns are similar to those observed in non-living systems, e.g., in electrochemical deposition and crystal growth [21]. The underlying mechanisms in such non-living systems is the Mullins-Sekerka or diffusive instability, which is manifested when outward prostitutions at the interface advance faster that their surroundings [85, 154].

For an intermediate level of agar and high level of nutrient, patterns consisting of concentric rings have been observed [52, 158]. Finally, on nutrient-rich soft medium bacteria exhibit homogeneous compact colonies [159]. Detailed summary of the experimental observations can be found on [73] (see also [55, 94] and the

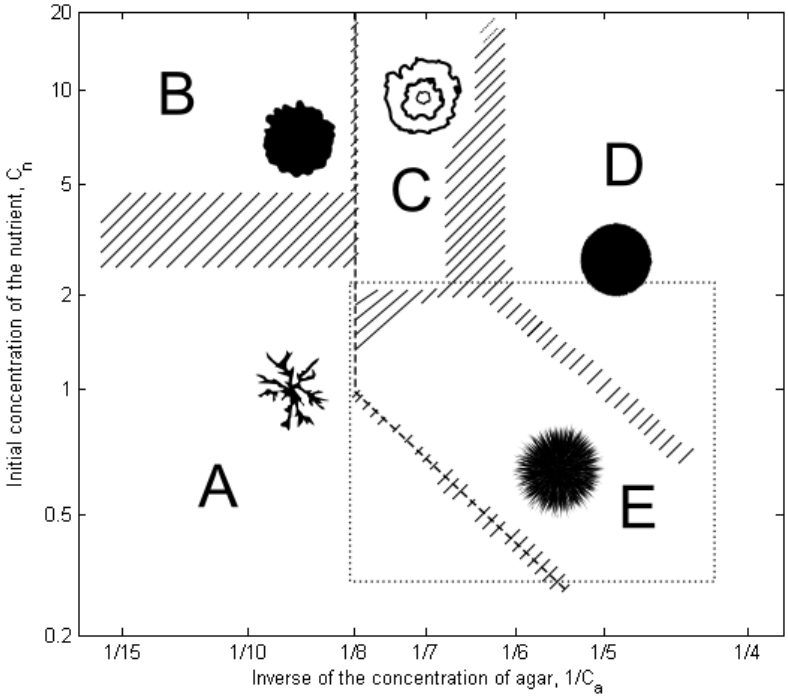

Figure 3.1: Depiction of the morphological diagram of the aggregation patterns exhibited by colonies of *B. subtilis* as a function of the concentration nutrient C_n (vertical axis) and the solidity of the agar medium expressed as $1/C_a$ (horizontal axis). This diagram is redrawn from the one in [73].

references therein).

The observable patterns emerge depending on the nutrient level C_n and agar concentration C_a. Typically, the experimental observations are summarized schematically in a morphological diagram as the one shown in Fig. 3.1.

The horizontal axis is the inverse of agar concentration, $1/C_a$, and the vertical axis is the nutrient level C_n. For high agar concentrations and low nutrient level, patterns are DLA-like (region A). As the nutrient level increases, but still on a hard surface, colony assumes an Eden-like configuration (region B). When agar's concentration is intermediate (semi-solid medium) and nutrient is low, DBM-like patterns emerge (region E), with smooth round envelope propagating outward. In nutrient-rich semi-solid medium the observed patterns are concentric rings (region C). In region D, where the medium is softer and nutrient level is high, bacteria develop homogeneous circular patterns with no openings. Dashed regions on Fig.

3.1 represent regions for the growth parameters (agar and nutrient levels) where the observed patterns show an ambiguous morphology.

Thanks to all the experimental work done, the qualitative picture of *B. subtilis* colonies is well understood; nevertheless it is susceptible to further improvements: for example, Bonachela *et al.* [28] propose the possibility of a richer morphological variety for patterns in the Eden regime (region B) (see also [164]).

In order to explain the experimental observations, different phenomenological mathematical models have been proposed, including continuous reaction-diffusion systems [106] and hybrid models [23]. Depending on the biological, models have been able to reproduce specific regions or all of the morphological diagram.

Typically, deterministic continuous modeling has been developed in the framework of reaction diffusion systems, consisting usually of two coupled equations to describe the evolution of bacteria and nutrient densities [106]. (It is to be observed, though, that homogeneously spreading patterns (region D) have been found as the solution of a single two-dimensional Fisher equation with linear diffusion [159].)

To reproduce more complex patterns, such as DLA and DBM-like, it is necessary to consider mechanisms that trigger the Mullins-Sekerka instability, as argued by Ben-Jacob and coworkers [20, 34, 55]. Examples of such mechanisms that have been previously considered are a meta-stable diffusion term [95], motivated by cell differentiation during growth process; a cut-off in the reaction term [78], due to a discreteness of bacteria; the incorporation of an additional lubricating field that influences the motion of bacteria [55]; and the inclusion of non-linear bacterial diffusion [73, 80]. To gain further insights of the biological mechanisms of the branching instability, these models have been compared and contrasted in [55] (see also [20]).

In the mid-90's Kawasaki *et al.* [73] introduced a R-D model with non-linear density-dependent degenerate (cross) diffusion coefficient to explain the experimental observations of Ohgiwari *et al.* [111] pertaining to DBM-like transition patterns between regions E and D of the morphological diagram. This model has been consistently studied due to its capabilities on reproducing the complex dense morphology patterns and to its rich non-linear mathematical structure (see, e.g., [47, 65, 106, 129]).

The aggregation patterns exhibited by bacteria are the result of a cooperative behavior that involve highly complex adaptive capabilities, such as, bacterial chemotaxis. Ben-Jacob and co-workers (cf. [17–20, 22, 23, 55]) have suggested that some of the features of the observable patterns can be only understood when the chemotactic response of bacteria is included.

Chemotaxis towards nutrients it is a well studied phenomenon in many bacterial species [1,2]. For instance, it is well documented that *B. subtilis* exhibits (positive) chemotaxis towards high nutrient levels and multiple aminoacids (cf. [102,115]; see

also [104, 157]).

Experimental evidence and theoretical arguments were given by Ben-Jacob *et al.* [20, 55] to justify the incorporation of nutrient chemotaxis into continuous reaction-diffusion models for bacterial growth. They suggested that nutrient chemotaxis play a key role in the branch-making dynamics, since it increases the diffusive instability and provides an outward drift to cellular movement. Although the authors did not propose a new chemotactic term for the particular model of Kawasaki and collaborators, they certainly discussed what the relation between a generic diffusion term an the appropriate chemotaxis should be (see Section 3.2.2 below).

In this fashion, we incorporate a suitable chemotactic term into the original model by Kawasaki *et al.* and explore the effects that the new chemotaxis term has on the bacterial aggregation patterns.

In the following section we briefly review the model of Kawasaki and collaborators, discuss the mathematical modeling of chemotaxis and the role it takes in the development of bacterial patterns.

3.2 The model by Kawasaki *et al.*

Kawasaki *et al.* [73] proposed a continuous model of reaction-diffusion type that captures many of the experimental features of the bacterial growth patterns in for the DBM and homogeneous circular morphologies.

We denote by $\Omega \subset \mathbb{R}^2$ a bounded domain, every point by $(x, y) \in \Omega$, and time $t \geq 0$. The nutrient concentration and cell density are represented by $n = n(x, y, t)$ and $b = b(x, y, t)$, respectively. The model has the following general form:

$$\begin{aligned} n_t &= D_n \Delta n - f(n, b) \\ b_t &= \nabla \cdot (D_b \nabla b) + \theta f(n, b). \end{aligned} \tag{3.2.1}$$

It is supposed that the bacteria and the nutrient diffuses, with diffusion coefficient D_b and D_n, respectively. The coefficient $D_n > 0$ is constant.

The key feature of this model is the choice of the non-linear diffusion coefficient D_b, which depends proportionally on b and n, and its design was motivated by the experimental findings of Ohgiwari *et al.* [111] on the growth patterns of bacterium *Bacillus subtilis* on agar plates. The authors systematically change the growth conditions, nutrient C_n and agar C_a concentrations, and found drastic morphology changes. These findings are summarized in the morphology diagram (see Fig. 3.1). They acknowledge that colonies apply different strategies to develop depending on the environmental conditions. For hard agar conditions, high C_a (corresponding to regions A and B in the morphological diagram), colonies tend to be more static, since the outermost part of the colony grows by cell division and individuals in the

inner part become dormant. In contrast, for soft agar (low and intermediate C_a) colony growth is due to the dynamic movement of bacteria in the periphery. This growth strategy correspond to regions C, D and E of the diagram, where softness of the agar promotes bacterial movement. The colony envelope is determined by a thin layer of bacteria whose movement is dull. Cells inside the colony, far from the front, are inactive.

Kawasaki and co-workers conjectured that the bacteria are immotile when either n or b is low and become active as n or b increases. Furthermore, they noted that bacteria deviate from the random diffusion exhibiting stochastic fluctuations. Hence, motivated by the previous observations, they proposed D_b to be a nonlinear cross diffusion coefficient of the following form

$$D_b = \sigma n b, \tag{3.2.2}$$

where $\sigma = \sigma_0(1 + \Delta)$, denoting σ_0 the inverse of the agar concentration. The softness of the agar increases with σ_0. The stochastic fluctuation of the movement is introduced by the parameter Δ, which is drawn from a triangular distribution with support in $[-1, 1]$ (see Section 3.5.3 below).

The term $f(n, b)$ represents the local interaction between the bacteria and the nutrient, i.e., is the consumption rate. The term $\theta f(n, b)$ is the growth rate of bacteria, where $\theta > 0$ is the conversion rate factor. The functional form of the consumption rate f was assumed to be of Michaelis-Menten type,

$$f(n, b) = \frac{\kappa n b}{1 + \gamma n}, \tag{3.2.3}$$

where $\kappa > 0$ and $\gamma > 0$ are constants. In the low-nutrient limit, f can be approximated as

$$f(n, b) = \kappa n b. \tag{3.2.4}$$

The consumption rate (3.2.4) was adopted by Kawasaki and co-workers for the majority of their analysis in [73], although, they also discuss the effects of the saturation term γn. For the rest of the chapter, we shall use the consumption rate defined in equation (3.2.4) for our calculations.

3.2.1 The role of chemotaxis in aggregation patterns

Ohgiwari *et al.* [111] discussed that for patterns in the regions C, D and E, the active bacterial movement enhances the growth rate of the colony. In addition, they noted that the DBM-like patterns cannot be described by the diffusion field of nutrient alone and suggested that additional mechanisms must be considered to explain some of the features of colony patterns.

Ben-Jacob and co-workers [18, 20, 22, 55] have proposed that the development of bacterial colonies is the result of a complex process of self-organization in which individual bacteria and the colony use various communication capabilities to form spatio-temporal patterns that enhance the adaptability to environmental conditions. The communication is done through chemotatic signaling. They suggested that there are at least three kinds of signals, each expected to be dominant in different regimes of the morphology diagram. One of the signals is the nutrient attractive chemotaxis, which is dominant for certain levels of the nutrient. Another type of signal is a long-range repulsive one, secreted by starving bacteria at center of the colony. The last one, is a short-range attractive signal produced at the front of the colony where bacteria ask for help to metabolize the excess of toxic waste products. The range of each signal is determined by the diffusion coefficient and the rate of decomposition.

Although, bacterial patterns are reminiscent to those of inorganic material [21], Ben-Jacob *et al.* [55] have pointed that in non-living systems, the DBM (lower fractal dimension) patterns are observed for lower growth velocity. In contrast, for bacterial colonies they have conjectured [20,55] that nutrient chemotaxis is the mechanism responsible for faster growth velocity together with a ramified pattern of low fractal dimension. Such a process should permit to increase the propagation of the front.

In view of these observations, the model we propose considers the nutrient chemotactic signal alone, inasmuch as it is the dominant signal in the DBM regime. Thus, we introduce a nutrient chemotactic term into system (3.2.1). For that purpose, we need to define a chemotaxis flux J_c which, in general, is written as

$$J_c = \xi(b)\chi(n)\nabla n, \tag{3.2.5}$$

where $\xi = \xi(b)$ is the bacterial response to the nutrient gradient, and $\chi(n)$ is the chemotactic sensitivity function.

3.2.2 Receptor's Law and the bacteria response function

The detection of chemical signals is done by bacteria using dedicated membrane receptors [157]. Bacteria can not sense chemical gradients spatially; instead, they compare between sequential registers of their occupied chemoreceptors [40]. Bacteria dynamically adapt to respond to higher concentrations of attractant; this has been previously explained through Weber's law [98], that states that the minimum detectable difference on the intensity of a stimulus is proportional to the previous stimulus intensity.

The process of interaction between a receptor and substrate (nutrient) can be explained through the law of mass-action (see [98, 119]). The binding of the

nutrient n to a protein P of a chemoreceptor forms the complex Pn according to $P + n \rightleftharpoons Pn$. When the equilibrium of the reaction is reached we get

$$K_d = \frac{[P][n]}{[Pn]}$$

where K_d is the *dissociation constant*, and the brackets notation [ ] indicate the corresponding concentration. Assuming that the velocity of association and dissociation are the same, and that the concentration of free protein $[P]$ is the total binding protein $[P_T]$ minus the concentration of the complex $[Pn]$, we can derive the following equation

$$[Pn] = \frac{[P_T][n]}{[Pn]}.$$

Then, the ratio of saturation of the chemoreceptors is expressed as

$$\phi(n) = \frac{\text{Occupied Receptors}}{\text{Total Receptors}} = \frac{[Pn]}{[P_T]} = \frac{[n]}{K_d + [n]}.$$

This allows us to consider the chemotactic potential $\phi(n)$, and we define the chemotactic sensitivity as $\chi(n) = \phi'(n)$. The dissociation constant K_d has nutrient units, and is the concentration of nutrient needed for half of receptor to be occupied. Moreover, K_d is the nutrient level where the chemotactic sensitivity $\chi(n)$ is maximum.

In the literature, cf. [55,106], this form for the chemotactic sensitivity is known as "receptor's law" and was proposed by Lapidus and Schiller [83],

$$\chi(n) = \frac{\chi_0 K_d}{(K_d + n)^2} \tag{3.2.6}$$

where $\chi_0 > 0$ is a constant that represents the strength of the chemotaxis. The chemotactic response vanishes for large nutrient concentrations due to the saturation of the receptors. This receptor sensitivity law has been derived and applied in several models for chemotaxis [51, 134, 135]. (See [149] for a review on mathematical modeling of bacterial chemotaxis, including a comparison of models that consider different chemotactic sensitivity functions.)

It is to be noted that the dissociation constant K_d for the attractor-receptor molecular interaction has a unique value that depends on the bacterial strain, nutrient type and other in-vitro conditions, and has to be determined experimentally (see [56] for values of K_d on various substrates of *B. subtilis*). We shall use K_d as normalization factor, as we shall see below.

The bacterial response function $\xi = \xi(b)$ is positive for attractive chemotaxis and negative for a repulsive one. In [55] (see also [20]), Ben-Jacob and his group

suggest that, if the bacteria move within a liquid and the colony density is low, then the bacterial response should be proportional to the bacteria concentration times the diffusion, i.e.,

$$|\xi(b)| \propto bD_b. \tag{3.2.7}$$

For the linear (constant) diffusion case the bacterial response function is proportional to the density b, as in the classical Keller-Segel model [76, 77]. When a non-linear diffusion coefficient D_b is considered, the authors suggested that, the chemotactic flux J_c should be changed according to (3.2.7) in order to incorporate the density dependence of the bacterial movement. For example, for the non-linear diffusion $D_b = D_0 b^k$ where D_0 is constant and $k > 0$ is an integer, as considered by Kitzunezaki [80], the adequate response function is $\xi(b) = bD_b = D_0 b^{k+1}$.

3.3 Nutrient chemotaxis

We introduce a suitable nutrient chemotaxis term into system (3.2.1), that is compatible with (3.2.7). Thus, considering the non-linear diffusion (3.2.2) we propose the following attractive chemotactic flux

$$J_c = \sigma n b^2 \chi(n) \nabla n, \tag{3.3.1}$$

where $\chi(n)$ is the receptor law. Subtracting the divergence of J_c to the bacterial density evolution equation we obtain

$$\begin{aligned} n_t &= D_n \Delta n - \kappa n b, \\ b_t &= \nabla \cdot (\sigma n b \nabla b) + \theta \kappa n b - \nabla \cdot \left(\sigma n b^2 \frac{\chi_0 K_d}{(K_d + n)^2} \nabla n \right), \end{aligned} \tag{3.3.2}$$

for $(x, y) \in \Omega, t \geq 0$. Initial conditions are given as

$$n(x, y, 0) = \bar{n}_0, \quad b(x, y, 0) = \bar{b}_0(x, y), \tag{3.3.3}$$

where $\bar{n}_0$ is the uniformly distributed initial constant concentration of nutrient, and $\bar{b}_0$ is a given function that represents the initial inoculum of bacteria. Further, no-flux boundary conditions are imposed on system (3.3.2),

$$\nabla n \cdot \nu = 0, \quad \nabla b \cdot \nu = 0, \quad (x, y) \in \partial\Omega, \tag{3.3.4}$$

where $\nu \in \mathbb{R}^2$, is the unitary outer normal vector to the boundary of the domain.

3.4 Normalization

In order to reduce the number of free parameters in system (3.3.2) we consider the following non-dimensional rescaled variables:

$$\bar{x} = \left(\frac{\theta K_d \kappa}{D_n}\right)^{1/2} x, \quad \bar{y} = \left(\frac{\theta K_d \kappa}{D_n}\right)^{1/2} y, \quad \bar{t} = (\theta K_d \kappa) t,$$

$$\bar{n} = \frac{n}{K_d}, \quad \bar{b} = \frac{b}{\theta K_d}, \quad \bar{\sigma} = \left(\frac{\theta K_d^2}{D_n}\right) \sigma.$$

The partial derivatives change in the following manner

$$\frac{\partial}{\partial t} = (\theta K_d \kappa) \frac{\partial}{\partial \bar{t}}\,, \quad \frac{\partial}{\partial x} = \left(\frac{\theta K_d \kappa}{D_n}\right)^{1/2} \frac{\partial}{\partial \bar{x}}.$$

Then, vector operators change as

$$\nabla_x = \left(\frac{\theta K_d \kappa}{D_n}\right)^{1/2} \nabla_{\bar{x}}, \quad \Delta_x = \left(\frac{\theta K_d \kappa}{D_n}\right) \Delta_{\bar{x}},$$

where the subscripts x and $\bar{x}$ stands for old and new variables, respectively. Upon substitution of the rescaled variables into (3.3.2) we obtain for the nutrient equation

$$\begin{aligned}
(\theta K_d \kappa)(K_d \bar{n})_{\bar{t}} &= \frac{\theta K_d \kappa}{D_n} D_n \Delta_{\bar{x}} (K_d \bar{n}) - \kappa (K_d \bar{n})(\theta K_d \bar{b}) \\
(\theta K_d^2 \kappa) \bar{n}_{\bar{t}} &= (\theta K_d^2 \kappa) \Delta_{\bar{x}} \bar{n} - (\theta K_d^2 \kappa) \bar{n} \bar{b} \\
\bar{n}_{\bar{t}} &= \Delta_{\bar{x}} \bar{n} - \bar{n} \bar{b},
\end{aligned}$$

and for the bacterial density equation

$$\begin{aligned}
&(\theta K_d \kappa)(\theta K_d) \bar{b}_{\bar{t}} = \\
&= \left(\frac{\theta K_d \kappa}{D_n}\right)^{1/2} \nabla_{\bar{x}} \cdot \left(\frac{D_n}{\theta K_d^2} \bar{\sigma} (K_d \bar{n})(\theta K_d \bar{b}) \left(\frac{\theta K_d \kappa}{D_n}\right)^{1/2} \nabla_{\bar{x}} (\theta K_d \bar{b}) \right) \\
&+ \theta \kappa (K_d \bar{n})(\theta K_d \bar{b}) \\
&- \left(\frac{\theta K_d \kappa}{D_n}\right)^{1/2} \nabla_{\bar{x}} \cdot \left(\frac{D_n}{\theta K_d^2} \bar{\sigma} (K_d \bar{n})(\theta K_d \bar{b})^2 \frac{\chi_0 K_d}{(K_d + K_d \bar{n})^2} \left(\frac{\theta K_d \kappa}{D_n}\right)^{1/2} \nabla_{\bar{x}} (K_d \bar{n}) \right),
\end{aligned}$$

which simplifies to

$$\bar{b}_{\bar{t}} = \nabla_{\bar{x}} \cdot \left(\bar{\sigma} \bar{n} \bar{b} \nabla_{\bar{x}} \bar{b} \right) + \bar{n} \bar{b} - \nabla_{\bar{x}} \cdot \left(\bar{\sigma} \bar{n} \bar{b}^2 \frac{\chi_0}{(1+\bar{n})^2} \nabla_{\bar{x}} \bar{n} \right).$$

We drop the bar notation for simplicity and obtain the following rescaled system of equations

$$\begin{aligned} n_t &= \Delta n - nb, \\ b_t &= \nabla \cdot (\sigma nb \nabla b) + nb - \chi_0 \nabla \cdot \left(\frac{\sigma nb^2}{(1+n)^2} \nabla n \right), \end{aligned} \tag{3.4.1}$$

where $\sigma = \sigma_0(1 + \Delta)$, and Δ is the stochastic fluctuation, drawn from a triangular distribution with support in $[-1, 1]$ (see Section 3.5.3 below) . The initial conditions are

$$\begin{aligned} n(x, y, 0) &= \hat{n}_0/K_d \equiv n_0, \\ b(x, y, 0) &= \hat{b}_0/(\theta K_d) \equiv b_0(x, y), \end{aligned} \tag{3.4.2}$$

for $(x, y) \in \Omega$. We impose the no-flux boundary conditions on the rescaled variables

$$\nabla n \cdot \nu = 0, \quad \nabla b \cdot \nu = 0, \quad (x, y) \in \partial\Omega. \tag{3.4.3}$$

For the rescaled system (3.4.1) the free parameters are $\sigma_0 > 0$, that represents the hardness of the agar, $n_0 > 0$ measures the initial nutrient concentration, and $\chi_0 \geq 0$, is the chemotactic signal strength. The stochastic

3.5 Numerical Simulations

In order to explore the qualitative effects of the chemotactic signal in the colony patterns, we performed several numerical simulations of system (3.4.1) for various values of the free parameters. We implemented a explicit second order Runge-Kutta and finite differences numerical scheme using the NVIDIA CUDA libraries for the C/C++ programming language. CUDA is a general purpose parallel computing platform that is designed to run in the Graphic Processing Units (GPUs) compute architecture [79]. The GPUs are well-suited to address problems that can be expressed as data-parallel computations, the same program (finite differences) is executed on many data elements (grid points) at once [109]. This programming model is known as simple program/multiple data (SPMD). The parallel programming model allowed us to process large data sets, and thus we overcome the inconvenience of small time steps required by explicit numerical schemes for solving stiff equations. In this fashion, we speeded up the computations and made thousand of iterations in a couple of hours. Our numerical simulations were performed on a NVIDIA Tesla© C2070 graphics card with 448 CUDA cores.

In the following section we describe the numerical scheme for which we considered a square of side $L = 680$ as the spatial domain. We selected a square lattice mesh of $N = 2048$ points per side, i.e., a mesh containing more than 4 million points (see discussion below on Section 3.5.3). Therefore, the used grid width was

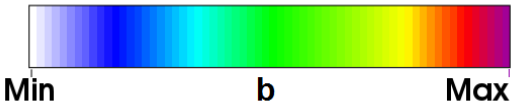

Figure 3.2: The bacteria density scale used for plotting solutions.

$\Delta x = \Delta y = L/N \approx 0.3320$. We considered two values for the time step depending on the value of σ_0. For $\sigma_0 = 1$, we used $\Delta t = 0.0231$, and for $\sigma_0 = 4$, we used $\Delta t = 0.0110$. Although we did not include a proper stability analysis, we observed that the numerical scheme was not susceptible to the round-off errors induced by the discretization for the values of Δt that we considered.

The visualization of the results was made with Paraview© [3]. Simulations data are plotted as a 3-D surface, this means that bacteria density is the height (positive z-axis) plotted over the mesh points(x-y plane), and the view is of the positive z-axis pointing outward of the paper. The colonies are colored according to the bacterial density level. Figure 3.2 shows the scale of the color map used for all numerical simulations, where purple is the maximum and white is the minimum of the bacterial density. For all simulations, the minimum is zero, but in each case, the maximum varies.

For the sake of comparison, following reference [73], we took the initial conditions as $n_0 = 0.71$ and 1.07, for the initial uniformly distributed nutrient level. For the bacteria we took the initial inoculum

$$b_0(x, y) = b_M e^{-(x^2+y^2)/6.25},$$

where $b_M = 0.71$ is the maximum density at the center of the domain. For a summary of the values of the free parameters used in the numerical simulations see Table 3.1.

We remark that for the chemotaxis strength χ_0 we included the value $\chi_0 = 0$, this means that we solved the original system (3.2.1) (in its normalized version). As the reader may see below (see Section 3.6), we compare the simulations of system (3.4.1) when the chemotactic signal is present to those without chemotaxis, and confirm that the colony speed of propagation is enhanced by the nutrient chemotaxis as predicted by asymptotic calculations.

3.5.1 Numerical scheme

In the implementation of the finite difference for discretizing space, and of the second order Runge-Kutta numerical scheme for the resulting ODE system we discretized system (3.4.1). To proceed so, let us write the system (3.4.1) in the

Description	Symbol	Values
Initial condition for the nutrient	n_0	1.07, 0.71
Agar softness	σ_0	1.0, 4.0
Chemotactic signal strength	χ_0	0, 2.5, 5.0, 7.5, 10.0

Table 3.1: Free parameter values used during the numerical simulations.

following explicit form

$$\begin{aligned} n_t &= \Delta n - nb, \\ b_t &= \sigma\left(nb\Delta b + n|\nabla b|^2 + b\nabla b\cdot\nabla n\right) + nb \\ &\quad - \frac{\chi_0\sigma}{(1+n)^2}\left(nb^2\Delta n + 2nb\nabla b\cdot\nabla n + b^2\left(1-\frac{2n}{1+n}\right)|\nabla n|^2\right). \end{aligned} \tag{3.5.1}$$

Let Δx, Δy denote the spatial step increments, and Δt the time step. We made the numerical computations in the domain

$$\{(x,y,t) : 0 \le x, y \le L, t \ge 0\},$$

which we discretized considering a regular squared grid, that is defined by the discrete point set

$$\{(i\Delta x, j\Delta y, k\Delta t) : i, j = 0, \ldots, N, k \ge 0\}.$$

In all our computations we took $\Delta x = \Delta y = L/N$, where $N = 2048$.

We considered approximations to the derivatives using central finite differences for the spatial derivatives and forward differences for the temporal derivative [69]. Thus, for the first order spatial derivatives of the bacteria density we have

$$\begin{aligned} \frac{\partial b}{\partial x}(x,y,t) &= \frac{1}{2\Delta x}(b(x+\Delta x,y,t) - b(x-\Delta x,y,t)) + O((\Delta x)^2), \\ \frac{\partial b}{\partial y}(x,y,t) &= \frac{1}{2\Delta y}(b(x,y+\Delta y,t) - b(x,y-\Delta y,t_k)) + O((\Delta y)^2). \end{aligned} \tag{3.5.2}$$

And for the second order derivatives we have

$$\begin{aligned} \frac{\partial^2 b(x,y,t)}{\partial x^2} &= \frac{1}{(\Delta x)^2}(b(x+\Delta x,y,t) - 2b(x,y,t) + b(x-\Delta x,y,t)) + O((\Delta x)^2), \\ \frac{\partial^2 b(x,y,t)}{\partial x^2} &= \frac{1}{(\Delta y)^2}(b(x,y+\Delta y,t) - 2b(x,y,t) + b(x,y-\Delta y,t)) + O((\Delta y)^2). \end{aligned} \tag{3.5.3}$$

Therefore, for the laplacian operator we have the approximation known as the five point stencil

$$\begin{aligned}\Delta b(x,y,t) &= \frac{\partial^2 b(x,y,t)}{\partial x^2} + \frac{\partial^2 b(x,y,t)}{\partial x^2} \\ &\simeq \frac{b(x+\Delta x,y,t) - 2b(x,y,t) + b(x-\Delta x,y,t)}{(\Delta x)^2} \\ &+ \frac{b(x,y+\Delta y,t) - 2b(x,y,t) + b(x,y-\Delta y,t)}{(\Delta y)^2}.\end{aligned} \tag{3.5.4}$$

For the temporal derivative we have the approximation,

$$\frac{\partial b}{\partial t}(x,y,t) = \frac{1}{\Delta t}\left(b(x,y,t+\Delta t) - b(x,y,t)\right) + O(\Delta t). \tag{3.5.5}$$

Similar approximations hold for the first and second order derivatives of the nutrient concentration $n(x,y,t)$.

We denote an approximation to the bacterial and nutrient densities, $b(x_i,y_j,t_k)$ and $n(x_i,y_j,t_k)$, at the mesh points $(x_i,y_j,t_k) = (i\Delta x, j\Delta y, k\Delta t)$ by

$$b^k_{i,j} \simeq b(x_i,y_j,t_k), \quad n^k_{i,j} \simeq n(x_i,y_j,t_k).$$

Note that the superscript denotes the time step.

Let $h = \Delta x = \Delta y$, denote the regular spatial spacing in both space coordinates. Substituting the approximations of the derivatives, (3.5.2) and (3.5.4), at the grid points in the vector differential operators for the bacterial density we have:

$$\Delta b^k_{i,j} = \frac{\left(b^k_{i+1,j} + b^k_{i-1,j} + b^k_{i,j+1} + b^k_{i,j-1} - 4b^k_{i,j}\right)}{h^2}, \tag{3.5.6}$$

$$|\nabla b^k_{i,j}|^2 = \left(\frac{b^k_{i+1,j} - b^k_{i-1,j}}{2h}\right)^2 + \left(\frac{b^k_{i,j+1} - b^k_{i,j-1}}{2h}\right)^2, \tag{3.5.7}$$

similar approximations hold for $n^k_{i,j}$. For the inner product $\nabla b \cdot \nabla n$ we have

$$\begin{aligned}\nabla b^k_{i,j} \cdot \nabla n^k_{i,j} = &\left(\frac{b^k_{i+1,j} - b^k_{i-1,j}}{2h}\right)\left(\frac{n^k_{i+1,j} - n^k_{i-1,j}}{2h}\right) + \\ &+ \left(\frac{b^k_{i,j+1} - b^k_{i,j-1}}{2h}\right)\left(\frac{n^k_{i,j+1} - n^k_{i,j-1}}{2h}\right).\end{aligned} \tag{3.5.8}$$

For notational convenience, we define the right-hand side of (3.5.1) as the functions

$$\begin{aligned}F(b,n) &:= \Delta n - nb, \\ G(b,n) &:= \sigma\left(nb\Delta b + n|\nabla b|^2 + b\nabla b \cdot \nabla n\right) + nb \\ &\quad - \frac{\chi_0 \sigma}{(1+n)^2}\left(nb^2\Delta n + 2nb\nabla b \cdot \nabla n + b^2\left(1 - \frac{2n}{1+n}\right)|\nabla n|^2\right).\end{aligned}$$

Therefore, using expression (3.5.6) for $n_{i,j}^k$ we obtain

$$F(b_{i,j}^k, n_{i,j}^k) = \Delta n_{i,j}^k - n_{i,j}^k b_{i,j}^k. \tag{3.5.9}$$

The expression for G is long, so we divide it in two pieces

$$G(b,n) = G_{r-d}(b,n) + G_{chem}(b,n),$$

where

$$\begin{aligned} G_{r-d}(b,n) &= \sigma\left(nb\Delta b + n|\nabla b|^2 + b\nabla b\cdot\nabla n\right) + nb, \\ G_{chem}(b,n) &= -\frac{\chi_0\sigma}{(1+n)^2}\left(nb^2\Delta n + 2nb\nabla b\cdot\nabla n + b^2\left(1-\frac{2n}{1+n}\right)|\nabla n|^2\right). \end{aligned}$$

Hence, substituting the approximation of the derivatives, (3.5.6), (3.5.7) and (3.5.8), we have

$$G_{r-d}(b_{i,j}^k, n_{i,j}^k) = \sigma\left(n_{i,j}^k b_{i,j}^k \Delta b_{i,j}^k + n_{i,j}^k|\nabla b_{i,j}^k|^2 + b_{i,j}^k \nabla b_{i,j}^k\cdot\nabla n_{i,j}^k\right) + b_{i,j}^k n_{i,j}^k, \tag{3.5.10}$$

$$\begin{aligned} G_{chem}(b_{i,j}^k, n_{i,j}^k) = -\frac{\chi_0\sigma}{(1+n_{i,j}^k)^2}\Bigg(& n_{i,j}^k (b_{i,j}^k)^2 \Delta n_{i,j}^k + 2n_{i,j}^k b_{i,j}^k \nabla b_{i,j}^k\cdot\nabla n_{i,j}^k \\ &+ (b_{i,j}^k)^2\left(1-\frac{2n_{i,j}^k}{1+n_{i,j}^k}\right)|\nabla n_{i,j}^k|^2\Bigg), \end{aligned} \tag{3.5.11}$$

and hence

$$G(b_{i,j}^k, n_{i,j}^k) = G_{r-d}(b_{i,j}^k, n_{i,j}^k) + G_{chem}(b_{i,j}^k, n_{i,j}^k). \tag{3.5.12}$$

For the temporal derivative, we use the forward approximation (3.5.5) that, when considered at the mesh points, has the following form

$$\frac{\partial b_{i,j}^k}{\partial t} = \frac{b_{i,j}^{k+1} - b_{i,j}^k}{\Delta t}, \quad \frac{\partial n_{i,j}^k}{\partial t} = \frac{n_{i,j}^{k+1} - n_{i,j}^k}{\Delta t}.$$

Hence, substituting the previous approximation into system (3.5.1) and considering the expressions for the right-hand sides, (3.5.9) and (3.5.12), yields the Euler method

$$\begin{aligned} n_{i,j}^{k+1} &= n_{i,j}^k + \Delta t F(b_{i,j}^k, n_{i,j}^k), \\ b_{i,j}^{k+1} &= b_{i,j}^k + \Delta t G(b_{i,j}^k, n_{i,j}^k). \end{aligned}$$

Using the Euler method, we implemented a second order Runge-Kutta method of two-stages. The first stage considers the Euler method with half time step,

$$\begin{aligned} n_{i,j}^{k+1/2} &= n_{i,j}^k + \frac{\Delta t}{2} F(b_{i,j}^k, n_{i,j}^k), \\ b_{i,j}^{k+1/2} &= b_{i,j}^k + \frac{\Delta t}{2} G(b_{i,j}^k, n_{i,j}^k), \end{aligned} \tag{3.5.13}$$

and the second stage consists of the Euler method with full time step, but the right-hand sides are evaluated at the previous "halfway" approximations of the first stage, namely

$$\begin{aligned} n_{i,j}^{k+1} &= n_{i,j}^{k} + \Delta t F(b_{i,j}^{k+1/2}, n_{i,j}^{k+1/2}), \\ b_{i,j}^{k+1} &= b_{i,j}^{k} + \Delta t G(b_{i,j}^{k+1/2}, n_{i,j}^{k+1/2}). \end{aligned} \tag{3.5.14}$$

The numerical scheme (3.5.13)-(3.5.14) is defined for $k \geq 0$, $i, j = 1, ..., N-1$. For the points at the boundaries, we apply the no-flux boundary conditions (3.4.3).

We supplement the initial conditions (3.4.2), discretized according to the grid points

$$n_{i,j}^{0} = n(x_i, y_j, 0) = n_0, \quad b_{i,j}^{0} = b_0(x_j, y_j).$$

3.5.2 Parallelization and boundary conditions

Graphics Processing Units (GPUs) are parts of a computer that produce high quality graphics, providing accelerations on 2D and 3D images and light transforms. Since the year 2000, GPUs allow to apply arithmetic operations simultaneously on pixels using stream multiprocessors (SMs). Later applications of this operations to other data resulted in the development of general purpose graphics processing unit (GPGPU) computing. CUDA was first proposed in 2007 by NVIDIA to unify the GPGPU programming model on their own video cards, but other programming models on GPUs have been proposed such as OpenCL and OpenACC.

Typically processing units on GPUs are simpler and slower if compared with traditional CPUs. It is the number of cores in SM that provides a graphics card more computational power; a GPU can have over 100 times more cores that a CPU. GPUs are designed to deliver maximum throughput and are very efficient at performing repetitive tasks in which only data change. In this sense, the parallelism model offered by GPUs consists of executing a single program on many data elements. This programming model is known as simple program/multiple data (SPMD), and in CUDA consists in that all cores execute the same instructions with different data. In our case, it is the finite differences scheme applied to the different grid points.

On the other hand, the architecture of GPUs includes different types of memory that are located physically at different places, for instance on-board and on-chip. Moreover, the CUDA programming platform is designed to launch the programs from a host (CPU) and run on separated device (GPU), maintaining their memories separated. For this reason, CUDA programming is focused to minimize the data transfer between host and device, since these operations are significantly time consuming.

CUDA model offers different types of memory, being the global, shared and texture the most commonly used in practice. In the implementation of finite

differences scheme we used a combination of both global and texture memories.

Global memory is the most used since it can be accessed by all SMs. It is the largest of all types, being measured in Gigabytes, but it is also the slowest. The texture memory has important features over the other types of memory from which we benefited in the coding of the numerical scheme.

We took advantage of the spatial locality feature of texture memory (data can be handled in 2D arrays), in contrast with global memory which only access data as a 1D array. In this way, the coding of the local interactions of the finite differences was more transparent.

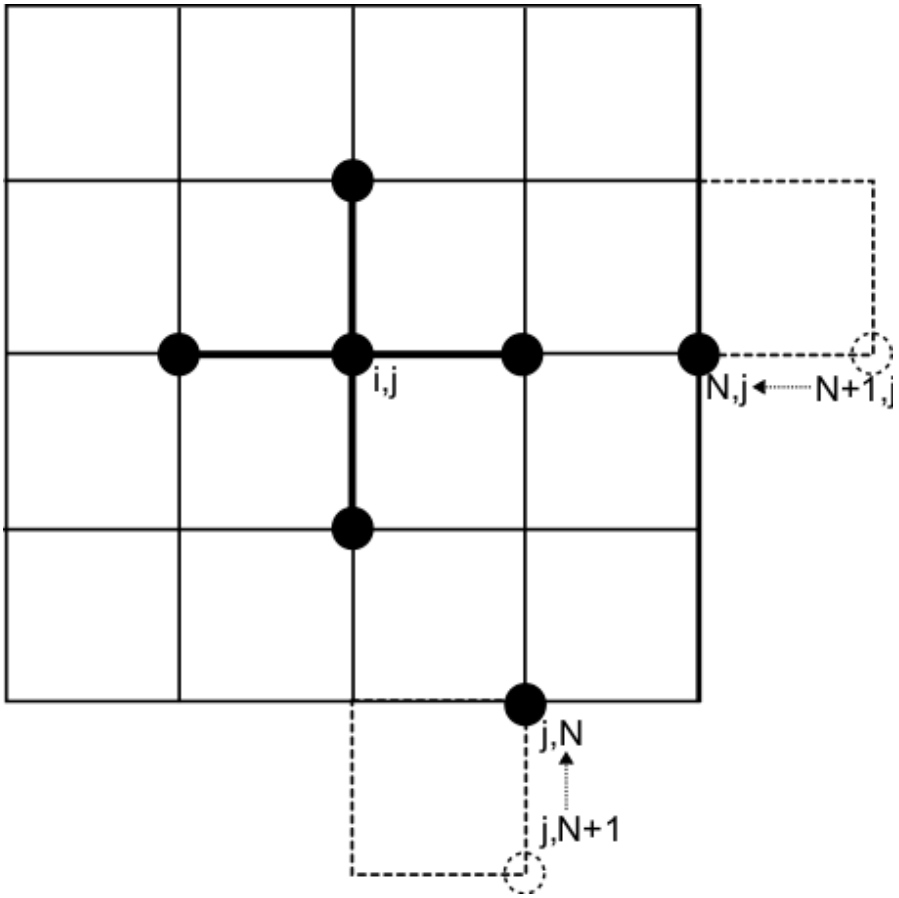

Figure 3.3: Graphical representation of the spatial locality of finite differences interactions. Example of texture memory clamping on the boundaries.

The most important capability of texture memory that we benefited from is the address mode: it describes the behavior of out-of-range data fetching. In particular, we used the *cudaAddressModeClamp* [110], which specifies that an out-

of-bounds coordinates are replaced with the closest boundary. In the context of finite differences method this is equivalent to automatically impose no-flux boundary conditions with no further coding. For example, consider the approximation of the nutrient density at right boundary, this is $n^k_{N,j} = n(N\Delta x, j\Delta y, k\Delta t)$, for $0 \leq j \leq N$ and $k \geq 0$. The discrete no-flux boundary condition at the right boundary considering a forward approximation for the derivative is

$$\frac{n^k_{N+1,j} - n^k_{N,j}}{\Delta x} = 0.$$

Thus we have the condition at the right boundary $n^k_{N+1,j} = n^k_{N,j}$. Similar conditions hold for the other boundaries, using the appropriate shifted derivative approximations, for both bacterial and nutrient densities. (See Figure 3.3.)

3.5.3 A note on the grid size, symmetry and random fluctuations

It has been suggested that numerical simulations might depend on the grid size [100]. Presumably, it is necessary to consider high spatial resolutions to correctly display the finer structures present in the solutions, e.g., authors in [73] used a grid size of 1600×1600 in their simulations. To avoid this possibility, we performed simulations with parameter values $\sigma_0 = 1$, $n_0 = 0.71$ and $\chi_0 = 5$, for the following grid size: 1024×1024, 2048×2048, 4096×4096 and 8192×8192. The results are depicted in Fig. 3.4.

Notice that for the grid size 1024×1024 (Fig. 3.4(a)) solutions have a cross shape with a rhomboid envelope, resembling DLA clusters in discrete growth models [96]. When grid size is increased to 2048×2048 (Fig. 3.4(b)), we observe drastic morphology changes. Solutions exhibit a more dense branching morphology, with radially oriented ramifications having a round envelope. For the bigger grid size of 4096×4096, these morphological features are kept by solutions, as can be observed in Figs. 3.4(c). (We must point that the results for the grid size 8192×8192 are not shown here, due to technical limitations. It can be seen in Fig. 4(d), page 5653 of reference [86].) Therefore, since there is no major morphological changes between higher grid sizes and 2048×2048, we select this last one as the grid size for all the numerical simulation that we performed.

On the other hand, models that reproduce fingering patterns are susceptible to anisotropy, including continuous [20, 80] and discrete [96, 103]. The underlying square lattice imposes an artificial anisotropy to growth patterns, giving rise to symmetries in the numerical solutions. However, these might not be a feature of the model.

One way to reduce induced symmetries is to consider random lattices [80]. In our setting, we introduced a random fluctuation into the diffusion coefficient

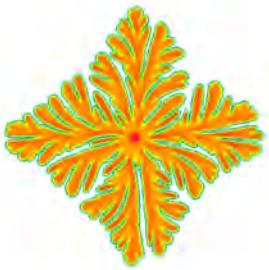

(a) 1024×1024

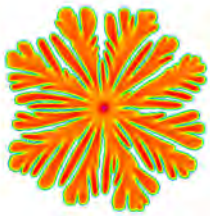

(b) 2048×2048

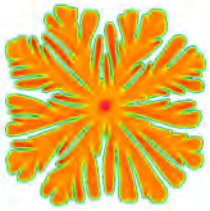

(c) 4096×4096

Figure 3.4: Simulations of system (3.4.1), with parameter values $\sigma_0 = 1, n_0 = 0.71$ and $\chi_0 = 5$, under random fluctuation for the diffusion coefficient for different grid sizes. Symmetries shown in the patterns are due to the implicit anisotropy of the grid.

of bacteria, relying on the fact that bacteria move performing biased random walks. This alternative was also considered by authors in [73]. Hence, the diffusion coefficient for bacteria σ is perturbed from the mean σ_0 through a stochastic fluctuation Δ,

$$\sigma = \sigma_0(1 + \Delta),$$

where σ_0 is the agar softness. The stochastic fluctuation was applied to the diffusion coefficient on every grid point, at every time step.

We used the inversion method [38] to generate Δ as random variable with a

triangular distribution with support in $[-1, 1]$, defined in the following form:

$$\Delta = \begin{cases} \sqrt{2u} - 1, & 0 \leq u < 1/2, \\ 1 - \sqrt{2(1-u)}, & 1/2 \leq u < 1, \end{cases}$$

where u is a uniform $[0, 1]$ random variable. The variable u was generated using a pseudo-random number generator from the CUDA CURAND library, which is optimize to produce highly independent pseudo-random numbers in parallel computations.

The introduction of the random perturbation Δ serves as a way to consider a more realistic model, but is not enough to prevent symmetries in the patterns. Figure 3.5 shows a highly symmetric pattern, less branched (compare with Fig. 3.4(b)) as the result of simulation of system (3.4.1) without the random fluctuation, i.e., $\Delta = 0$.

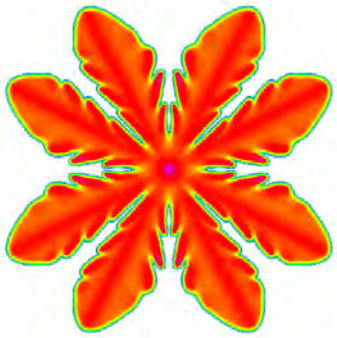

Figure 3.5: Simulations of system (3.4.1), with parameter values $n_0 = 0.71$ and $\chi_0 = 5$, in the absence of random fluctuations for the diffusion coefficient ($\sigma = \sigma_0 = 1$) on a grid of size 2048×2048. The reader may observe a higher degree of symmetry due to the implicit anisotropy of the grid.

In the following section we present and discuss the results of the numerical simulations.

3.6 Results

We present the results of the numerical simulations of system (3.4.1) with initial conditions (3.4.2) and subject to boundary conditions (3.4.3).

We consider two regimes in the agar softness parameter σ_0 value, namely, semi-solid agar that corresponds to $\sigma_0 = 1$, and soft agar that corresponds to the value $\sigma_0 = 4$. The morphology of the reproducible patterns correspond to regions D and E in the morphology diagram, and the transition region between theses (see the region enclosed by rectangle in Fig. 3.1). Solutions to the bacterial density b are shown in Figs. 3.6 through 3.10. Each figure has two columns and four rows. The rows represent different time steps and each column is associated to a value of the chemotaxis strength parameter χ_0.

We remark that the main qualitative effect of the chemotactic term of the bacterial patterns is the enhancement of the growth speed of the outer envelope, as expected from the asymptotic estimations of the speed (see Chapter 4).

3.6.1 Semi-solid agar

This case corresponds to the parameter value $\sigma_0 = 1$. The agar concentration is intermediate and the diffusion of bacteria is limited. The morphological features are from dense branching morphology patterns pertaining to region E of the morphological diagram (Fig. 3.1).

Fig. 3.6 shows the time evolution of ramified patterns for the initial nutrient level $n_0 = 0.71$. On the left column it is shown the time evolution in the case without chemotaxis, i.e., $\chi_0 = 0$. This case corresponds to the original model by Kawasaki *et al.*, and the observed patterns are comparable to those of the authors (see Fig 3 (b) in Ref. [73]). To be more precise, for the case $\chi = 0$ we solved the original system of [73], but due to the random fluctuation included in the diffusion coefficient, the patterns we obtained have the same qualitative features to those in [73] but are not totally equal. On the right column we observe the case where the chemotaxis sensitivity is $\chi_0 = 5$. The morphology is similar in both cases, ramified patterns with radially aligned branches. Taking a closer look, we can see that the number of branches is consistent. In both cases, with and without chemotaxis, the number of branches is of the same order. We remark that there is an increase in the growth speed of the outer envelope of the branches when the chemotaxis signal is present.

The results of the numerics for the nutrient level $n_0 = 1.07$ are shown in Fig. 3.7 . Once again, left column displays the pattern evolution for the case without chemotaxis, $\chi_0 = 0$. At the center of the colony there is a peak of bacterial concentration, shown by dark purple dot that according to the coloring scale in Fig. 3.2 corresponds to the maximum of the bacterial density. This is so, because

at early times bacteria deplete the nutrient at the inoculum site. This is a feature of the model, as mentioned before, bacteria move around actively when both n or b are high. Meanwhile, bacteria at the interior of the colony become stationary because the nutrient is depleted. This behavior allows the leading branches at the front of the colony to search for higher concentrations of food, while, inner bacteria have its movement limited by the lowered nutrient concentration. Then, every branch tip at the front is immersed in similar environmental conditions, favoring the evenly expansion of colony by which a round envelope is developed.

In the right column of Fig. 3.7 are depicted patterns corresponding to case with chemotaxis strength $\chi_0 = 5$. It can be observed that chemotaxis provides an outward drift to the movement of bacteria, increasing the speed of propagation of the envelope, as discussed in [55]. Comparing Fig. 3.7(h) with Fig. 3.7(g) we observe that when the chemotaxis signal is present the pattern has a more ramified structure with almost a size twice as large.

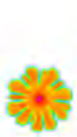

(a) $\chi_0 = 0$, $t = 694.5$

(b) $\chi_0 = 5$, $t = 694.5$

(c) $\chi_0 = 0$, $t = 1389.0$

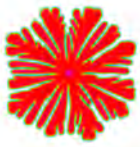

(d) $\chi_0 = 5$, $t = 1389.0$

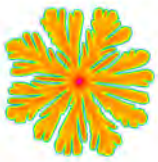

(e) $\chi_0 = 0$, $t = 2083.5$

(f) $\chi_0 = 5$, $t = 2083.5$

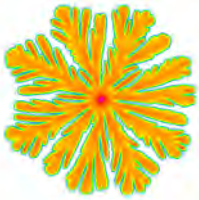

(g) $\chi_0 = 0$, $t = 2824.0$

(h) $\chi_0 = 5$, $t = 2824.0$

Figure 3.6: Colony growth snapshots as a result of simulations of system (3.4.1), taking $\sigma_0 = 1.0, n_0 = 0.71$, with chemotaxis sensitivity $\chi_0 = 0$ (no chemotaxis - left), and $\chi_0 = 5.0$ (right), at different running times (values of t). The four-fold symmetry of the branching patterns is due to an inherent anisotropy due to the square lattice.

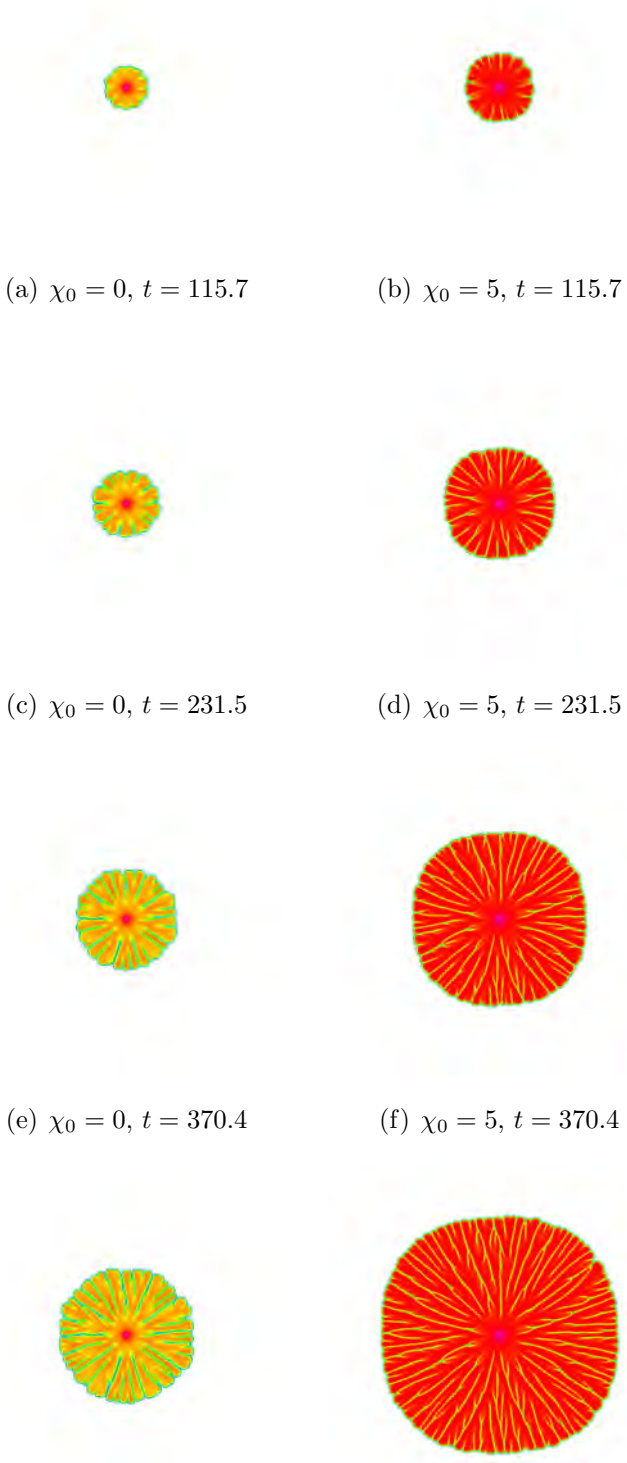

(a) $\chi_0 = 0$, $t = 115.7$ (b) $\chi_0 = 5$, $t = 115.7$

(c) $\chi_0 = 0$, $t = 231.5$ (d) $\chi_0 = 5$, $t = 231.5$

(e) $\chi_0 = 0$, $t = 370.4$ (f) $\chi_0 = 5$, $t = 370.4$

(g) $\chi_0 = 0$, $t = 509.3$ (h) $\chi_0 = 5$, $t = 509.3$

Figure 3.7: Colony growth snapshots as a result of simulations of system (3.4.1), taking $\sigma_0 = 1.0, n_0 = 1.07$, with chemotaxis sensitivity $\chi_0 = 0$ (no chemotaxis - left), and $\chi_0 = 5.0$ (right), at different running times (values of t).

3.6.2 Soft agar

We set the value of parameter $\sigma_0 = 4$. Recall that the agar hardness decreases as the value of the parameter σ_0 increases. Hence, the diffusion of the bacteria is increased in this case. The reproducible patterns belong to region D of homogeneous circular colonies for high enough initial nutrient level, but for lower levels patterns fall into DBM-like region E of the morphological diagram.

The results for $n_0 = 0.71$ are shown in Figs. 3.8 and 3.9. In this case the comparison is made through the two figures, where the initial nutrient level is fixed and we took the values $\chi_0 = 0, 2.5, 5$ and 7.5 for the chemotaxis sensitivity. Left column of Fig. 3.8 shows the case without chemotaxis. It can be observed that the colony has thick radially oriented branches with round envelope. On the right column of Fig. 3.8 the colony growth, for $\chi_0 = 2.5$, is shown. Comparing both columns of Fig. 3.8, we observe that the patterns exhibit similar morphologies, but as expected the growth speed is increased when the chemotactic signal is present (compare Figs. 3.8(g) and 3.8(h)). In addition to the greater propagation speed of the envelope, we observe morphological changes for higher values of χ_0. Presumably, at higher values of χ_0, the enhanced mobility of bacteria at the front, due to a stronger chemotactic signal, makes thin branches start to fuse (slower tips catch up faster ones) (Fig. 3.9(g)). Eventually, patterns show no more branches and become homogeneous disks (Fig. 3.9(h)). In other words, bacteria at the front move faster, allowing them to close the dips that form at the front due to the diffusing instability of the nutrient field. Hence, the results of Figs. 3.8 and 3.9 suggest that the underlying mechanism responsible for transitions between patterns in region E and D, is the suppressing effect of the chemotaxis on the onset of the diffusing instability (as discussed on [15]). Therefore, the effect of increasing the chemotaxis strength is the homogenization of patterns and the expected increased velocity of propagation of the envelope. At $\chi_0 = 7.5$ colony has almost doubled its size (compare Figs. 3.8(h) and 3.9(h)). Finally, in Fig. 3.10 are depicted the results for the nutrient level $n_0 = 1.07$, and chemotaxis sensitivities $\chi_0 = 0$ and $\chi_0 = 7.5$. The observable patterns are homogeneous disks belonging to region D of the morphological diagram. Left column shows the case when there is no chemotaxis signal, and it can be observed the evolution of an homogeneous disk with a peak concentration at the center of the colony (dark purple dot). In the right column, it is observed the increase of the speed of propagation of the envelope due to the chemotaxis signal with strength $\chi_0 = 7.5$. The pattern is an homogeneous disk with a small depression at the center, shown as a red spot which according to the coloring scale (Fig. 3.2) is a lower than the maximum (dark purple) bacterial density. This last feature presumably is due to the enhanced mobility of bacteria, that allows them to leave the center before the nutrient is depleted. In this case, we observe an increased envelope velocity with no significant morphology change.

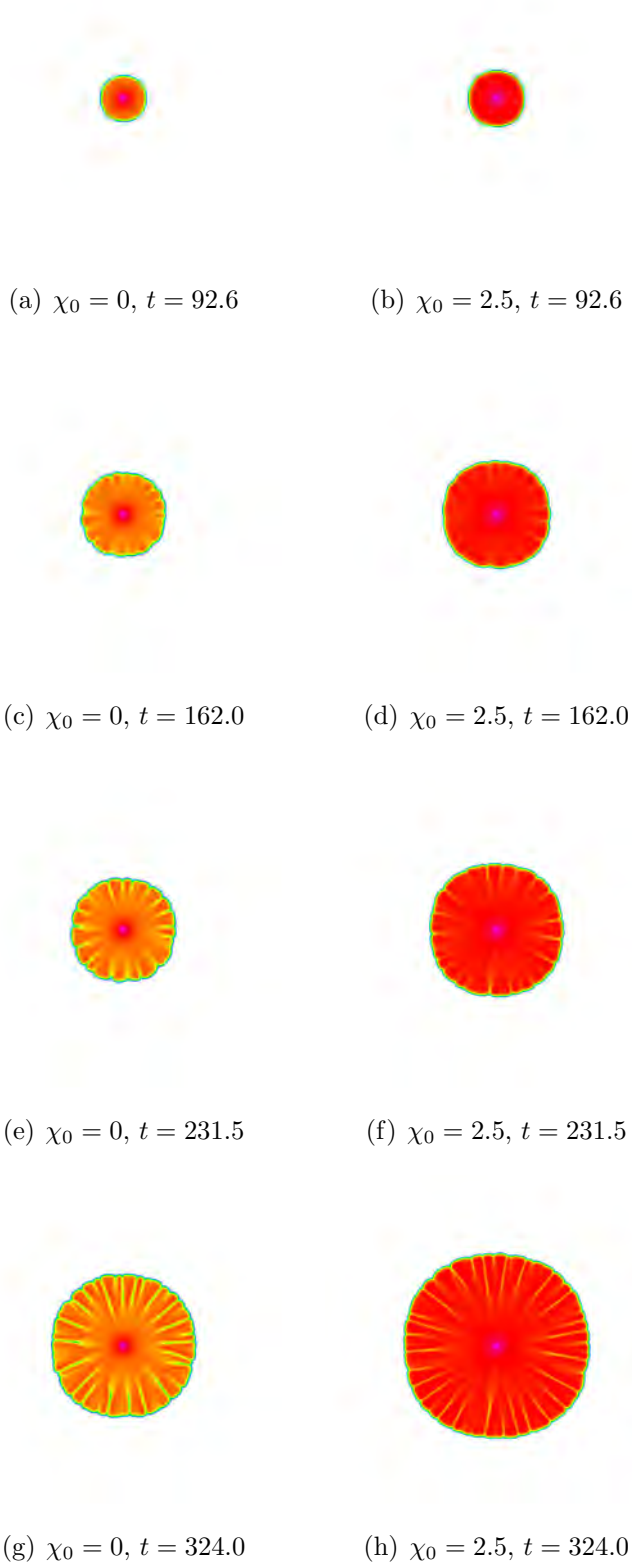

(a) $\chi_0 = 0$, $t = 92.6$ (b) $\chi_0 = 2.5$, $t = 92.6$

(c) $\chi_0 = 0$, $t = 162.0$ (d) $\chi_0 = 2.5$, $t = 162.0$

(e) $\chi_0 = 0$, $t = 231.5$ (f) $\chi_0 = 2.5$, $t = 231.5$

(g) $\chi_0 = 0$, $t = 324.0$ (h) $\chi_0 = 2.5$, $t = 324.0$

Figure 3.8: Colony growth snapshots as a result of simulations of system (3.4.1), taking $\sigma_0 = 4.0, n_0 = 0.71$, with chemotaxis sensitivity $\chi_0 = 0$ (left) and $\chi_0 = 2.5$ (right), at different running times (values of t).

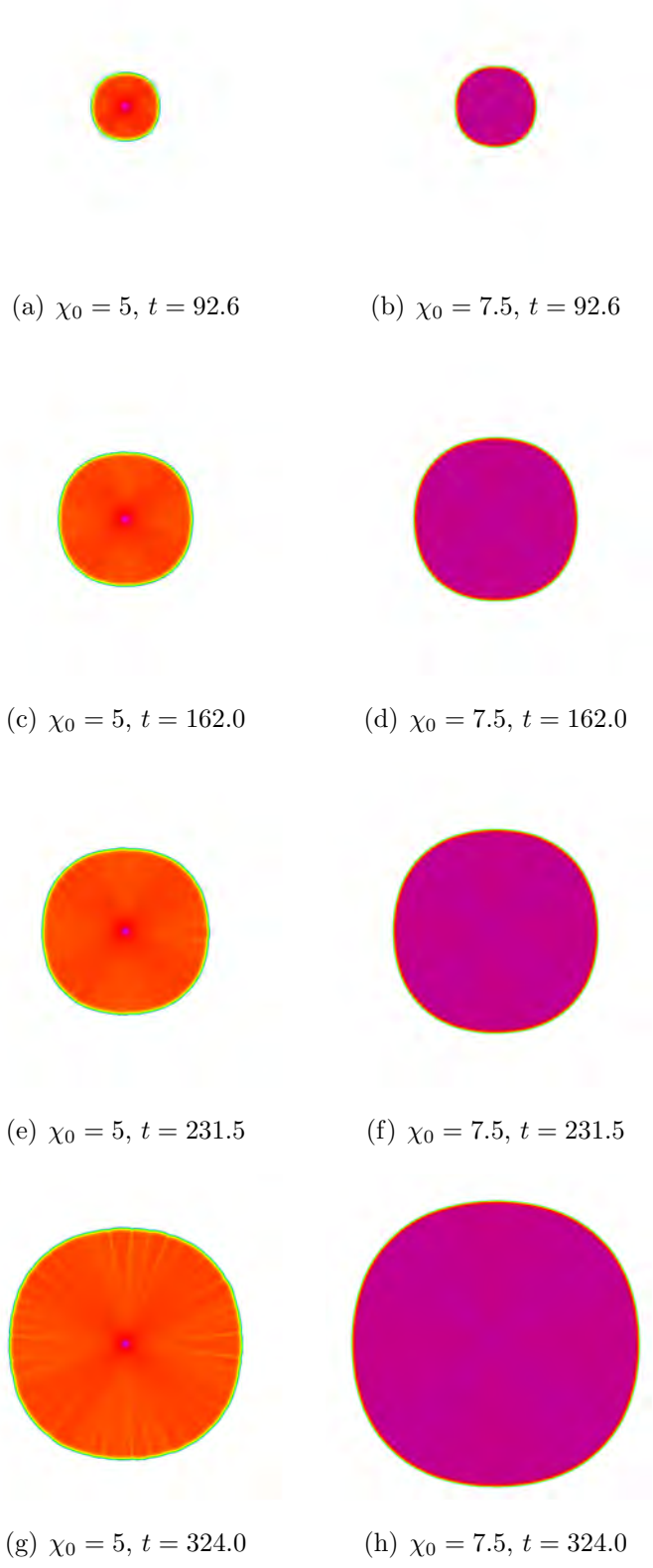

(a) $\chi_0 = 5$, $t = 92.6$ (b) $\chi_0 = 7.5$, $t = 92.6$

(c) $\chi_0 = 5$, $t = 162.0$ (d) $\chi_0 = 7.5$, $t = 162.0$

(e) $\chi_0 = 5$, $t = 231.5$ (f) $\chi_0 = 7.5$, $t = 231.5$

(g) $\chi_0 = 5$, $t = 324.0$ (h) $\chi_0 = 7.5$, $t = 324.0$

Figure 3.9: Colony growth snapshots as a result of simulations of system (3.4.1), taking $\sigma_0 = 4.0, n_0 = 0.71$, with chemotaxis sensitivity $\chi_0 = 5.0$ (left) and $\chi_0 = 7.5$ (right), at different running times (values of t).

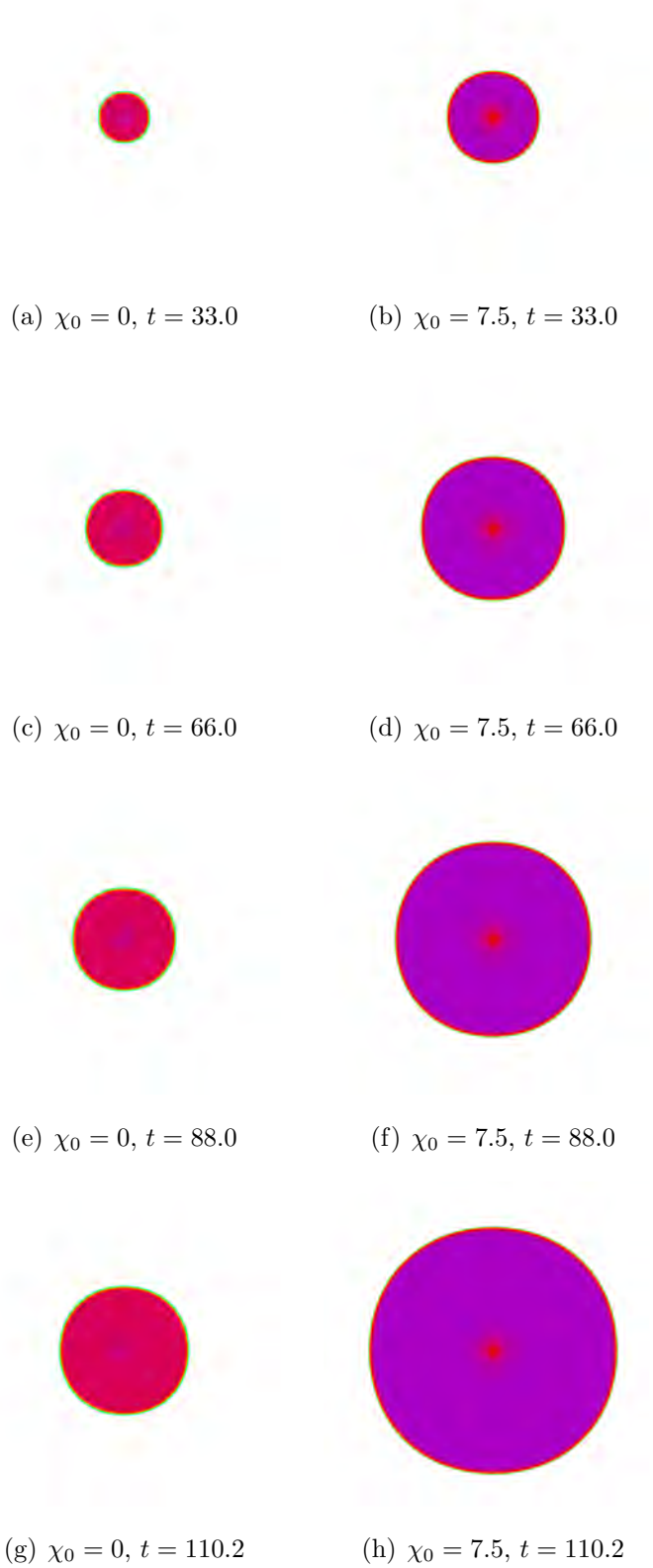

(a) $\chi_0 = 0$, $t = 33.0$ (b) $\chi_0 = 7.5$, $t = 33.0$

(c) $\chi_0 = 0$, $t = 66.0$ (d) $\chi_0 = 7.5$, $t = 66.0$

(e) $\chi_0 = 0$, $t = 88.0$ (f) $\chi_0 = 7.5$, $t = 88.0$

(g) $\chi_0 = 0$, $t = 110.2$ (h) $\chi_0 = 7.5$, $t = 110.2$

Figure 3.10: Colony growth snapshots as a result of simulations of system (3.4.1), taking $\sigma_0 = 4.0, n_0 = 1.07$, with chemotaxis sensitivity $\chi_0 = 0$ (left) and $\chi_0 = 7.5$ (right), at different running times (values of t).

3.7 Discussion

The bacterial aggregation patterns have interested many researchers from various fields such as biology, chemistry, physics and mathematics.

In particular, the morphological diversity shown by the bacterium *B. subtilis* [94, 111], summarized in the morphological diagram (see Fig. 3.1), has motivated many models, including continuous deterministic [73, 80, 100, 132, 159] and discrete ones [23], to explain the growth patterns that have been classified in five distinct types (regions A to E in the morphological diagram).

The models reproduce parts of the morphological diagram depending on the phenomenological assumptions made to include the key features involved in the development of patterns. Two of the biological features may be the reproduction and the motility of bacteria. During in-vitro experiments, these features are "controlled" by changing the nutrient and agar concentrations.

It is to be highlighted that none of the models available in the literature has been able to reproduce all the morphological diagram, except for the model recently proposed by Schwarcz *et al.* [132]. The authors in [132] proposed a reaction-diffusion system for bacterial and nutrient densities. The model considers the reproduction and mortality of the bacteria, and includes two novel modeling features. First, a non-linear density dependent diffusion coefficient for the bacterial density, $D_b = D_0 b^k$, with $k = k(t)$ as a time dependent parameter that is defined in terms of the hardness of the agar and takes the values 0 or 1. This feature makes the diffusion coefficient D_b to switch between non-linear (density dependent) and linear regimes. This allows the model to include different mechanism, such as the hardness of the substrate, that modify the bacterial motion. And second, an adaptive bacterial reproduction rate defined through non-local mechanisms based on colony-level communication.

On the other hand, an important aspect of the mathematical modeling of the branched bacterial patterns has been to consider mechanisms that trigger the Mullins-Sekerka or diffusive instability. An example of such a mechanism is the non-linear density dependent diffusion, and is included in the model originally proposed by Kawasaki *et al.* [73], that considers a non-linear cross degenerate diffusion, and it is recognized for being able to successfully reproduce the patterns in regions D and E of the morphological diagram.

Ben-Jacob and coworkers [20, 34, 55] claim that the diffusion of bacteria alone is not capable of explaining some of the experimental observations, and it is necessary to consider additional mechanism, such as bacterial chemotaxis.

In the light of these arguments, we introduced a suitable chemotactic term into system (3.2.1), the model of Kawasaki *et al.*, and we proposed a new reaction-diffusion-chemotaxis system (3.3.2). The definition of the chemotactic term that we considered was based on the experimental findings and theoretical arguments

of Ben-Jacob and co-workers [20, 55], and considers only the chemotaxis due to the nutrient field. They suggested that nutrient chemotaxis is the mechanism responsible for a increased growth velocity in conjunction with a pattern equally ramified.

Although is not theoretically justified, for example from microscopic considerations, the chemotactic flux that we proposed (see equation (3.3.1)) is biological supported by the observations of Ben-Jacob's group of the bacterial response function (see equation (3.2.7)), and it is compatible with the non-linear cross diffusion of the model by Kawasaki and collaborators. In this way, the density dependence is introduced in the biased movement produced by the nutrient chemotaxis.

We explored the effects of the new chemotactic term on the aggregation patterns by doing high resolution numerical simulations of system (3.4.1) for several values of the free parameters (see Table 3.1), including the case without chemotaxis. Thus, comparing the numerical simulation between the cases with and without chemotaxis, we highlight that the main qualitative effects of the nutrient chemotaxis over the patterns are:

(i) Enhancement of the growth speed when the chemotactic signal is present.

(ii) Morphological change for the soft agar, poor nutrient regime.

Concerning point (i), we may observe in figures 3.6 to 3.10 of section 3.6 that when the chemotaxis signal is present the bacterial movement is greatly increased in the outward direction, hence, increasing the propagation of the envelope front of the colony. The morphology of patterns show no major changes, except in the regime of soft agar and poor nutrient regime, in relation to point (ii). Compare figures 3.8 and 3.9 of section 3.6.2, where it is observed that chemotaxis induces a homogenization of the patterns as the chemotaxis strength is increased. There is a morphological transition between branching patterns of region E to homogeneously spreading disks pertaining to region D, of the morphological diagram.

The following chapter is devoted to address point (i). We explore the effects of the chemotactic term has on the propagation velocity of the envelope front of the colony. We estimate the velocity of the envelope front numerically, and doing asymptotic calculations we predict the velocity of the front as a function of both the nutrient concentration and the chemotaxis strength. The results of this chapter have been reported in [86].

Chapter 4

Chemotaxis model - approximation of propagation velocity

In this chapter we continue exploring the effects that nutrient chemotaxis has on the bacterial aggregation patterns. The chemotactic signal provides an outward drift to the bacterial movement, and hence, increasing the propagation rate of the colony envelope front, as the numerical simulations contained in Chapter 3 showed. Therefore, in this chapter we focus on exploring the effects of chemotaxis on the velocity of the front.

In Section 4.1 we numerically estimated the velocity of the envelope front. Then, in section 4.2 we present an asymptotic approximation of the propagation velocity of the front. We compare both theoretical and numerical approximations of the velocity when the chemotaxis is present, to those approximations without chemotaxis.

4.1 Numerical approximation of the velocity

We are interested in the effects that the chemotactic term induces in the colony pattern, in particular in the propagation velocity of the front. Hence, we consider that the influence of the stochastic fluctuations on the diffusion is negligible for the approximation of the propagation speed. Thus, we approximate $\sigma \approx \sigma_0$; furthermore, for simplicity we consider a constant chemotactic sensitivity function, $\chi = \chi_0$. Hence, the system of equations that we consider now has the form

$$n_t = \Delta n - nb, \tag{4.1.1a}$$

$$b_t = \nabla \cdot (\sigma_0 nb \nabla b) + nb - \chi_0 \sigma_0 \nabla \cdot \left(nb^2 \nabla n \right). \tag{4.1.1b}$$

As discussed by Kawasaki and coworkers [73], despite the fact that colony patterns grow in two dimensions on a Petri dish, the tip of each branch extends linearly in one dimension. This is clearly observed in our numerical simulations (see Section 3.6 on Chapter 3), since branches are radially oriented. We approximate the velocity of front solving numerically the one-dimensional version of system (4.1.1). This is

$$\begin{aligned} \frac{\partial n}{\partial t} &= \left(\frac{\partial n}{\partial x}\right)_x - nb, \\ \frac{\partial b}{\partial t} &= \sigma_0 \left(nb\frac{\partial b}{\partial x}\right)_x + nb - \chi_0\sigma_0 \left(nb^2\frac{\partial n}{\partial x}\right)_x, \end{aligned} \tag{4.1.2}$$

together with the initial conditions

$$n(x,0) = n_0, \quad b(x,0) = b_M e^{-x^2/6.25}, \tag{4.1.3}$$

where $b_M = 0.71$. The simulations were performed on the spatial domain $[0, 20]$. We imposed zero-flux boundary conditions. The free parameters are: n_0 that denote the initial level of nutrient, χ_0 which measures the chemotaxis strength, and σ_0 the hardness of the agar. In all simulations we fixed $\sigma_0 = 1$, and took several values of $n_0 = \{0.35, 0.71, 1.07, 2, 3, 4\}$ and $\chi_0 = \{0, 1, 2.5, 5, 10\}$. Figure 4.1 depicts numerical solutions for system (4.1.2) at different time steps, and for various values of n_0 and χ_0.

It is to be noted that solutions for the bacteria do not exhibit a traveling wave profile initially, but eventually solutions resemble a traveling wave. Thus, we considered profiles at later time steps and selected points around $b = 0.5$ of the bacteria density to estimate the velocity, as shown in figure 4.1.

4.2 Approximation of the speed

We now discuss the consequences on the envelope propagation speed by means of an asymptotic geometric front expansion.

We will explore the reduction proposed by Kawasaki *et al.* [73]. They made a simplifying assumption to obtain an approximate scalar equation for the bacterial concentration b. They noted that in the absence of diffusion the total mass is conserved.

In our setting, ignoring both diffusion and chemotaxis in system (4.1.1) we have

$$\begin{aligned} \dot{n} &= -nb, \\ \dot{b} &= nb. \end{aligned} \tag{4.2.1}$$

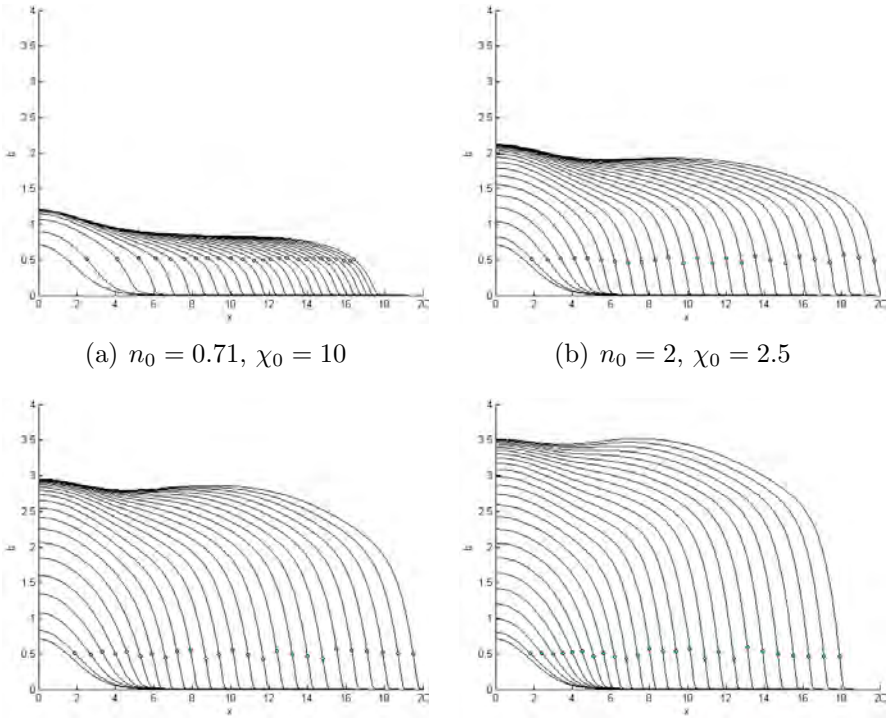

(a) $n_0 = 0.71$, $\chi_0 = 10$ (b) $n_0 = 2$, $\chi_0 = 2.5$

(c) $n_0 = 3$, $\chi_0 = 1$ (d) $n_0 = 4$, $\chi_0 = 1$

Figure 4.1: Numerical solution of the bacterial density b from the system (4.1.2) at different time steps and different values of n_0 and χ_0. The corresponding time intervals are: (a) $t \in [0, 35]$, (b) $t \in [0, 5]$, (c) $t \in [0, 3.3]$ and (d) $t \in [0, 1.9]$. Circles represent selected points to numerically estimate the velocity of the profile.

Adding both equations we obtain

$$\frac{d}{dt}(n + b) = 0,$$

and integrating in time once we have

$$n + b = C, \tag{4.2.2}$$

where C is a constant of integration, that we choose as $C = n_0$. Thus $n = n_0 - b$, and substituting in (4.2.1) we obtain a logistic equation for b,

$$b_t = n_0 b \left(1 - \frac{b}{n_0}\right). \tag{4.2.3}$$

This equation represents the nutrient-limited growth of bacteria. In order to obtain a approximated scalar equation for b, Kawasaki *et al.* substituted $\sigma_0 nb$ by $\sigma_0 n_0 b$

and nb by $n_0 b(1 - b/n_0)$. They arrive to a porous medium reaction-diffusion equation of the form

$$b_t = \sigma_0 n_0 (b b_x)_x + n_0 b(1 - b/n_0), \tag{4.2.4}$$

for which the authors quoted results by Newman [107] to approximate the growth velocity.

In our case, we substitute (4.2.2) into (4.1.1b) to get

$$b_t = \nabla \cdot (\sigma_0 (n_0 - b) b \nabla b) + (n_0 - b)b - \chi_0 \sigma_0 \nabla \cdot \left((n_0 - b) b^2 \nabla (n_0 - b) \right), \tag{4.2.5}$$

which is an approximated scalar equation for b with a Fisher-KPP reaction term. Equation (4.2.5) represents a more accurate approximation and as we will see below it is also consistent with the numerical simulations which, at first order, show that the conservation of mass (4.2.2) is valid away from the front. The diffusion and chemotaxis terms, in equation (4.2.5), can be rearranged into one term written in divergence form to arrive to

$$b_t = \sigma_0 \nabla \cdot (\tilde{D}(b, \chi_0) \nabla b) + g(b), \tag{4.2.6}$$

where

$$\tilde{D}(b, \chi_0) = n_0 b \left(1 - \frac{b}{n_0} \right) (1 + \chi_0 b), \tag{4.2.7}$$

may be interpreted as a effective diffusion term that incorporates contributions from both diffusion and chemotaxis. We notice that the non-linear diffusion $\tilde{D}(b, \chi_0)$ is doubly degenerated, it vanishes at $b = 0$ and $b = n_0$; meanwhile, the diffusion coefficient for (4.2.4) only vanishes at $b = 0$. The reaction term is of Fisher-KPP type

$$g(b) = n_0 b \left(1 - \frac{b}{n_0} \right). \tag{4.2.8}$$

We assume that the location of the front is known, although the task of describing the front position at every time is a non-linear free boundary two dimensional problem [8]. We describe the motion of the front in local curvilinear coordinates with components $\zeta(x, y, t)$ and $\tau(x, y, t)$, the normal and tangent unitary vectors to the front, respectively. According to custom, ζ is the normal component pointing inside the colony front, so that $-\zeta_t$ is the outer normal speed. We assume that the dependence of b with respect to the tangent component is negligible and we consider the approximation

$$b(x, y, t) \approx \bar{b}(\zeta(x, y, t)). \tag{4.2.9}$$

We substitute $\bar{b}$ into equation (4.2.6) to obtain

$$\begin{aligned}\bar{b}'\zeta_t &= \sigma_0(\nabla\tilde{D}(b,\chi_0)\cdot\nabla b + \tilde{D}(b,\chi_0)\Delta b) + g(b)\\ &= \sigma_0(\tilde{D}'(b,\chi_0)\bar{b}'\nabla\zeta\cdot\bar{b}'\nabla\zeta + \tilde{D}(b,\chi_0)(\bar{b}'\Delta\zeta + \bar{b}''|\nabla\zeta|^2)) + g(b)\\ &= \sigma_0(\tilde{D}'(b,\chi_0)(\bar{b}')^2 + \tilde{D}(\bar{b},\chi_0)\bar{b}'\Delta\zeta + \tilde{D}(D)(\bar{b},\chi_0)\bar{b}'') + g(b)\\ &= \sigma_0(\tilde{D}(b,\chi_0)\bar{b}')' + \sigma_0\tilde{D}(b,\chi_0)\Delta\zeta\bar{b}' + g(b).\end{aligned} \tag{4.2.10}$$

Hence, dropping the bar notation for convenience, we arrive to the ordinary differential equation

$$-cb' = \sigma_0(\tilde{D}(b,\chi_0)b')' + b(n_0 - b), \tag{4.2.11}$$

where

$$c = -\zeta_t + \sigma_0\tilde{D}(b,\chi_0)\Delta\zeta, \tag{4.2.12}$$

and $-\zeta_t$ is the velocity we want to estimate.

The approximated equation (4.2.6) is similar to those studied by Malaguti and Marcelli [92], and in the next section we summarize the theoretical results of the authors that we applied to prove that the speed of the envelope front is greater when the chemotaxis terms is present. Recall that we have mentioned earlier (see Definition 1 in Chapter 2) the concept of traveling wave solutions of front and sharp type.

4.2.1 Bounds for the velocity

In [130] the authors stated the problem of traveling wave solutions (TWS) for a double degenerate diffusion equation, and they used numerical techniques to study the wavefront profiles. Afterwards, Malaguti and Marcelli [92] showed the existence of TWS of equation

$$u_t = (D(u)u_x)_x + g(u), \tag{4.2.13}$$

with $D \in C^1([0,1]), g \in C^1([0,1])$, where the diffusion satisfies

$$D(0) = D(1) = 0, \quad D(u) > 0,\ u \in (0,1),$$

and the reaction term is of Fisher-KPP type,

$$g(0) = g(1) = 0, \quad g(u) > 0,\ u \in (0,1).$$

They proved that TWS of equation (4.2.13) exhibit a minimal threshold velocity feature. This means that there exists $c_* > 0$ such that equation (4.2.13) has

(i) no TWS for $0 < c < c_*$,

(ii) a monotone TWS of sharp type with wave speed $c = c_*$,

(iii) a monotone TWS of front type for every wave speed $c > c_*$,

and c_* satisfies

$$0 < c_* \leq 2\sqrt{\sup_{s\in(0,1]} \frac{D(s)g(s)}{s}}. \tag{4.2.14}$$

The authors discussed that the double degeneracy of the diffusion coefficient $D(u)$ do not produce any further sharpness phenomenon at the degeneracy point $u = 1$. In other words, the TWS for the speed $c = c_*$ is of (single) sharp type connecting the equilibrium $u = 1$ to $u = 0$.

The authors carried out the proof showing that the existence of TWS for (4.2.13) is equivalent to the existence of a negative solution $z = z(u)$ of the boundary-value problem

$$\begin{aligned} \frac{dz}{du} &= -c - \frac{D(u)g(u)}{z}, \\ z(0^+) &= z(1^-) = 0, \end{aligned}$$

for fixed $c > 0$, and $u \in (0, 1)$.

The aforementioned result can be extrapolated to a one dimensional equation of the form

$$b_t = (\tilde{D}(b, \chi_0)b_x)_x + g(b), \tag{4.2.15}$$

on $[0, n_0]$ and $\tilde{D}(b, \chi_0)$, $g(b)$ are as in (4.2.7) and (4.2.8), respectively. For each χ_0, the one dimensional threshold wave speed can be estimated in terms of χ_0, n_0, and the functions $\tilde{D}$ and g. We want to compare the velocity in the cases with and without chemotaxis.

The existence of a TWS to the equation (4.2.15) with $\chi_0 > 0$ is related to the solution to the boundary-value problem

$$\begin{aligned} \frac{dz}{db} &= -c - \frac{\tilde{D}(b, \chi_0)g(b)}{z}, \\ z(0^+) &= z(n_0^-) = 0. \end{aligned} \tag{4.2.16}$$

For the case without chemotaxis, $\chi_0 = 0$, the existence of TWS is related to the boundary-value problem

$$\begin{aligned} \frac{dz}{db} &= -c - \frac{\tilde{D}(b, 0)g(b)}{z}, \\ z(0^+) &= z(n_0^-) = 0. \end{aligned} \tag{4.2.17}$$

Following Theorem 9 in Ref. [92] we may consider the sets

$$A_{\chi_0} = \{c > 0 \,:\, \text{problem (4.2.16) has a non-positive solution}\}, \tag{4.2.18}$$

$$A_0 = \{c > 0 \,:\, \text{problem (4.2.17) has a non-positive solution}\}, \tag{4.2.19}$$

that define the range of velocities c for which there exist a TWS to equation (4.2.15). These sets are non empty and its infimum, in either case, correspond to the threshold speed c_*. In addition, the one dimensional TWS to equation (4.2.15) must travel with velocity $c(\chi_0)$, bounded below by $c(\chi_0) \geq c_*(\chi_0)$, where $c_*(\chi_0)$ satisfies the bound

$$0 < c_*(\chi_0) \leq \bar{c}(n_0, \chi_0) := 2\sqrt{\sup_{b\in(0,n_0]} \frac{\sigma_0 \tilde{D}(b,\chi_0) g(b)}{b}},$$

with $\tilde{D}$ and g given by (4.2.7) and (4.2.8). We shall compute the bound $\bar{c}(n_0, \chi_0)$; substituting $\tilde{D}$ and g, we arrive to

$$\bar{c}(n_0, \chi_0) = 2n_0\sqrt{\sigma_0}\sqrt{\max_{b\in[0,n_0]} \tilde{\psi}(b)},$$

where

$$\tilde{\psi}(b) := b\left(1 - \frac{b}{n_0}\right)^2 (1 + \chi_0 b),$$

is a non-negative function for each $\chi_0 \geq 0$ and $0 \leq b \leq n_0$. To be more specific,

$$\tilde{\psi}(0) = \tilde{\psi}(n_0) = 0, \quad \tilde{\psi}(b) > 0,\ b \in (0, n_0).$$

Thus,

$$\tilde{\psi}'(b) = \frac{(b - n_0)}{n_0^2}(4\chi_0 b^2 + (3 - 2n_0\chi_0)b - n_0),$$

and the critical points of $\tilde{\psi}(b)$ are

$$b_1 = n_0,\ b_2^{\pm} = \frac{1}{2}\left(\frac{n_0}{2} - \frac{3}{4\chi_0}\right) \pm \frac{1}{2}\sqrt{\left(\frac{n_0}{2} - \frac{3}{4\chi_0}\right)^2 + \frac{n_0}{\chi_0}}.$$

Therefore, $\tilde{\psi}(b)$ attains its global maximum $\tilde{\psi}_{max} = \tilde{\psi}(b_*)$ at

$$b_* = \frac{1}{2}\left(\frac{n_0}{2} - \frac{3}{4\chi_0}\right) + \frac{1}{2}\sqrt{\left(\frac{n_0}{2} - \frac{3}{4\chi_0}\right)^2 + \frac{n_0}{\chi_0}} \in (0, n_0),$$

for all values of χ_0 and any fixed value of $n_0 > 0$. Hence,

$$\bar{c}(n_0, \chi_0) = 2n_0\sqrt{\sigma_0}\sqrt{\tilde{\psi}_{max}}. \tag{4.2.20}$$

If there is no chemotaxis, i.e. $\chi_0 = 0$, $\tilde{\psi}(b)$ reduces to

$$\psi(b) = b\left(1 - \frac{b}{n_0}\right)^2,$$

and

$$\psi'(b) = \frac{(b - n_0)(3b - n_0)}{n_0^2},$$

whose zeros are $b = n_0$ and $b = n_0/3$. Hence, ψ has global maximum

$$\psi_{max} = \psi\left(\frac{n_0}{3}\right) = \frac{4n_0}{27}.$$

This implies that

$$\bar{c}(n_0, 0) = 2n_0\sqrt{\sigma_0}\sqrt{\frac{4n_0}{27}} = \frac{4}{3\sqrt{3}}n_0^{3/2}\sigma_0^{1/2}. \tag{4.2.21}$$

The bounds for the velocity are given by (4.2.20) and (4.2.21), for the cases with and without chemotaxis. These equations predict the speed of a sharp front, and will be used when comparing the numerical estimates of the velocity.

The following proposition compares the two velocity thresholds (with and without chemotaxis).

Proposition 4.2.1. *For any fixed value of $n_0 > 0$ and for all values of $\chi_0 \geq 0$ there hold,*

(i) $\bar{c}(\chi_0) \geq \bar{c}(0)$, *and*

(ii) $c_*(\chi_0) \geq c_*(0)$.

Proof. The proof of (i) is straightforward: for all values of $\chi_0 \geq 0$ and for each $b \in (0, n_0)$ there holds

$$\psi(b, \chi_0) = b(1 - b/n_0)^2(1 + \chi_0 b) \geq \psi(b, 0) = b(1 - b/n_0)^2.$$

Therefore $\max_{b\in[0,n_0]} \psi(b, \chi_0) \geq \max_{b\in[0,n_0]} \psi(b, 0)$, yielding (i).

To show (ii), let us suppose that $c > 0$ is a velocity such that $c \in A_{\chi_0}$ for some $\chi_0 > 0$. This means that the problem (4.2.16) has a non-positive solution $\zeta(b)$.

Therefore, since $\tilde{D}(b,\chi_0) > \tilde{D}(b,0)$ for all $b \in (0,n_0)$ inasmuch as $\chi_0 > 0$, we have that

$$\frac{d\zeta}{db} = -c - \frac{\tilde{D}(b,\chi_0)}{\zeta(b)} > -c - \frac{\tilde{D}(b,0)}{\zeta(b)}.$$

By Lemma 8 in [92], there exists a negative solution $z = z(b)$ to problem (4.2.17), with the same constant c. This shows that $c \in A_0$. Therefore, $A_{\chi_0} \subseteq A_0$ for all $\chi_0 \geq 0$, and consequently $c_*(\chi_0) = \inf A_{\chi_0} \geq c_*(0) = \inf A_0$. This yields (ii). □

We are assuming that the propagation of the front of the colony is only in the radial direction (see (4.2.9)), and estimate the normal velocity $s = -\zeta_t$. Hence, we compare the one dimension TWS speed for equation (4.2.15) with (4.2.12). The existence of the TWS is guaranteed for $c \geq c_*$, thus

$$c = -\zeta_t + \sigma_0 \tilde{D}(b)\Delta\zeta \geq c_*(\chi_0).$$

We are considering regions where the colony exhibit an outer growth. Recall that for this regions the local curvature is positive there, i.e., $\kappa = -\Delta\zeta > 0$. This implies that

$$s = -\zeta_t \geq c_*(\chi_0) + \sigma_0 \tilde{D}(b)\kappa > 0.$$

It follows from Proposition 4.2.1 that

$$s = -\zeta_t \geq c_*(\chi_0) + \sigma_0 \tilde{D}(b)\kappa \geq c_*(0) + \sigma_0 \tilde{D}(b)\kappa \geq c_*(0). \tag{4.2.22}$$

Therefore, the normal outer velocity is greater than the wave speed corresponding to the sharp TWS without chemotaxis, and that it is increased/decreased by a term proportional to the local curvature and the chemotactic strength $\chi_0 > 0$.

We highlight that in the vicinity of the front the diffusion coefficient $\tilde{D}$ vanishes, there is no bacteria ahead of the envelope front. Therefore, regardless of the curvature sign, we may approximate the normal velocity s by the one dimensional sharp front velocity when the chemotaxis signal is present,

$$s \gtrsim c_*(\chi_0). \tag{4.2.23}$$

Assuming the conservation of total mass, equation (4.2.23) and Proposition 4.2.1 (*ii*) imply that the population front will propagate faster, in the normal direction, when the chemotaxis signal is present.

4.2.2 Comparison of velocity approximations

In this section, we present the comparison between the numerical estimates for the speed of propagation of solutions of the one-dimensional system (4.1.2) and

the theoretical predictions for the speed of the sharp front defined in equations (4.2.20), (4.2.21) for the cases with and without chemotaxis, respectively.

We plotted equations (4.2.20) for $\chi_0 > 0$, and (4.2.21) for $\chi_0 = 0$, as functions of the initial nutrient level n_0, and these are shown as solid lines in Fig. 4.2. The numerical estimates of the speed for the 1-D system (4.1.2) are shown as solid dots in Fig. 4.2.

We may observe that there is a match between the numerical estimates (solid dots) and the theoretical thresholds (solid lines) defined for the scalar equation (4.2.15) for b. Therefore, this shows that the assumption on the conservation of total mass (see equation (4.2.2)) represents a good approximation to solutions of the system (4.1.1).

4.3 Discussion

We explored the effects of the nutrient chemotaxis on the propagation velocity of colony envelope front. We numerically estimated the velocity of the front by solving numerically system (4.1.2), a one-dimensional version of system (4.1.1). Afterwards, we applied an asymptotic geometric front approach, and we approximated the velocity of propagation of the front. Under the assumption of mass conservation (see Eq. (4.2.2)) we found an approximated scalar equation for the bacterial density (Eq. (4.2.6)). Then, applying a result from Malaguti and Marcelli [92] we proved that the normal velocity is greater than the speed associated to the sharp front when there is no chemotaxis. We derived theoretical speed thresholds, defined in Eqs. (4.2.20) and (4.2.21), for the sharp front associated to the scalar equation (4.2.5). We then compare both, numerical and theoretical, velocity approximations (see Fig. 4.2) from which we note the following:

(i) The velocity of propagation is increased when the nutrient chemotaxis is present.

(ii) Numerical estimates approximate well the velocity thresholds for the sharp traveling wave solution (TWS) for equation (4.2.5).

The observation of point (i) was expected from the numerical simulations of the full PDE system in 2-D shown in Chapter 3. Moreover, the asymptotic approximation predicts the front velocity as an increasing function of the chemotactic strength parameter χ_0. The observation from point (ii) implies that the conservation-like Eq. (4.2.2) is a good approximation to solutions of system (4.1.1).

On the other hand, our results for the case without chemotaxis (Fig. 4.2(a)) are comparable to those found by Kawasaki *et al.* [73], however we note that in our calculations we used a more accurate approximation to the bacterial density.

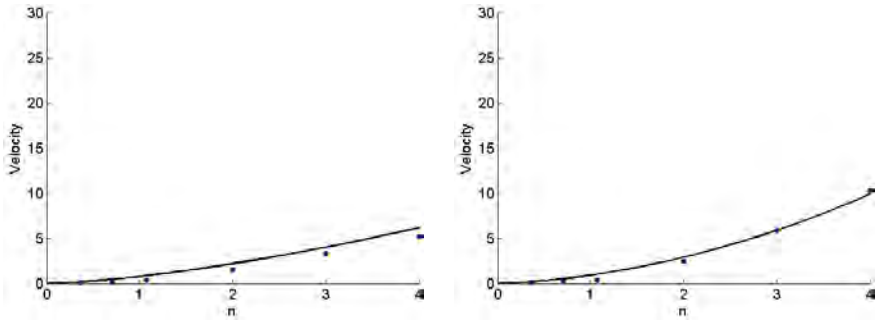

(a) $\chi_0 = 0$ (b) $\chi_0 = 1.0$

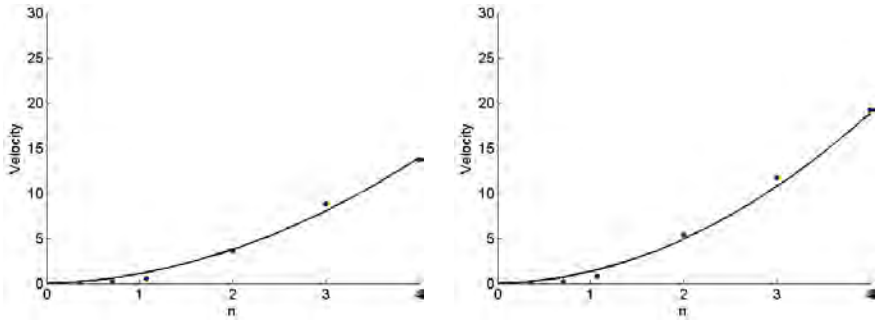

(c) $\chi_0 = 2.5$ (d) $\chi_0 = 5.0$

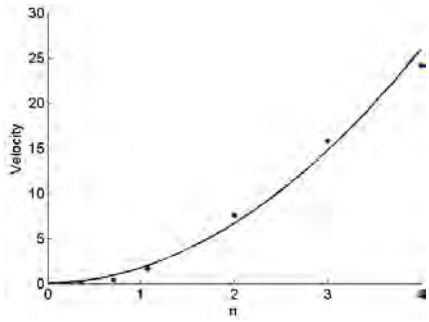

(e) $\chi_0 = 10.0$

Figure 4.2: Comparison of the propagation speeds of the front for the one-dimensional system (4.1.2) as a function of the initial nutrient concentration for different values of the chemotactic sensitivity χ_0. The solid dots depict the numerical estimations of the velocity. The solid line is the velocity threshold given by equation (4.2.21) in the absence of chemotaxis (case 4.2(a)), and by equation (4.2.20) when chemotactic term is present (cases 4.2(b), 4.2(c), 4.2(d) and 4.2(e)), both as functions of the initial nutrient concentration n_0. Here $\sigma_0 = 1$.

Bacterial populations develop well defined spatially structures (aggregation patterns) that have been experimentally observed [20, 111]. These structures have been recognized as biological waves or traveling invasion fronts [141]. We used mathematical modeling, in particular reaction-diffusion models, to explain the basic mechanism behind the formation of such patterns. These patterns are the result of the interaction of two basic physical/biological phenomena, namely, diffusion and chemotaxis. As we observed in the numerical simulation from Chapter 3, bacterial colonies spread towards the diffusing nutrient field which they seek chemotactically. Bacteria propagate (approximately) in one dimension for the dense branch and homogeneous disk morphologies. These results have been reported in [86].

The mathematical representation of the propagating biological waves is given by the traveling wave solutions to the reaction-diffusion system used for the mathematical modeling of the biological systems. The relevance of TWS's stem from the phenomenological and mathematical point of view. Biologically, TWS's represent a structure that in time does not change of form yet it moves with a constant speed, propagating information in one direction that either could be the concentration of certain substance or biomass. Mathematically speaking, the method of looking for TWS is one of few methods known to analytically deal with non-linear partial differential equations.

On the other hand, once it is known a TWS exist, it is of great importance to determine if it is stable under perturbations of the initial conditions. The stable TWS's are those that represent in a more realistic manner the waves that we observe in nature.

Therefore, motivated by the derivation of the scalar equation (4.2.5) for the bacterial density b and the evidence that the speed of its TWS represent a fair approximation to the velocity of the solutions of system (4.1.2), we decided to delve into the stability of TWS to degenerate scalar reaction-diffusion equations of the form (4.2.5). This seems to be a natural approach to gain further understanding on the mechanics of the spreading bacterial patterns.

It is to be highlighted that equation (4.2.5) represents an approximation, based on the conservation-like principle (4.2.2), to the solutions of proposed system (4.1.1). Thus, the stability of the TWS to the scalar equation will not imply directly the stability of the full model. Although, we can not expect stability of the solutions to the full model without the stability of the solutions to the scalar equation.

In the following chapter we will address the stability in exponentially weighted spaces of some subsets of the spectrum corresponding to the linearized operator around smooth-monotone-degenerate traveling waves supported by degenerate scalar reaction-diffusion with reaction term of Fisher-KPP type. The multidimen-

sional stability of TWS for systems poses a fairly complicated problem that we will not discuss in this thesis.

Chapter 5

Stability of diffusion-degenerate traveling fronts

In this chapter we establish the stability, in exponential weighted spaces, of a subset of the spectrum of the linearized differential operator around smooth traveling monotone fronts for reaction diffusion equations of Fisher-KPP type with nonlinear degenerate diffusion coefficient.

In Section 5.1 we explain the motivation and give a brief background to the stability problem we are interested in. Afterwards, in Section 5.2, we cite the results of Sánchez-Garduño and Maini [126, 127] on the existence of sharp and smooth degenerate traveling fronts supported by the non-linear scalar reaction-diffusion equation (5.1.1), and we present information about the structure of the fronts. In Section 5.3 we define the spectral problem by linearizing equation (5.1.1) around the degenerate front. Later, we introduce an alternative partition of the spectrum of the linearized operator and rigorously define the spectral stability of the degenerate Fisher-KPP fronts. We prove the stability of the point spectrum by using energy estimates technique in Section 5.4. In Section 5.5 we introduce a regularization technique to circumvent the difficulties posed by the degeneracy in diffusion, and in Section 5.6 we prove the generalized convergence of the family of regularized operators to the original degenerate operator. In turn, this will allow us to locate a subset of the compression spectrum. In Section 5.7 we introduce exponentially weighted spaces and prove that under certain restriction on the velocity of the front, we can find an appropriate weighted space where the point spectrum and subset of the compression spectrum of the linearized operator are stable. Finally, in Section 5.8 we give a detailed analysis of the asymptotic behavior of the solutions to the spectral equation on the degenerate side. These decay estimates are needed to close the energy estimates of Section 5.4.

5.1 Motivation and background

We will study the scalar reaction-diffusion equation

$$u_t = (D(u)u_x)_x + f(u), \quad (x,t) \in \mathbb{R} \times \mathbb{R}_+, \tag{5.1.1}$$

where $u = u(x,t)$, and the diffusion coefficient $D(u)$ is a nonlinear non-negative function which is degenerate at $u = 0$. We consider the following hypothesis on D,

$$\begin{aligned} D(0) = 0 \text{ and } D(u) > 0, \text{ for } u \in (0,1], \\ D \in \mathcal{C}^2([0,1],\mathbb{R}) \text{ with } D'(u) > 0 \text{ and } D''(u) \neq 0, \quad \forall u \in [0,1]. \end{aligned} \tag{5.1.2}$$

The reaction term $f(u)$ is supposed to be of Fisher-KPP type [50, 81], more precisely,

$$\begin{aligned} f(0) = f(1) = 0, \text{ and } f(u) > 0, \quad \forall u \in (0,1), \\ f \in \mathcal{C}^2([0,1],\mathbb{R}) \text{ with } f'(0) > 0 \text{ and } f'(1) < 0. \end{aligned} \tag{5.1.3}$$

Specific examples of diffusion and reaction functions satisfying the above hypothesis are

$$D(u) = u^2 + bu, \quad f(u) = u(1-u),$$

for a constant $b > 0$.

Reaction-diffusion equations of the form (5.1.1) arise in the modeling of biological phenomena such as population migrations. These models are more realistic, when compared with the classical constant diffusivity models, since they consider that diffusivity of individuals may depend on the population density. For instance, in some biological situations, individuals avoid overcrowded areas moving away from highly populated regions [30]; or in other situations it is the population that segregates the individuals exerting a repulsive influence, increasing the dispersion [101,140].These biological situations have been previously considered in various mathematical models [59, 60, 112, 140]. In the context of development of bacterial colonies these models have been used as tool to understand the aggregation patterns, as we saw in Chapters 3 and 4 (see also [20, 55, 80, 86]).

One of the characteristic behaviors of spreading populations is that of developing a well-defined spatial distribution (or structure) that does not change its form with time, yet it moves at constant speed. This behavior has been recognized in invading species, and sometimes is termed as biological waves or traveling fronts of invasion [141]. Mathematically speaking, this type of behavior corresponds to the emergence of traveling front solutions to the models of interest. As we observed in Chapters 3 and 4, the behavior of traveling front is present in the development of

bacterial colonies, and can be seen in the outward growth of the colony envelope front which propagates (approximately) in one dimension for patterns pertaining to morphologies densely ramified and of homogeneous disks. Our main subject of study in this chapter will be the traveling wave solution of front type (see Definition 1 in Chapter 2).

The introduction of the degeneration in the diffusion has various important mathematical features that contrast with those of the classical strict parabolic case of constant diffusion [144]. One is the finite speed of propagation of disturbances from rest. Biologically speaking, this means that a population that it is initially confined to a bounded region will spread at finite rate. In contrast, for the constant diffusion case, perturbations propagate with a infinite speed. Again, in biological terms this means that a population initially confined to a bounded region will spread instantly to all space [60]. Other important mathematical feature, is the emergence of the traveling front solutions of *sharp* type, as well as smooth front waves [11, 126]. In contrast, the constant diffusion case only supports smooth front waves. Briefly, the difference between the sharp and smooth fronts, is that the former have a discontinuity in their derivative at a finite point in space; while the latter have a continuous derivative.

In 1937, Kolmogorov *et al.* [81] and Fisher [50] introduced the model

$$u_t = u_{xx} + f(u), \tag{5.1.4}$$

where $f(u) = u(1-u)$, to describe the propagation of an advantageous gene in a population within a one-dimensional habitat. These pioneer works lay the foundations for the theory of existence of traveling wave solutions to reaction-diffusion equations, and the methods (phase plane analysis) introduced in [81] represent now the classical approach to delve in the existence of traveling waves solutions. The authors showed that there exists $c_* > 0$ such that equation (5.1.4) has monotonically decreasing front that travels with velocity $c \geq c_*$, and that there are no traveling fronts for $c < c_*$. This means that the velocity c defines an infinite family of traveling fronts. In addition, in [81] the authors obtain the first results on stability of traveling fronts for the equation (5.1.4) in the following sense, they proved that for a class on initial conditions the solutions to the initial value problem (IVP) converge in certain sense to the traveling wave with minimum speed c_*.

Since the publication of the now classical works [50] and [81], traveling wave solutions have attracted great interest, and extension and generalization to the analysis of Kolmogorov *et al.* of equation (5.1.4) regarding traveling fronts can be seen in [14, 48, 49, 105].

The existence of fronts for reaction-diffusion equations with degenerate diffusion was first analyzed for the particular case of porous medium diffusion type,

$D(u) = u^m$ and $m \geq 1$, in [11, 105, 107, 108]. For results on existence of traveling waves for more general equations of reaction-diffusion-convection type see [53].

The first general existence results for degenerate diffusion satisfying hypotheses (5.1.2), and generic reaction functions of Fisher-KPP type satisfying (5.1.3), is due to Sánchez-Garduño and Maini [126, 127]. In these works, the authors prove the existence of a positive threshold speed $c_* > 0$ such that: (i) there exist no traveling fronts with speed $0 < c < c_*$; (ii) there exists a traveling wave of *sharp* type with speed $c = c_*$, with $\varphi(-\infty)$ and $\varphi(\xi) = 0$ for all $\xi \geq \xi_*$ with $\xi_* \in \mathbb{R}$; and (iii) there exist a family of smooth monotone decreasing traveling fronts with speed $c > c_*$, and such that $\varphi(-\infty) = 1$ and $\varphi(+\infty) = 0$ (see Theorem 5.2.1 below). In this chapter we are interested in analyzing the stability properties of smooth monotone Fisher-KPP degenerated fronts (case (iii) above).

The study of the stability properties of traveling waves is fundamental, since the stable TWS to an equation that models a phenomenon will be the only solutions physically relevant.

One approach to the stability of traveling waves is to linearize the non-linear partial differential equation around the wave. Hence, the stability problem consists of two parts: (i) Localize the spectrum of the linearized differential operator; and (ii) use the linear information to prove the non-linear stability, that is, stability of the wave with respect to the full non-linear partial differential equation.

Earlier results for point (ii) in the case of semi-linear parabolic equations are due to Sattinger [131] and Henry [61]. More recent results for (i) and (ii) in the case of quasi-linear parabolic equations with non-degenerate density dependent diffusion coefficient are provide by Meyries *et al.* [99].

The methods to study the stability of traveling waves incorporate the techniques of functional analysis and dynamical systems, and the paper by Alexander, Gardner and Jones [4] is a canonical reference. In addition, we refer to the review article by Sandstede [128] and the recent monograph by Kapitula and Promislow [71] for an updated exposition on the subject and additional references related to the stability of traveling waves.

There exist previous results regarding the stability of traveling fronts to reaction-diffusion equations with degenerate diffusion. Hosono [67] showed the existence of smooth and sharp fronts to the porous medium degenerate reaction-diffusion equation

$$u_t = (u^m)_{xx} + u(1-u)(u-\alpha),$$

where $m > 1$ and $\alpha \in (0, 1)$. Using techniques from parabolic PDEs the author constructed sub and supersolutions, and then using comparison techniques he proved that solutions to IVP with initial conditions close to the stationary front converge asymptotically to a translated of the front. These results rely heavily of the properties of the porous medium equation.

For the case of Fisher-KPP reaction type and a diffusion coefficient of the form $D(u) = u$, Sherrat and Marchant [139] studied numerically the asymptotic behavior of solutions, and they showed that for certain initial conditions, the solutions to the IVP evolve to a traveling wave solution. Biró [27] and Medevev *et al.* [97] showed, for equations of porous medium type together with a reaction of Fisher-KPP type and more general coefficients, using comparison techniques that solutions with initial data with compact support converge to the traveling wave with minimum velocity (the sharp wave).

In this chapter we are interested in studying the spectral stability of the smooth degenerate Fisher-KPP fronts to equation (5.1.1). The spectral stability, formally is the non-existence of eigenvalues with positive real part of the linearized differential operator around the front (see Definition 3 below). We highlight that our analysis is based on the spectral analysis of operators, and we do not use techniques from parabolic PDEs. As we shall se below, the degeneracy in the diffusion poses various technical difficulties that are not present in the standard parabolic case.

In particular, the degeneracy of the diffusion at one of the equilibrium points of the reaction term precludes the application of the standard methods to localize the essential spectrum of the linearized operator around the wave. Hence, we propose an alternative but equivalent partition of the spectrum of the linearized operator in the form $\sigma = \sigma_{pt} \cup \sigma_{\pi} \cup \sigma_{\delta}$, where σ_{pt} is the point spectrum, σ_{π} is a subset of the approximate spectrum and σ_{δ} is a subset of the compressed spectrum (see Definition 2 below).

Our primary interest is to prove the spectral stability (see Definition 3), of the smooth degenerate Fisher-KPP fronts to equation (5.1.1). In this chapter we provide the proof for the stability of the subsets of spectrum σ_{pt} and σ_{δ}.

Using an appropriate change of variables and energy estimates we show the stability of the point spectrum σ_{pt}. To justify the change of variables, a detailed analysis of the asymptotic behavior of the eigenfunctions at the degenerates stationary state is performed.

In addition, we introduced a regularization technique which, together with the generalized convergence of operators, allowed us to exploit the robustness of the Fredholm properties under "small" perturbations to localize the subset σ_{δ} of the compressed spectrum. This approach relates the Fredholm properties of the regularized operators to those of the original degenerate operator. Fredholm borders determine the location of σ_{δ}.

It is known from the parabolic Fisher-KPP case [61, 131] that is it necessary to recast the spectral problem in an exponentially weighted space. In particular, point spectrum σ_{pt} is invariant under conjugation by an exponential weight, while the Fredholm borders are pushed into the stable region of the complex with the

same weight (see [71]). Thus, we show that if the velocity of the front satisfy certain restriction then there exist an appropriate weighted L^2- space, in which σ_{pt} and σ_δ are stable.

In the following section we review the existence results of smooth degenerate traveling front to equation (5.1.1) due to Sanchez-Garduño and Maini [126, 127].

5.2 Structure of the traveling wave fronts

In this section we state the results of Sánchez-Garduño and Maini [126] concerning the existence of traveling wave solutions of equation (5.1.1). For further details, see [126, 127].

Consider a solution $u(x,t) = \varphi(x - ct) = \varphi(\xi)$ of (5.1.1), where $c \in \mathbb{R}$ denotes the wave velocity and ξ is the galilean variable in the co-moving frame of the traveling wave. Substituting the solution φ in (5.1.1) we arrive to the profile equation

$$(D(\varphi)\varphi_\xi)_\xi + c\varphi_\xi + f(\varphi) = 0. \tag{5.2.1}$$

Boundary conditions are imposed, requiring that the traveling wave have finite asymptotic limits

$$u_- := \lim_{\xi\to-\infty} \varphi(\xi) = 1, \quad u_+ := \lim_{\xi\to+\infty} \varphi(\xi) = 0. \tag{5.2.2}$$

In this framework, the traveling wave solutions of equation (5.1.1) with speed c correspond to solutions of the second order ODE (5.2.1) for the same speed. The asymptotic limits $u_\pm$ are assumed to be equilibrium points of the reaction function f.

We rewrite equation (5.2.1) as first order ODE system, of the following form

$$\begin{aligned} \frac{d\varphi}{d\xi} &= v, \\ D(\varphi)\frac{dv}{d\xi} &= -cv - D'(\varphi)v^2 - f(\varphi). \end{aligned} \tag{5.2.3}$$

Observe that system (5.2.3) has a singularity at $\varphi = 0$, since $D(0) = 0$. To overcome this singularity, Aronson [11] introduced the change of variable $\tau = \tau(\xi)$ such that

$$\frac{d\tau}{d\xi} = \frac{1}{D(\varphi(\xi))}. \tag{5.2.4}$$

We define

$$\varphi(\xi) = \varphi(\tau(\xi)), \quad v(\xi) = v(\tau(\xi)).$$

Hence, the derivative with respect the new independent variable τ is given by

$$\frac{d\varphi}{d\xi} = \frac{1}{D(\varphi)}\frac{d\varphi}{d\tau}, \quad \frac{dv}{d\xi} = \frac{1}{D(\varphi)}\frac{dv}{d\tau}. \tag{5.2.5}$$

Substituting in (5.2.3) we arrive to the non-singular system

$$\begin{aligned} \frac{d\varphi}{d\tau} &= D(\varphi)v, \\ \frac{dv}{d\tau} &= -cv - D'(\varphi)v^2 - f(\varphi), \end{aligned} \tag{5.2.6}$$

which have the equilibrium points $(\varphi, v) = P_0 = (0,0), P_1 = (1,0)$, and $P_c = (0, -c/D'(0))$. As Aronson [11] points out, the effect of the change of variable (5.2.4) is to resolve the singularity at $\varphi = 0$ into two critical points $(0,0)$ and $(0, -c/D'(0))$. Also, observe that relation (5.2.5) states a reparametrization of the trajectories of systems (5.2.3) and (5.2.6), and since $D(\varphi) > 0$ for $\varphi > 0$ the orientation of trajectories is the same. This means that systems (5.2.3) and (5.2.6) are topologically equivalent in the region $\{(\varphi, v) | \varphi > 0, -\infty < v < \infty\}$.

Linear analysis of equilibria shows that $(1,0)$ and $(0, -c/D'(0))$ are a saddle points and $(0,0)$ is a non-hyperbolic point with a center eigenspace of dimension one. Then, it is necessary to consider higher order terms in the Taylor series to determine the behavior of the trajectories in the vicinity of the origin. Applying the methods from Andronov *et al.* [10] it is found that the equilibrium $(0,0)$ is a saddle-node for system (5.2.6) and for system (5.2.3) as well.

Sánchez-Garduño and Maini [126] proved the existence of traveling waves by doing a detailed phase plane analysis of system (5.2.6). They showed that there exists a c_*, such that for each $c > c_*$ there exists a heteroclinic trajectory connecting the equilibrium points $(0,0)$ and $(0,1)$, corresponding to a decreasing smooth traveling wave with speed c that satisfies boundary conditions (5.2.2). Furthermore, for $0 < c < c_*$, the authors proved that the trajectory leaving the equilibrium $(0,1)$ terminates at $(-\infty, 0)$, implying that there is no traveling wave; and for $c = c_*$ the trajectory hits the equilibrium $(0, -c_*/D'(0))$, this corresponds to a "sharp" traveling wave. In particular they proved the following (see Theorem 2 in [126])

Theorem 5.2.1. *If the function $D = D(u)$ satisfies* (5.1.2) *and $f = f(u)$ is of Fisher-KPP type satisfying* (5.1.3)*, then there exist a unique speed value $c_* > 0$ such that equation* (5.1.1) *has:*

(i) No traveling wave solutions for $0 < c < c_*$,

(ii) A traveling wave solution $u(x,t) = \phi(x - c_* t)$ of sharp type satisfying: $\phi(-\infty) = 1$, $\phi(\xi) = 0 \quad \forall \xi \geq \xi_*$; $\phi'(-\infty) = 0$, $\phi'(\xi_*) = -\frac{c_*}{D'(0)}$ and $\phi'(\xi) = 0 \quad \forall \xi \geq \xi_*$,

(iii) A monotone decreasing traveling front φ for each $c > c_*$, with

$$u_+ = \varphi(+\infty) = 0, \quad u_- = \varphi(-\infty) = 1,$$

and $\varphi_\xi < 0$ for all $\xi \in \mathbb{R}$. Each front is diffusion degenerate at $u_+ = 0$, as $\xi \to +\infty$.

In this chapter we are interested in analyzing the stability properties of the family of monotone decreasing smooth Fisher-KPP degenerate traveling fronts indexed by the velocity c, that connect the equilibrium points $u_- = 1$ and $u_+ = 0$, which existence is given by point (iii) of Theorem 5.2.1. We give the asymptotic behavior of the monotone decreasing degenerate traveling fronts in the following

Lemma 5.2.2 (asymptotic decay)**.** *Let $\varphi = \varphi(\xi)$ be a monotone decreasing Fisher-KPP degenerate front, traveling with speed $c > c_* > 0$, and with $u_+ = 0, u_- = 1$. Then φ behaves asymptotically as*

$$|\partial_\xi^j(\varphi - u_+)| = |\partial_\xi^j \varphi| = O(e^{-f'(0)\xi/c}), \quad \text{as} \quad \xi \to +\infty, j = 0, 1,$$

on the degenerate side; and as,

$$|\partial_\xi^j(\varphi - u_-)| = |\partial_\xi^j(\varphi - 1)| = O(e^{\eta\xi}), \quad \text{as} \quad \xi \to -\infty, j = 0, 1,$$

on the non-degenerate side, with $\eta = (2D(1))^{-1}\left(-c + \sqrt{c^2 - 4D(1)f'(1)}\right) > 0$.

Proof. The asymptotic decay of the front φ on the non degenerate side, as $\xi \to -\infty$, can be found using the linearization of the profile equation (5.2.1) around the point $\tilde{\varphi} = \varphi - 1$, that has the following form

$$D(1)\tilde{\varphi}'' + c\tilde{\varphi}' + f'(1)\tilde{\varphi} = 0. \tag{5.2.7}$$

The general solution of the second order constant coefficient ODE (5.2.7) is a linear combination of the form $\tilde{\varphi} = C_1 e^{\eta\xi} + C_2 e^{\varrho\xi}$ where

$$\eta = \frac{-c + \sqrt{c^2 - 4D(1)f'(1)}}{2D(1)} > 0, \quad \varrho = \frac{-c - \sqrt{c^2 - 4D(1)f'(1)}}{2D(1)} < 0.$$

Therefore, $\tilde{\varphi}$ will decay as $\xi \to -\infty$ only if $C_2 = 0$. Hence, the decaying solutions of equation (5.2.7) have the form $\tilde{\varphi} = e^{\eta\xi}$. Thus, we have the exponential decay

$$|\varphi - 1| \sim e^{\eta\xi}, \quad \text{as} \quad \xi \to -\infty.$$

Likewise, we have

$$|\partial_\xi(\varphi - 1)| \sim Ce^{\eta\xi}, \quad \text{as} \quad \xi \to -\infty.$$

The authors in [126] showed that the trajectory coming from P_1 approaches P_0 through the local center manifold of system (5.2.6) at P_0. This is because P_0 is a non-hyperbolic equilibrium point. The Centre Manifold Theorem [31] guarantees that the dynamics around P_0 is given by the dynamics on the centre manifold. In general, the centre manifold is no unique, but the equilibrium P_0 will be contained in any centre manifold. Moreover, all approximations of centre manifolds coincide at all orders. Thus, to verify the asymptotic decay rate on the degenerate side we have to approximate the centre manifold.

The decay rate of φ, as $\xi \to +\infty$ depends on the leading order of $v = h(\varphi)$, where $h(\varphi)$ is the approximated centre manifold of the system (5.2.6) at equilibrium $(0, 0)$. Up to second order, we found that the centre manifold for system (5.2.6) (and hence for system (5.2.3)) has the following form (details can be found in [126]):

$$h(\varphi) = -\frac{f'(0)}{c}\varphi - \frac{1}{2c^3}(f''(0)c^2 + 4D'(0)f'(0)^2)\varphi^2 + O(\varphi^3),$$

as $\varphi \to 0$.

Thus, the reduced dynamics on the center manifold is given by

$$\frac{d\varphi}{d\tau} = D(\varphi)v = D(\varphi)h(\varphi).$$

Returning to the original galilean variable, via equation (5.2.5), we have

$$\frac{d\varphi}{d\xi} = h(\varphi) \approx -\frac{f'(0)}{c}\varphi \leq 0, \tag{5.2.8}$$

as $\xi \to +\infty$. Therefore, we obtain the asymptotic behavior

$$\varphi = O(e^{-f'(0)\xi/c}),$$

as $\xi \to +\infty$. Finally, taking the absolute value of (5.2.8) and substituting the previous decay rate we have

$$|\partial_\xi \varphi| = O(e^{-f'(0)\xi/c}),$$

as $\xi \to +\infty$. □

Lemma 5.2.3. *Let $\varphi = \varphi(\xi)$ be a monotone decreasing Fisher-KPP degenerate front, traveling with speed $c > c_* > 0$. Then, $\varphi_\xi \in H^2(\mathbb{R})$.*

Proof. We corroborate that $\partial_\xi^j(\varphi) \in L^2(\mathbb{R})$, for $j = 1, 2, 3$.

For $j = 1$, it holds that $\varphi_\xi \in L^2(\mathbb{R})$. This is a consequence of Lemma 5.2.2, because of the exponential decay to zero, $\varphi_\xi \to 0$, as $|\xi| \to \infty$.

From the profile equation (5.2.1) we have that

$$\varphi_{\xi\xi} = -\frac{1}{D(\varphi)}\left(c\varphi_\xi + f(\varphi) + D'(\varphi)(\varphi_\xi)^2\right).$$

In order to find the asymptotic behavior of $\varphi_{\xi\xi}$ on the degenerate side, as $\xi \to +\infty$, we take the following Taylor expansions around $\varphi = 0$:

$$\begin{aligned} D(\varphi) &= D'(0)\varphi + O(\varphi^2), \quad D(\varphi)^{-1} = D'(0)^{-1}\varphi^{-1} + O(1), \\ D'(\varphi) &= D'(0) + O(\varphi), \quad f(\varphi) = f'(0)\varphi + O(\varphi^2) \end{aligned}$$

Likewise, we use the centre manifold approximation

$$\varphi_\xi = -f'(0)\varphi/c + O(\varphi^2).$$

Hence, as $\varphi \to 0$, we have

$$\begin{aligned} \varphi_{\xi\xi} =& -\left(\frac{\varphi^{-1}}{D'(0)} + O(1)\right)\left(c\left(-\frac{f'(0)}{c}\varphi + O(\varphi^2)\right)\right. \\ &\left. + f'(0)\varphi + O(\varphi^2) + (D'(0) + O(\varphi))\left(\frac{f'(0)^2}{c^2}\varphi^2 + O(\varphi^3)\right)\right) \\ =& -\left(\frac{\varphi^{-1}}{D'(0)} + O(1)\right)\left(\frac{f'(0)^2}{c^2}\varphi^2 + O(\varphi^2) + O(\varphi^3)\right) \\ =& -\left(\frac{\varphi^{-1}}{D'(0)} + O(1)\right)O(\varphi^2) = O(\varphi). \end{aligned} \tag{5.2.9}$$

Therefore,

$$|\varphi_{\xi\xi}| = O(e^{-f'(0)\xi/c}), \quad \text{as} \quad \xi \to +\infty. \tag{5.2.10}$$

On the non degenerate side, it follows from Lemma 5.2.2 that

$$|\varphi_{\xi\xi}| = O(e^{\eta\xi}), \quad \text{as} \quad \xi \to -\infty. \tag{5.2.11}$$

Therefore, $\varphi_{\xi\xi}$ decays exponentially to zero as $|\xi| \to \infty$. This implies that $\varphi_{\xi\xi} \in L^2(\mathbb{R})$.

Observe that from the center manifold approximation (5.2.8) we have

$$\varphi_\xi = h(\varphi) = -\frac{f'(0)}{c}\varphi + \alpha\varphi^2 + O(\varphi^3),$$

as $\varphi \to 0$ and where

$$\alpha = -\frac{f''(0)c^2 + 4D'(0)f'^2(0)}{2c^3}.$$

Then, we differentiate twice $h(\varphi)$ with respect ξ, arriving to

$$\varphi_{\xi\xi\xi} = \frac{f'(0)}{c}\varphi_{\xi\xi} + 2\alpha(\varphi\varphi_{\xi\xi} + \varphi_\xi^2).$$

Then, as $\varphi \to 0$, the nonlinear terms $\varphi\varphi_{\xi\xi}$ and φ_ξ^2 are smaller than the linear term $\varphi_{\xi\xi}$, and hence

$$\varphi_{\xi\xi\xi} \approx \frac{f'(0)}{c}\varphi_{\xi\xi}.$$

Hence it follows from (5.2.10) that on the degenerate side we have

$$|\varphi_{\xi\xi\xi}| = O(e^{-f'(0)\xi/c}), \quad \text{as } \xi \to +\infty.$$

On the other hand, to find the decay for $\varphi_{\xi\xi\xi}$ at the non-degenerate side, as $\xi \to -\infty$, we differentiate once the profile equation (5.2.1) with respect ξ, and we get

$$(D(\varphi)\varphi_\xi)_{\xi\xi} + c\varphi_{\xi\xi} + f'(\varphi)\varphi_\xi = 0.$$

Hence, as $\xi \to -\infty$, the solutions of the previous equations are approximated by the solutions of

$$D(1)\varphi_{\xi\xi\xi} + c\varphi_{\xi\xi} + f'(1)\varphi_\xi = 0.$$

Thus,

$$\varphi_{\xi\xi\xi} = -\frac{1}{D(1)}(c\varphi_{\xi\xi} + f'(1)\varphi_\xi),$$

and it follows from Lemma 5.2.2 and (5.2.11) that

$$|\varphi_{\xi\xi\xi}| = O(e^{\eta\xi}), \quad \text{as } \xi \to -\infty.$$

Therefore, $\varphi_{\xi\xi\xi}$ decays exponentially to zero as $|\xi| \to \infty$. This implies that $\varphi_{\xi\xi\xi} \in L^2(\mathbb{R})$. Then the proof follows. □

In the following section we define the spectral problem by linearizing the nonlinear reaction-diffusion equation (5.1.1) around the front φ. We introduce an alternative but equivalent partition of the spectrum of the linearized operator (see Definition 2), and we give the rigorous definition of spectral stability (see Definition 3).

5.3 Spectral problem

Let us consider equation (5.1.1) under assumptions (5.1.2) and (5.1.3). Suppose that $u(x,t) = \varphi(x - ct)$ is a monotone traveling front solution to equation (5.1.1) with velocity $c > c_* > 0$. For notation simplicity, we make the change of variables

$x \to x - ct$, where now x denotes the Galilean variable of translation. Thus, equation (5.1.1) written in the co-moving frame of the Galilean variable is

$$u_t = (D(u)u_x)_x + cu_x + f(u). \tag{5.3.1}$$

Traveling fronts with velocity c, $u(x,t) = \varphi(x)$, correspond to stationary solutions of above equations, and satisfy

$$(D(u)\varphi_x)_x + c\varphi_x + f(\varphi) = 0. \tag{5.3.2}$$

Now, we consider solutions of equation (5.3.1) that are perturbations of the traveling front $\varphi(x)$ of the form $\varphi(x) + u(x,t)$. Substituting in (5.3.1) we obtain a nonlinear perturbation equation

$$u_t = (D(\varphi + u)(\varphi + u)_x)_x + c(\varphi + u)_x + f(\varphi + u). \tag{5.3.3}$$

Linearizing around the front $\varphi(x)$ we obtain

$$\begin{aligned} u_t =&((D(\varphi) + D'(\varphi)u)(\varphi_x + u_x))_x + c\varphi_x + u_x + f(\varphi) + f'(\varphi)u \\ =&(D(\varphi)\varphi_x)_x + (D(\varphi)u_x)_x + (D'(\varphi)\varphi_x u)_x + (D'(\varphi)uu_x)_x \\ &+ c\varphi_x + cu_x + f(\varphi) + f'(\varphi)u. \end{aligned} \tag{5.3.4}$$

On account of the profile equation (5.3.2) and keeping only the linear terms we arrive to

$$u_t = (D(\varphi)u)_{xx} + cu_x + f'(\varphi)u. \tag{5.3.5}$$

We can rewrite the linear evolution equation (5.3.5) as $u_t = \mathcal{L}u$, where $\mathcal{L}$ is the linear operator

$$\begin{aligned} &\mathcal{L} : \mathcal{D}(\mathcal{L}) \subset X \to X, \\ &\mathcal{L}u = (D(\varphi)u)_{xx} + cu_x + f'(\varphi)u, \end{aligned} \tag{5.3.6}$$

acting on an adequate Banach space X. We may define the spectral problem as

$$\mathcal{L}u = \lambda u, \tag{5.3.7}$$

where $\lambda \in \mathbb{C}$ is the spectral parameter.

The spectral stability of the traveling front $\varphi(x)$, formally, is defined as the non-existence of solutions $u \in X$ to equation (5.3.7) for $\operatorname{Re}\lambda > 0$ (see Definition 3 below). This condition assures the non-existence of solutions to equation (5.3.5) of the form $e^{\lambda t}u$ that grow exponential in time.

5.3.1 Spectral stability

This section is devoted to define rigorously the concept of spectral stability. We begin giving a particular partition of the spectra of a linear operator, suitable for our needs.

Let X and Y be Banach spaces, and let $\mathscr{C}(X,Y)$ and $\mathscr{B}(X,Y)$ denote the sets of all closed and bounded linear operators from X to Y, respectively. For any $\mathcal{L} \in \mathscr{C}(X,Y)$ we denote its domain as $\mathcal{D}(\mathcal{L}) \subset X$ and its range as $\mathcal{R}(\mathcal{L}) := \mathcal{L}(\mathcal{D}(\mathcal{L})) \subseteq Y$. We say that $\mathcal{L}$ is densely defined if $\overline{\mathcal{D}(\mathcal{L})} = X$.

Definition 2. The *resolvent set* $\rho(\mathcal{L})$ of a closed, densely defined operator $\mathcal{L} \in \mathscr{C}(X,Y)$ is the set of all scalars $\lambda \in \mathbb{C}$ for which $\mathcal{L} - \lambda$ is bijective with bounded inverse, this is,

$$\rho(\mathcal{L}) := \{\lambda \in \mathbb{C} : \mathcal{L} - \lambda \text{ is injective, } \mathcal{R}(\mathcal{L} - \lambda) = Y, \text{ and } (\mathcal{L} - \lambda)^{-1} \in \mathscr{B}(Y,X)\}.$$

Its *spectrum* is defined as $\sigma(\mathcal{L}) := \mathbb{C} \setminus \rho(\mathcal{L})$. We define the following subsets of the complex plane, characterized by the way in which the invertibility of $\mathcal{L} - \lambda$ could fail.

$$\begin{aligned}
\sigma_{pt}(\mathcal{L}) &:= \{\lambda \in \mathbb{C} : \mathcal{L} - \lambda \text{ is not injective}\},\\
\sigma_{\delta}(\mathcal{L}) &:= \{\lambda \in \mathbb{C} : \mathcal{L} - \lambda \text{ is injective, } \mathcal{R}(\mathcal{L} - \lambda) \text{ is closed, and } \mathcal{R}(\mathcal{L} - \lambda) \neq Y\},\\
\sigma_{\pi}(\mathcal{L}) &:= \{\lambda \in \mathbb{C} : \mathcal{L} - \lambda \text{ is injective, } \mathcal{R}(\mathcal{L} - \lambda) \text{ is not closed}\}.
\end{aligned}$$

The set $\sigma_{pt}(\mathcal{L})$ is called the *point spectrum*. Each $\lambda \in \sigma_{pt}(\mathcal{L})$ is called an *eigenvalue*, and each $u \in \mathcal{D}(\mathcal{L}), u \neq 0$ such that $(\mathcal{L} - \lambda)u = 0$, is called an *eigenfunction* associated to λ.

Remark 1. For a closed operator $\mathcal{L} \in \mathscr{C}(X,Y)$, if $\mathcal{L} - \lambda$ is bijective, for some $\lambda \in \mathbb{C}$, then $(\mathcal{L} - \lambda)^{-1}$ is alway bounded (cf. [72, p. 167]). It is clear that the sets $\sigma_{pt}(\mathcal{L})$, $\sigma_{\pi}(\mathcal{L})$ and $\sigma_{\delta}(\mathcal{L})$ are pairwise disjoint, and that

$$\sigma(\mathcal{L}) = \sigma_{pt}(\mathcal{L}) \cup \sigma_{\pi}(\mathcal{L}) \cup \sigma_{\delta}(\mathcal{L}).$$

Additional partitions of the spectrum for an unbounded operator are found in the literature, for instance, the larger subset of *approximate spectrum*, defined as

$$\sigma_{app}(\mathcal{L}) := \{\lambda \in \mathbb{C} : \mathcal{L} - \lambda \text{ is not injective or } \mathcal{R}(\mathcal{L} - \lambda) \text{ is not closed}\}.$$

It is clear from the definition that $\sigma_{\pi}(\mathcal{L}) \subset \sigma_{app}(\mathcal{L})$ and $\sigma_{pt}(\mathcal{L}) \subset \sigma_{app}(\mathcal{L})$. The set $\sigma_{app}(\mathcal{L})$ is characterized by the following fact (cf. [41, p. 242]): $\lambda \in \sigma_{app}(\mathcal{L})$ if and only if there exist a sequence $\{u_n\} \in \mathcal{D}(\mathcal{L})$ with $||u_n|| = 1$, called *singular sequence*, such that $(\mathcal{L} - \lambda)u_n \to 0$ in Y as $n \to \infty$. The elements of $\sigma_{app}(\mathcal{L})$ are called *approximate eigenvalues*.

The set $\sigma_\delta(\mathcal{L})$ is contained in the residual spectrum, also called the compression spectrum (see [125]),

$$\sigma_\delta(\mathcal{L}) \subset \sigma_{com}(\mathcal{L}) := \{\lambda \in \mathbb{C} : \mathcal{L} - \lambda \text{ is injective, } \overline{\mathcal{R}(\mathcal{L}-\lambda)} \neq Y\}.$$

(Since $\overline{\mathcal{R}(\mathcal{L}-\lambda)} \neq Y$ it is said that the range has been compressed).

In Definition 2, we propose a partition of the spectrum in which the nature of the failure of the invertibility of $\mathcal{L} - \lambda$ is given by the points for which the range $\mathcal{L} - \lambda$ is closed and those for which is not. Obviously this is not the only way in which the invertibility of $\mathcal{L} - \lambda$ could fail. In contrast, the classical partition of spectrum of continuous, residual and point spectra (cf. [39]), is defined in terms of points for which the range of $\mathcal{L} - \lambda$ is dense and those for which is not.

Definition 3. We say the traveling front φ is *X-spectrally stable* if

$$\sigma(\mathcal{L}) \subset \{\lambda \in \mathbb{C} : \operatorname{Re}\lambda \leq 0\}.$$

We shall consider $X = L^2(\mathbb{R};\mathbb{C})$ and $\mathcal{D}(\mathcal{L}) = H^2(\mathbb{R};\mathbb{C})$, so that $\mathcal{L}$ is closed, densely defined operator acting on L^2. Definition 3 in conjunction with choice of the base space L^2 correspond to the stability analysis with respect to spatially localized perturbations. In the following, $\sigma(\mathcal{L})$ will denote the L^2-spectrum of the linearized operator (5.3.6) with domain $\mathcal{D} = H^2$, except where it is otherwise computed with respect to a space X and explicitly denoted as $\sigma(\mathcal{L})_{|X}$.

Definition 4. Let $\mathcal{L} \in \mathscr{C}(X, Y)$, and denote the nullity and deficiency of $\mathcal{L}$ as $\text{nul}\mathcal{L} = \dim\ker\mathcal{L}$, $\text{def}\mathcal{L} = \text{codim}\mathcal{R}(\mathcal{L})$, respectively. The operator $\mathcal{L}$ is said to be Fredholm if its range $\mathcal{R}(\mathcal{L})$ is closed, and its nullity and deficiency are both finite. The operator $\mathcal{L}$ is said to be semi-Fredholm if $\mathcal{R}(\mathcal{L})$ is closed and at least one of $\text{nul}\mathcal{L}$ and $\text{def}\mathcal{L}$ is finite. In both cases, the index of $\mathcal{L}$ is defined (see [71]) as

$$\text{ind}\mathcal{L} = \text{nul}\mathcal{L} - \text{def}\mathcal{L}.$$

Usually, in the framework of spectral stability analysis of traveling waves the partition of the spectrum is defined in terms of the Fredholm properties of the linearized operator around the wave, and relies on the hyperbolicity of the asymptotic rest states [71, 128]. This partition of the spectrum is composed of the essential spectrum, $\sigma_{ess}(\mathcal{L})$, which is the set of $\lambda \in \mathbb{C}$ such that $\mathcal{L} - \lambda$ is not Fredholm or is Fredholm with index not zero. The point spectrum $\tilde{\sigma}_{pt}(\mathcal{L})$ is the complement of $\sigma_{ess}(\mathcal{L})$, that is, the set of $\lambda \in \mathbb{C}$ such that $\mathcal{L} - \lambda$ is Fredholm with index zero, but the kernel is not trivial. This definition of spectrum, $\sigma(\mathcal{L}) = \sigma_{ess}(\mathcal{L}) \cup \tilde{\sigma}_{pt}(\mathcal{L})$, is due to Weyl [162] and makes the essential spectrum σ_{ess} a larger set but easier to compute, while $\tilde{\sigma}_{pt}$ only contains isolated eigenvalues (see Remark 2.2.4 in [128]).

In our setting, this definition of the spectrum for the linearized operator $\mathcal{L}$ around one of the degenerate traveling fronts φ is not particularly useful, since upon substitution of the coefficients of $\mathcal{L}$ by their constant values at $\pm\infty$, the degeneracy of the diffusion coefficient precludes a direct application of standard techniques to localize the essential spectrum [71, 128]. Such approach rely on the hyperbolicity of the asymptotic matrices (see Section 5.5 below). In particular for the operator $\mathcal{L}$ the asymptotic matrix, at the stationary state u_+, in $+\infty$ is not well defined.

5.4 Stability of the point spectrum

This section concerns with the stability of the point-spectrum of the monotone diffusion-degenerate Fisher-KPP fronts. We use energy estimates in conjunction with an appropriate change of variables, which is motivated by the monotonicity of the fronts. In order to justify the change of variables, a detailed analysis of the asymptotic behavior of solution to the spectral equation is necessary (see Section 5.8 for details).

5.4.1 Energy estimate

Let $\varphi(x)$ be any member of the family of monotone diffusion-degenerate Fisher-KPP fronts, and $\mathcal{L}$ the corresponding linearized operator around φ defined in (5.3.6). Let $\lambda \in \mathbb{C}$ be fixed. Assume that there exists a solution $u \in \mathcal{D}(\mathcal{L}) = H^2(\mathbb{R};\mathbb{C})$ of the spectral equation

$$\begin{aligned} (\mathcal{L}-\lambda)u &= 0 \\ D(\varphi)u_{xx} + (2D(\varphi)_x + c)u_x + (D(\varphi)_{xx} + f'(\varphi) - \lambda)u &= 0. \end{aligned} \tag{5.4.1}$$

Let $x_0 \in \mathbb{R}$ be fixed, but arbitrary. Denote the function

$$\theta(x) := -\frac{c}{2}\int_{x_0}^{x} \frac{ds}{D(\varphi(s))}. \tag{5.4.2}$$

Observe that $\theta(x)$ is well defined for all $x \in \mathbb{R}$, and satisfies

$$\theta_x = -\frac{c}{2D(\varphi(x))}, \quad \theta_{xx} = \frac{c}{2}\frac{D(\varphi)_x}{D(\varphi)^2},$$

for all $x \in \mathbb{R}$. Consider the transformation

$$u(x) = w(x)e^{\theta(x)}. \tag{5.4.3}$$

We compute the first and second derivatives of (5.4.3),

$$\begin{aligned} u_x &= w_x e^{\theta(x)} + w\theta_x e^{\theta(x)} \\ &= \left(w_x - \frac{c}{2D(\varphi)} w \right) e^{\theta(x)}, \end{aligned} \tag{5.4.4}$$

$$\begin{aligned} u_{xx} &= w_{xx} e^{\theta(x)} + 2w_x\theta_x e^{\theta(x)} + w\theta_{xx} e^{\theta(x)} + w\theta_x^2 e^{\theta(x)} \\ &= \left(w_{xx} - \frac{c}{D(\varphi)} w_x + \left(\frac{cD(\varphi)_x}{2D(\varphi)^2} + \frac{c^2}{4D(\varphi)^2} \right) w \right) e^{\theta(x)}. \end{aligned} \tag{5.4.5}$$

Thus, upon substitution of equations (5.4.4) and (5.4.5) in equation (5.4.1) we arrive to

$$D(\varphi) w_{xx} + 2D(\varphi)_x w_x + H(x) w - \lambda w = 0, \tag{5.4.6}$$

where

$$H(x) = D(\varphi)_{xx} + f'(\varphi) - \frac{c}{2} \frac{D(\varphi)_x}{D(\varphi)} - \frac{c^2}{4D(\varphi)}.$$

Observe that $e^{-\theta(x)}$ may diverge as $x \to +\infty$. Nevertheless, we have that $w \in H^2$ whenever $u \in H^2$, and the details are provided by the following

Lemma 5.4.1. *Let $x_0 \in \mathbb{R}$ be fixed, but arbitrary. If $u \in H^2(\mathbb{R}; \mathbb{C})$ is a solution to the spectral equation $(\mathcal{L} - \lambda)u = 0$, for fixed $\lambda \in \mathbb{C}$, then*

$$w(x) = \exp\left(\frac{c}{2} \int_{x_0}^{x} \frac{ds}{D(\varphi(s))} \right) u(x),$$

belongs to $H^2(\mathbb{R}; \mathbb{C})$.

Proof. On the non degenerate side, as $x \to -\infty$, observe that

$$\int_{x_0}^{x} \frac{ds}{D(\varphi)} = -\int_{x}^{x_0} \frac{ds}{D(\varphi)} \leq 0,$$

for all $x \leq x_0$, since the integrand is positive. Denote

$$\Theta(x) := \exp\left(\frac{c}{2} \int_{x_0}^{x} \frac{ds}{D(\varphi)} \right)$$

Hence, $\Theta(x) \to 0$ as $x \to -\infty$. Thus $\Theta(x)$ is bounded and

$$\Theta(x) \leq 1$$

for $x \in (-\infty, x_0)$.This implies that

$$|w(x)| = \Theta(x)|u(x)| \leq |u(x)|$$

for $x \in (-\infty, x_0]$, and hence $w \in L^2(-\infty, x_0)$.

For $x_0 \in \mathbb{R}$ fixed, let

$$\delta_0 := \inf_{x\in(-\infty,x_0]} D(\varphi(x)) > 0.$$

Thus, for all $x < x_0$

$$\frac{c}{2}\int_{x_0}^{x} \frac{ds}{D(\varphi)} \leq \frac{c}{2}\int_{x_0}^{x} \frac{ds}{\delta_0} = -\frac{c}{2\delta_0}|x - x_0|.$$

This implies that

$$\Theta(x) \leq \exp\left(-\frac{c}{2\delta_0}|x - x_0|\right) \to 0,$$

as $x \to -\infty$.

Computing the derivative $\Theta(x)$ with respect x we have

$$\Theta_x = \frac{c}{2}\frac{\Theta(x)}{D(\varphi)}.$$

Thus, due to the monotonicity of $D = D(\cdot)$ we obtain

$$0 < \frac{c}{2}\frac{\Theta(x)}{D(1)} \leq \Theta_x \leq \frac{c}{2\delta_0}\Theta(x) \to 0,$$

as $x \to -\infty$. This implies that $w_x = \Theta_x u + \Theta u_x \in L^2(-\infty, x_0)$.

The second derivative of $\Theta(x)$ with respect x is

$$\Theta_{xx} = \left(\frac{c^2}{4D(\varphi)} - \frac{c}{2}\frac{D'(\varphi)\varphi_x}{D(\varphi)^2}\right)\Theta(x).$$

Denote $\delta_1 = \sup_{x\in(-\infty,x_0)} |D'(\varphi(x))\varphi_x(x)| < \infty$. Hence, we estimate

$$|\Theta_{xx}| \leq \left(\frac{c^2}{4\delta_0^2} + \frac{c}{2}\frac{\delta_1}{\delta_0}\right)\Theta(x) \to 0$$

as $x \to -\infty$. This implies that $w_{xx} = \Theta_{xx}u + 2\Theta_x u_x + \Theta u_{xx} \in L^2(-\infty, x_0)$.

On the degenerate side, as $x \to +\infty$, for $x_0 \gg 1$ fixed, by Lemma 5.8.5 we have $w(x) = C\zeta(x) \in H^2(x_0, +\infty)$. This implies $w \in H^2(\mathbb{R}; \mathbb{C})$, and the proof is complete.

□

Multiply equation (5.4.6) by $D(\varphi)$, and arrange terms to get

$$(D(\varphi)^2 w_x)_x + D(\varphi)H(x)w - \lambda D(\varphi)w = 0. \tag{5.4.7}$$

Recall that $\varphi_x \in \ker \mathcal{L}$, thus $u = \varphi_x$ is solution to equation (5.4.1) for $\lambda = 0$. Consider the transformation

$$\varphi_x = \psi(x)e^{\theta(x)}, \tag{5.4.8}$$

and substituting in (5.4.1), with $\lambda = 0$, we obtain

$$D(\varphi)\psi_{xx} + 2D(\varphi)_x\psi_x + H(x)\psi = 0.$$

Multiplying last equation by $D(\varphi)$ yields

$$(D(\varphi)^2\psi_x)_x + D(\varphi)H(x)\psi = 0.$$

Observe that $\psi(x) \neq 0$ for all $x \in \mathbb{R}$, due to the monotonicity of the front, $\varphi_x < 0$. Therefore, we may write

$$D(\varphi)H(x) = -\frac{(D(\varphi)^2\psi_x)_x}{\psi}. \tag{5.4.9}$$

Hence, substituting (5.4.9) in (5.4.7) yields

$$(D(\varphi)^2 w_x)_x - \frac{(D(\varphi)^2\psi_x)_x}{\psi}w = \lambda D(\varphi)w.$$

Take the L^2-product of w with last equation, we obtain

$$\lambda\int_{\mathbb{R}} D(\varphi)|w|^2dx = \int_{\mathbb{R}}(D(\varphi)^2 w_x)_x w^* dx - \int_{\mathbb{R}}\frac{(D(\varphi)^2\psi_x)_x}{\psi}|w|^2dx. \tag{5.4.10}$$

Integrate by parts on the right hand side of (5.4.10) to get

$$\begin{aligned}\lambda\int_{\mathbb{R}} D(\varphi)|w|^2dx &= -\int_{\mathbb{R}} D(\varphi)^2|w_x|^2dx + \int_{\mathbb{R}} D(\varphi)^2\psi_x\left(\frac{|w|^2}{\psi}\right)_x dx \\ &= \int_{\mathbb{R}} D(\varphi)^2\left(\psi_x\left(\frac{|w|^2}{\psi}\right)_x - |w_x|^2\right)dx.\end{aligned} \tag{5.4.11}$$

Before proceeding any further we provide the following

Lemma 5.4.2.

$$\psi_x\left(\frac{|w|^2}{\psi}\right)_x - |w_x|^2 = -\psi^2\left|\left(\frac{w}{\psi}\right)_x\right|^2.$$

Proof. The proof is straightforward. Observe that by definition $\psi(x) < 0$ for all $x \in \mathbb{R}$. Thus,

$$\begin{aligned}
\psi^2 \left| \left(\frac{w}{\psi}\right)_x \right|^2 &= \psi^2 \left(\frac{w}{\psi}\right)_x \overline{\left(\frac{w}{\psi}\right)_x} \\
&= \psi^2 \left(\frac{w_x\psi - w\psi_x}{\psi^2}\right)\left(\frac{\bar{w}_x\psi - \bar{w}\psi_x}{\psi^2}\right) \\
&= \frac{1}{\psi^2}\left(|w_x|^2\psi^2 - (w_x\bar{w} + w\bar{w}_x)\psi\psi_x + |w|^2\psi_x^2\right) \\
&= \frac{1}{\psi^2}\left(|w_x|^2\psi^2 - (w\bar{w})_x\psi\psi_x + |w|^2\psi_x^2\right) \qquad (5.4.12) \\
&= \frac{1}{\psi^2}\left(|w_x|^2\psi^2 - (|w|^2)_x\psi\psi_x + |w|^2\psi_x^2\right) \\
&= |w_x|^2 - \frac{\psi_x}{\psi^2}\left((|w|^2)_x\psi - |w|^2\psi_x\right) \\
&= |w_x|^2 - \psi_x\left(\frac{|w|^2}{\psi}\right)_x
\end{aligned}$$

□

Therefore, using the identity from Lemma 5.4.2 in equation (5.4.11) we obtain

$$\lambda \int_{\mathbb{R}} D(\varphi)|w|^2 dx = -\int_{\mathbb{R}} D(\varphi)^2\psi^2 \left| \left(\frac{w}{\psi}\right)_x \right|^2 dx. \qquad (5.4.13)$$

Let us denote the standard L^2-product as

$$\langle u, v\rangle_{L^2} = \int_{\mathbb{R}} u^* v \, dx, \quad \|u\|_{L^2}^2 = \langle u, u\rangle_{L^2}.$$

Hence, we may write equation (5.4.13) as

$$\lambda\langle D(\varphi)w, w\rangle_{L^2} = -\|D(\varphi)\psi(w/\psi)_x\|_{L^2}^2.$$

Remark 2. Observe that, thanks to Lemma 5.4.1, $w \in H^2$, $\psi \in H^2$. Due to monotonicity of the front, $\psi < 0$, then the L^2-products of last equation are well-defined.

We summarize these calculations as follows.

Proposition 5.4.3 (basic energy estimate)**.** *For any $\lambda \in \mathbb{C}$, suppose that there exist a solution $u \in H^2(\mathbb{R};\mathbb{C})$ to the spectral equation $(\mathcal{L} - \lambda)u = 0$. Then there holds the energy estimate*

$$\lambda\langle D(\varphi)w, w\rangle_{L^2} = -\|D(\varphi)\psi(w/\psi)_x\|_{L^2}^2.$$

where $w = e^{-\theta}u \in H^2(\mathbb{R};\mathbb{C})$, and $\psi = e^{-\theta}\varphi_x \in H^2(\mathbb{R};\mathbb{C})$ is a non-vanishing real function, and $\theta = \theta(x)$ is defined in (5.4.2)*.*

5.4.2 Localization of the point spectrum

This section is concerned with the stability of the point spectrum, $\sigma_{pt}(\mathcal{L})$. For that purpose, we apply the basic energy estimate to show that the point spectrum is real and non-positive. We have the following

Theorem 5.4.4. *All monotone fronts of diffusion degenerate Fisher-KPP equations are point spectrally stable. More precisely,*

$$\sigma_{pt}(\mathcal{L}) \subset (-\infty, 0]$$

that is, L^2-point spectrum and non positive.

Proof. Let $\varphi = \varphi(x)$ be a degenerate Fisher-KPP monotone front and $\mathcal{L}$ the linearized operator around φ defined in (5.3.6). Let $\lambda \in \sigma_{pt}(\mathcal{L})$. Therefore, there exist $u \in H^2(\mathbb{R};\mathbb{C})$ such that $(\mathcal{L} - \lambda)u = 0$. Applying the Proposition 5.4.3 we arrive to the energy estimate

$$\lambda \langle D(\varphi)w, w\rangle_{L^2} = -\|D(\varphi)\psi(w/\psi)_x\|^2_{L^2} \leq 0. \tag{5.4.14}$$

The inequality holds because the diffusion coefficient $D(\varphi) > 0$ for all $x \in \mathbb{R}$. Therefore, we conclude that $\lambda \in \mathbb{R}$ and $\lambda \leq 0$. □

Corolary 5.4.5. $\lambda = 0$ *has geometric multiplicity equal to one, that is,* $\dim\ker \mathcal{L} = 1$. *Moreover,* $\ker \mathcal{L} = \operatorname{span}\{\varphi_x\}$.

Proof. It follows from equation (5.4.14), for $\lambda = 0$, that

$$\|D(\varphi)\psi(w/\psi)_x\|^2_{L^2} = \int_{\mathbb{R}} D(\varphi)^2\psi^2 \left|\left(\frac{w}{\psi}\right)_x\right|^2 dx = 0.$$

Thus, since $D(\varphi) > 0$ and $\psi(x) > 0$ for all $x \in \mathbb{R}$, we have that

$$\left(\frac{w}{\psi}\right)_x = 0, \quad \text{a.e. in } \mathbb{R}.$$

Hence, $w = \alpha\psi$ for some constant $\alpha \neq 0$. Therefore,

$$u = \alpha\varphi_x,$$

and we conclude that if $u \in \ker \mathcal{L}$ then necessarily is a constant multiple of φ_x, and the proof is complete. □

5.5 Localization of the compressed spectrum

In this section we introduce a regularization technique to circumvent the degeneracy of the diffusion coefficient, and to locate a subset of the compressed spectrum of the linearized operator around the front. This approach is based on the generalized convergence of operators and exploits the robustness of Fredholm properties.

5.5.1 The perturbed operator

Let $\epsilon > 0$. We denote

$$D^\epsilon(\varphi) := D(\varphi) + \epsilon \tag{5.5.1}$$

as a perturbation of the diffusion coefficient $D(\varphi)$. We define the regularized operator as

$$\begin{aligned} &\mathcal{L}^\epsilon : \mathcal{D}(\mathcal{L}^\epsilon) = H^2(\mathbb{R};\mathbb{C}) \subset L^2(\mathbb{R};\mathbb{C} \to L^2(\mathbb{R};\mathbb{C}) \\ &\mathcal{L}^\epsilon u = (D^\epsilon(\varphi)u)_{xx} + cu_x + f'(\varphi)u. \end{aligned} \tag{5.5.2}$$

Observer that, for every $\epsilon > 0$, operator $-\mathcal{L}^\epsilon$ is a linear, closed, densely defined and strongly elliptic operator acting on L^2, since $D^\epsilon(\varphi) \geq \epsilon > 0$. For the same reason, multiplication by $D^\epsilon(\varphi)^{-1}$ is an isomorphism. Thus, Fredholm properties of $(\mathcal{L}^\epsilon - \lambda)$ and those of the operator $\mathcal{J}^\epsilon(\lambda) : H^2(\mathbb{R};\mathbb{C}) \subset L^2(\mathbb{R};\mathbb{C}) \to L^2(\mathbb{R};\mathbb{C})$ defined as

$$\begin{aligned} \mathcal{J}^\epsilon(\lambda) &:= D^\epsilon(\varphi)^{-1}(\mathcal{L}^\epsilon - \lambda)u \\ &= u_{xx} + D^\epsilon(\varphi)^{-1}a_1(x)u_x + D^\epsilon(\varphi)^{-1}(a_0(x) - \lambda)u \end{aligned} \tag{5.5.3}$$

for $u \in H^2(\mathbb{R};\mathbb{C})$, are the same. The coefficients $a_1(x), a_0(x)$ are

$$a_1(x) = 2D^\epsilon(\varphi)_x + c, \quad a_0(x) = D(\varphi)_{xx} + f'(\varphi).$$

Following Alexander, Gardner and Jones [4], we rewrite operator (5.5.2) as a first order operator of the form

$$\begin{aligned} &\mathcal{T}^\epsilon(\lambda) : H^1(\mathbb{R};\mathbb{C}^2) \subset L^2(\mathbb{R};\mathbb{C}^2) \to L^2(\mathbb{R};\mathbb{C}) \\ &\mathcal{T}^\epsilon(\lambda) := \partial_x - A^\epsilon(\cdot;\lambda), \end{aligned} \tag{5.5.4}$$

where

$$A^\epsilon(x;\lambda) = \begin{pmatrix} 0 & 1 \\ D^\epsilon(\varphi)^{-1}(\lambda - a_0(x)) & -D^\epsilon(\varphi)^{-1}a_1(x) \end{pmatrix}.$$

It is a known fact (cf. [71, 128]) that operators $\mathcal{T}^\epsilon(\lambda)$ and $\mathcal{J}^\epsilon(\lambda)$ share the same Fredholm properties, and as result, $\mathcal{L}^\epsilon - \lambda$ will too (see Theorem 3.2 in

Ref. [99]). Furthermore, the Fredholm properties depend upon hyperbolicity of the asymptotic matrices [128]

$$\mathbb{A}^{\epsilon}_{\pm}(\lambda) := \lim_{x\to\pm\infty} \mathbb{A}^{\epsilon}(x;\lambda) = \begin{pmatrix} 0 & 1 \\ D^{\epsilon}(u_{\pm})^{-1}(\lambda - f'(u_{\pm})) & -D^{\epsilon}(u_{\pm})^{-1}c \end{pmatrix}. \quad (5.5.5)$$

Thus, we have to characterize the $\lambda \in \mathbb{C}$ for which $\mathbb{A}^{\epsilon}_{\pm}(\lambda)$ lose their hyperbolicity. For that purpose we compute the matrix eigenvalues, and define the characteristic polynomial of $\mathbb{A}^{\epsilon}_{\pm}(\lambda)$ as

$$\pi^{\epsilon}_{\pm}(\lambda,\mu) := \det(A^{\epsilon}_{\pm}(\lambda) - \mu). \quad (5.5.6)$$

Observe that the matrix eigenvalues μ depend continuously on the spectral parameter λ. By definition, asymptotic matrices will lose its hyperbolicity when there exist a matrix eigenvalue with zero real part, i.e., $\operatorname{Re}\mu(\lambda) = ik$ for $k \in \mathbb{R}$. We introduce the complex dispersion relation

$$\pi^{\epsilon}_{\pm}(\lambda, ik) = -k^2 + ikcD^{\epsilon}(u_{\pm})^{-1} + D^{\epsilon}(u_{\pm})^{-1}(f'(u_{\pm}) - \lambda) = 0. \quad (5.5.7)$$

Thus, the λ-roots of the dispersion relation (5.5.7) define algebraic curves in λ-complex plane with the following form

$$\lambda^{\epsilon}_{\pm}(k) := -D(u_{\pm})k^2 + ick + f'(u_{\pm}), \quad (5.5.8)$$

parametrized by the real parameter $k \in \mathbb{R}$. We note that for each curve $\lambda^{\epsilon}_{\pm}(k)$ the point at rightmost position is $f'(u_{\pm})$. Consider the following open connected subset of the complex plane

$$\Omega := \{\lambda \in \mathbb{C} : \operatorname{Re}\lambda > \max\{f'(u_-), f'(u_+)\}\},$$

which is called the region of consistent splitting. We denote, for each fixed $\lambda \in \mathbb{C}$ and $\epsilon > 0$, $S^{\epsilon}_{\pm}(\lambda)$, $U^{\epsilon}_{\pm}(\lambda)$ and $C^{\epsilon}_{\pm}(\lambda)$ as the stable, unstable and center eigenspaces of $\mathbb{A}^{\epsilon}_{\pm}(\lambda)$ in $\mathbb{C}^2$, respectively.

Lemma 5.5.1. *For each $\lambda \in \Omega$ and all $\epsilon > 0$, the asymptotic matrices $\mathbb{A}^{\epsilon}_{\pm}(\lambda)$ have no center eigenspace and* $\dim S^{\epsilon}_{\pm}(\lambda) = U^{\epsilon}_{\pm}(\lambda) = 1$.

Proof. A point $\lambda \in \mathbb{C}$ will be on the curves $\lambda^{\epsilon}_{\pm}(k)$ precisely when there exist a matrix eigenvalue that satisfy $\mu(\lambda) = ik$ for $k \in \mathbb{R}$. Thus, if $\lambda \in \Omega$ then $\dim C^{\epsilon}_{\pm}(\lambda) = 0$, since by definition

$$\operatorname{Re}\lambda > \max_{k\in\mathbb{R}} \operatorname{Re}\lambda^{\epsilon}_{\pm}(k) = f'(u_{\pm}),$$

and this last quantity is independent of ϵ. The characteritic polynomial (5.5.6) has one positive and one negative root:

$$\begin{aligned}\mu_1 &= \frac{1}{2D^\epsilon(u_\pm)}\left(-c+\sqrt{c^2+4D^\epsilon(u_\pm)(\eta-f'(u_\pm)}\right)>0,\\ \mu_2 &= \frac{1}{2D^\epsilon(u_\pm)}\left(-c-\sqrt{c^2+4D^\epsilon(u_\pm)(\eta-f'(u_\pm)}\right)<0,\end{aligned} \tag{5.5.9}$$

for $\eta > \max\{f'(u_\pm)\}$ large enough. By continuity on λ and by connectedness Ω, the dimensions $\dim S^\epsilon_\pm(\lambda) = \dim U^\epsilon_\pm(\lambda) = 1$ remain constant in Ω. □

Lemma 5.5.2. *For all $\epsilon > 0$ and for each $\lambda \in \Omega$, the operator $\mathcal{L}^\epsilon - \lambda$ is Fredholm with index zero.*

Proof. Let $\lambda \in \Omega$. Thus, by Lemma 5.5.1, the matrices $\mathbb{A}^\epsilon_\pm(\lambda)$ are hyperbolic. It follows from Theorem 3.3 in Ref. [128] that the system has exponential dychotomies on $\mathbb{R}^\pm$, with Morse indices $i_\pm(\lambda) = \dim U^\epsilon_\pm(\lambda) = 1$. It follows from Theorem 3.2 (and Remark 3.3) in [128], that the operators $\mathcal{T}^\epsilon(\lambda)$ are Fredholm with index

$$\mathrm{ind}\mathcal{T}^\epsilon(\lambda) = i_-(\lambda) - i_+(\lambda) = 0.$$

Therefore, we conclude that $\mathcal{J}^\epsilon(\lambda)$ and $\mathcal{L}^\epsilon - \lambda$ are Fredholm with index zero, as well. □

5.6 Generalized convergence

We shall seize the robustness of Fredholm properties under "small" perturbations of a closed operator, and use the independence of $\mathrm{ind}(\mathcal{L}^\epsilon - \lambda)$ with respect of $\epsilon > 0$ to make conclusions about the Fredholm properties of $\mathcal{L} - \lambda$. In turn, this will aid us to locate $\sigma_\delta(\mathcal{L})$. We introduce the succeeding notation following Kato [72].

Definition 5. Let Z be a Banach space, M and N nontrivial closed subspaces of Z. We denote by S_M the unitary sphere of M (the set of all $u \in M$ with $||u|| = 1$). For any two closed subspaces M, N we set

$$\delta(M,N) = \sup_{u\in S_M} \mathrm{dist}(u,N),$$

$$\hat{\delta}(M,N) = \max[\delta(M,N), \delta(N,M)].$$

$\hat{\delta}$ is called the *gap* between M and N.

Remark 3. In general, $\hat{\delta}(M,N)$ does not satisfy the triangle inequality, so the function $\hat{\delta}$ can not be used to define a distance between M and N. We modify slightly the definition of $\hat{\delta}$; we set

$$\mathrm{d}(M,N) = \sup_{u\in S_M} \mathrm{dist}(u, S_N),$$

$$\hat{\mathrm{d}}(M,N) = \max[\mathrm{d}(M,N), \mathrm{d}(N,M)].$$

The functions d and $\hat{\mathrm{d}}$ satisfy the triangle inequality; $\hat{\mathrm{d}}(M,N)$ is called the distance between M and N. Furthermore, we have the following inequalities

$$\delta(M,N) \le \mathrm{d}(M,N) \le 2\delta(M,N)$$
$$\hat{\delta}(M,N) \le \hat{\mathrm{d}}(M,N) \le 2\hat{\delta}(M,N).$$

Definition 6. Let X, Y be Banach spaces. Consider $\mathscr{C}(X,Y)$, set of all closed operators from X to Y. If $T, S \in \mathscr{C}(X,Y)$, then the graphs $G(T), G(S)$ are closed subspaces of $X \times Y$, and we set

$$\mathrm{d}(T,S) = \mathrm{d}(G(T), G(S)),$$

$$\hat{\mathrm{d}}(T,S) = \max[\mathrm{d}(T,S), \mathrm{d}(S,T)].$$

A sequence $T_n \in \mathscr{C}(X,Y)$ converges to $T \in \mathscr{C}(X,Y)$ if $\hat{\mathrm{d}}(T_n, T) \to 0$.

Remark 4. It follows from Remark 3 that the convergence $\hat{\mathrm{d}}(T_n, T) \to 0$ is equivalent to $\hat{\delta}(T_n, T) \to 0$. In this case we say that T_n converges to $T (T_n \to T)$ in a *generalized sense.*

Lemma 5.6.1. *For each fixed $\lambda \in \mathbb{C}$, the operators $\mathcal{L}^\epsilon - \lambda$ converge in generalized sense to $\mathcal{L} - \lambda$ as $\epsilon \to 0^+$.*

Proof. From the definition of $d(\cdot,\cdot)$ we have

$$\mathrm{d}(\mathcal{L}^\epsilon - \lambda, \mathcal{L} - \lambda) = d(G(\mathcal{L}^\epsilon - \lambda), G(\mathcal{L} - \lambda)) = \sup_{v \in S_{G(\mathcal{L}^\epsilon - \lambda)}} \left(\inf_{w \in S_{G(\mathcal{L}-\lambda)}} \|v - w\| \right).$$

Let $v \in S_{G(\mathcal{L}^\epsilon - \lambda)}$ be such that $v = \{p, (\mathcal{L}^\epsilon - \lambda)p\}$ for $p \in \mathcal{D}(\mathcal{L}^\epsilon - \lambda) = H^2$, and

$$\|v\|^2_{L^2 \times L^2} = \|p\|^2_{L^2} + \|(\mathcal{L}^\epsilon - \lambda)p\|^2_{L^2} = 1.$$

In a similar manner, let $w \in S_{G(\mathcal{L}-\lambda)}$ be such that $w = \{u, (\mathcal{L} - \lambda)u\}$, for $u \in \mathcal{D}(\mathcal{L} - \lambda) = H^2$ and

$$\|w\|^2_{L^2 \times L^2} = \|u\|^2_{L^2} + \|(\mathcal{L} - \lambda)u\|^2_{L^2} = 1.$$

Now, we find a upper bound for $\|v-w\|_{L^2\times L^2}$ so the set consisting of the infima taken over $S_{G(\mathcal{L}-\lambda)}$ is bounded, and consequently the supremum of $S_{G(\mathcal{L}^\epsilon-\lambda)}$ is bounded. Consider

$$\|v-w\|^2_{L^2\times L^2} = \|p-u\|^2_{L^2} + \|(\mathcal{L}^\epsilon-\lambda)p-(\mathcal{L}-\lambda)u\|^2_{L^2} \tag{5.6.1}$$

If we keep $v \in S_{G(\mathcal{L}^\epsilon-\lambda)}$ fixed, then it suffices to take $w = \{p, (\mathcal{L}-\lambda)p\}$, since $p \in \mathcal{D}(\mathcal{L}^\epsilon-\lambda) = \mathcal{D}(\mathcal{L}-\lambda)$. Observe that $(\mathcal{L}-\lambda)p = (\mathcal{L}^\epsilon-\lambda)p - \epsilon p_{xx}$. Therefore equation (5.6.1) reduces to

$$\|v-w\|^2_{L^2\times L^2} = \|(\mathcal{L}^\epsilon-\lambda)p-(\mathcal{L}-\lambda)p\|^2_{L^2} = \|\epsilon p_{xx}\|^2_{L^2}.$$

If we regard ∂_x^2 as a closed, densely defined operator acting on $L^2(\mathbb{R};\mathbb{C})$, with domain $\mathcal{D} = H^2(\mathbb{R};\mathbb{C})$, then it follows [72, Remark 1.5, pp. 191] that ∂_x^2 is $(\mathcal{L}^\epsilon - \lambda)-$bounded, i.e., there exist a constant $C>0$ such that

$$\|p_{xx}\|^2_{L^2} \le C(\|p\|^2_{L^2} + \|(\mathcal{L}^\epsilon-\lambda)p\|^2_{L^2}) = C,$$

for all $p \in H^2$.

We shall find an expression for C. For that purpose, we write down operator $(\mathcal{L}^\epsilon-\lambda)p$,

$$(\mathcal{L}^\epsilon-\lambda)p = (D(\varphi)+\epsilon)p_{xx} + (2D(\varphi)_x + c)p_x + (D(\varphi)_{xx} + f'(\varphi) - \lambda)p.$$

We denote

$$\begin{aligned} m_2 &= \inf_{x\in\mathbb{R}}(D(\varphi)+\epsilon), \\ M_1 &= \sup_{x\in\mathbb{R}}|2D(\varphi)_x + c|, \\ M_0 &= \sup_{x\in\mathbb{R}}|D(\varphi)_{xx} + f'(\varphi) - \lambda|. \end{aligned} \tag{5.6.2}$$

Observe that $m_2 = \epsilon > 0$, and $M_1, M_0 < \infty$. Thus, we have the lower bound

$$\|(\mathcal{L}^\epsilon-\lambda)p\|_{L^2} \ge m_2\|p_{xx}\|_{L^2} - M_1\|p_x\|_{L^2} - M_0\|p\|_{L^2}. \tag{5.6.3}$$

Let $\mu > 0$ be an arbitrary positive constant. By Lemma VI.6.1 in [54], there exist a constant $C_\mu > 0$ such that

$$\|p_x\|_{L^2} \le \mu\|p_{xx}\|_{L^2} + C_\mu\|p\|_{L^2}. \tag{5.6.4}$$

Hence, substituting (5.6.4) in (5.6.3) we obtain

$$\|(\mathcal{L}^\epsilon-\lambda)p\|_{L^2} \ge (m_2-\mu M_1)\|p_{xx}\|_{L^2} - (M_0+C_\mu)\|p\|_{L^2} \tag{5.6.5}$$

Let μ be such that $m_2 > \mu M_1$.Then

$$\frac{1}{(m_2-\mu M_1)}\|(\mathcal{L}^\epsilon-\lambda)p\|_{L^2} \geq \|p_{xx}\|_{L^2} - \frac{(M_0+C_\mu)}{(m_2-\mu M_1)}\|p\|_{L^2}.$$

Then,

$$\frac{1}{(m_2-\mu M_1)}\|(\mathcal{L}^\epsilon-\lambda)p\|_{L^2} + \frac{(M_0+C_\mu)}{(m_2-\mu M_1)}\|p\|_{L^2} \geq \|p_{xx}\|_{L^2}.$$

Denote,

$$a = \frac{1}{(m_2-\mu M_1)},\ b = \frac{(M_0+C_\mu)}{(m_2-\mu M_1)}. \tag{5.6.6}$$

Let $\eta > 0$. Hence,

$$(a^2+\eta ab)\|(\mathcal{L}^\epsilon-\lambda)p\|_{L^2}^2 + (b^2+ab/\eta)\|p\|_{L^2}^2 \geq \|p_{xx}\|_{L^2}^2. \tag{5.6.7}$$

We can choose

$$C = \max\left(a^2+\eta ab, b^2+ab/\eta\right). \tag{5.6.8}$$

Therefore

$$\|v-w\|_{L^2\times L^2}^2 = \|\epsilon p_{xx}\|_{L^2}^2 \leq \epsilon^2 C,$$

yielding

$$\mathrm{d}(\mathcal{L}^\epsilon-\lambda, \mathcal{L}-\lambda) \leq \epsilon^2 C.$$

In a similar fashion it can be proved that

$$\mathrm{d}(\mathcal{L}-\lambda, \mathcal{L}^\epsilon-\lambda) \leq \epsilon^2 C.$$

This shows

$$\hat{\mathrm{d}}(\mathcal{L}^\epsilon-\lambda, \mathcal{L}-\lambda) \to 0$$

as $\epsilon \to 0$, and the result is proved. □

We quote the following result from Kato [72], is known as the *general stability theorem*, and is the main tool to conclude the robustness of Fredholm properties.

Theorem 5.6.2 ([72]). *Let $T, S \in \mathscr{C}(X,Y)$ and let S be Fredholm. If*

$$\hat{\delta}(S,T) < \gamma(1+\gamma^2)^{-1/2},$$

where $\gamma = \gamma(S)$, then T is Fredholm and

$$\mathrm{nul}(T) \leq \mathrm{nul}(S), \qquad \mathrm{def}(T) \leq \mathrm{def}(S).$$

Furthermore, there exists $\delta > 0$ such that $\hat{\delta}(S,T) < \delta$ implies

$$\mathrm{ind}(S) = \mathrm{ind}(T).$$

Remark 5. If X, Y are Hilbert spaces we can take $\delta = \gamma(1+\gamma^2)^{-\frac{1}{2}}$ (cf. [72]).

Theorem 5.6.3. *Let $\varphi = \varphi(x)$ be a diffusion-degenerate Fisher-KPP front, and let $\mathcal{L} \in \mathscr{C}(L^2)$ be the linearized operator around φ defined in* (5.3.6)*. Then*

$$\sigma_\delta(\mathcal{L}) \subset \mathbb{C} \setminus \Omega.$$

Proof. Let $\lambda \in \sigma_\delta(\mathcal{L})$. By definition, $\mathcal{R}(\mathcal{L}-\lambda)$ is closed and $\mathcal{L}-\lambda$ is injective. Thus, $\mathrm{nul}(\mathcal{L}-\lambda) = 0$. In addition, being λ in the compression spectrum, the range $\mathcal{R}(\mathcal{L}-\lambda)$ is not all L^2 and $\mathcal{L}-\lambda$ is not surjective. This implies that $\mathrm{def}(\mathcal{L}-\lambda) = \mathrm{codim}\mathcal{R}(\mathcal{L}-\lambda) > 0$. Thus, $\mathcal{L}-\lambda$ is semi-Fredholm with index $\mathrm{ind}(\mathcal{L}-\lambda) \neq 0$.

Now, we proceed by contradiction and suppose that $\lambda \in \sigma_\delta(\mathcal{L}) \cap \Omega$. Hence, $\gamma := \gamma(\mathcal{L}-\lambda) > 0$, since $\mathcal{R}(\mathcal{L}-\lambda)$ is closed (see Theorem 5.2 in [72, p. 231].

By Lemma 5.6.1, $\hat{\delta}(\mathcal{L}^\epsilon - \lambda, \mathcal{L}-\lambda) \to 0$ as $\epsilon \to 0^+$. This implies that there exist $\epsilon > 0$ small enough such that

$$\hat{\delta}(\mathcal{L}^\epsilon - \lambda, \mathcal{L}-\lambda) < \gamma(1+\gamma^2)^{-1/2}.$$

Since $X = L^2(\mathbb{R};\mathbb{C})$ is a Hilbert space, Theorem 5.6.2 implies that

$$\mathrm{ind}(\mathcal{L}-\lambda) = \mathrm{ind}(\mathcal{L}^\epsilon - \lambda) = 0,$$

due to $\lambda \in \Omega$ and Lemma 5.5.2. This is a contradiction with $\mathrm{ind}(\mathcal{L}-\lambda) \neq 0$. Therefore, $\sigma_\delta(\mathcal{L}) \cap \Omega = \emptyset$, and

$$\sigma_\delta(\mathcal{L}) \subset \mathbb{C} \setminus \Omega.$$

□

Remark 6. Observe that the definition of the region of consistent splitting Ω depends on $f'(u_\pm)$. This in turn implies that the location, and hence stability of $\sigma_\delta(\mathcal{L})$ depend on the sign of $f'(u_\pm)$. In this case, $f'(0) > 0$, making $\sigma_\delta(\mathcal{L})$ unstable. It is, however, sensitive to changes at spatial infinity, and it is possible to find exponentially weighted spaces where the stability of σ_δ holds.

5.7 Spectral stability in exponentially weighted spaces

In this section we introduce the exponentially weighted spaces. Under certain conditions on the velocity, we found an appropriated weight function. Thus, in this suitable weighted space, the subset σ_δ of the spectrum of the linearized operator computed with respect to the new space, is stable.

5.7.1 Exponentially weighted spaces

We introduce the exponentially weighted spaces

$$H^m_a(\mathbb{R};\mathbb{C}) = \{v : e^{ax}v(x) \in H^m(\mathbb{R};\mathbb{C})\},$$

for $m \in \mathbb{N} \cup \{0\}$ and any $a \in \mathbb{R}$. These weighted spaces are Hilbert spaces with the inner product and norm

$$\langle u, v\rangle_{H^m_a} := \langle e^{ax}u, e^{ax}v\rangle_{H^m}, \quad \|v\|^2_{H^m_a} := \|e^{ax}v\|^2_{H^m} = \langle v, v\rangle_{H^m_a}.$$

As usual, we denote $L^2_a(\mathbb{R};\mathbb{C}) = H^0(\mathbb{R};\mathbb{C})$, equipped with the norm

$$\|v\|^2_{L^2_a} := \int_{-\infty}^{+\infty} |e^{ax}v(x)|^2 dx.$$

Note that the norms $\|\cdot\|_{L^2_a}$ for different values of a are not equivalent.

It is known [71] that if the spectral problem is recast in a exponentially weighted space then the Fredholm borders may move depending on the sign of a. In the sequel, we consider the operator $\mathcal{L}$ acting on L^2_a

$$\mathcal{L} : \mathcal{D}_a := H^2_a(\mathbb{R};\mathbb{C}) \subset L^2_a(\mathbb{R};\mathbb{C}) \to L^2_a(\mathbb{R};\mathbb{C}),$$

and compute its spectrum with respect to the norm $\|\cdot\|_{L^2_a}$ for appropriate values of a. To be more specific, for $a > 0$ the norm $\|\cdot\|_{L^2_a}$ penalizes perturbations at $+\infty$, while it tolerates perturbations at $-\infty$ which may grow exponentially with any rate less than $a > 0$. Thus, Fredholm borders calculated in the norm $\|\cdot\|_{L^2_a}$ move to the left, whereas the point spectrum remains the same [71].

Let $v = e^{ax}u$, thus $u \in L^2_a(\mathbb{R})$ if and only if $v \in L^2(\mathbb{R})$. The spectral problem for the operator $\mathcal{L}$ in L^2_a is taken to one for the conjugated operator $\mathcal{L}_a := e^{ax}\mathcal{L}e^{-ax}$ in L^2, where

$$\mathcal{L}_a : \mathcal{D}(\mathcal{L}_a) := H^2(\mathbb{R};\mathbb{C}) \subset L^2(\mathbb{R};\mathbb{C}) \to L^2(\mathbb{R};\mathbb{C}).$$

Consider the operator $\mathcal{L}$ defined in (5.3.6), thus operator $\mathcal{L}_a$ has the explicit form

$$\begin{aligned}
\mathcal{L}_a u &= e^{ax}[\mathcal{L}(e^{-ax}u)] \\
&= e^{ax}\left[(D(\varphi)e^{-ax}u)_{xx} + c(e^{-ax}u)_x + f'(\varphi)e^{-ax}u\right] \\
&= e^{ax}\big[D(\varphi)(u_{xx} - 2au_x + a^2u)e^{-ax} + (2D(\varphi)_x + c)(u_x - au)e^{-ax} + \\
&\quad + (D(\varphi)_{xx} + f'(\varphi))ue^{-ax}\big] \\
&= D(\varphi)u_{xx} + (2D(\varphi)_x - 2aD(\varphi) + c)u_x + \\
&\quad + (D(\varphi)_{xx} + f'(\varphi) + a^2D(\varphi) - 2aD(\varphi)_x - ac)u
\end{aligned} \tag{5.7.1}$$

for all $u \in H^2$. $\mathcal{L}_a$ is a closed, densely defined operator in L^2.

5.7.2 Calculation of the Fredholm curves

To select an appropriate value for the parameter a, we shall compute the curves that limit the set $\sigma_\delta(\mathcal{L}_a)$ in order to find in which form the weight function e^{ax} moves the set $\sigma_\delta(\mathcal{L})$.

We follow the methods of Section 5.5, and introduce a perturbation of the diffusion coefficient $D^\epsilon(\varphi) = D(\varphi) + \epsilon$, for $0 < \epsilon \ll 1$. Thus, the regularized operator $\mathcal{L}_a^\epsilon$ is defined by substituting $D(\varphi)^\epsilon$ in (5.7.1), and has the following form

$$\begin{aligned}\mathcal{L}_a^\epsilon u = D^\epsilon(\varphi)u_x x + (2D^\epsilon(\varphi)_x - 2aD^\epsilon(\varphi) + c)u_x + \\ + (D^\epsilon(\varphi)_{xx} + f'(\varphi) + a^2 D^\epsilon(\varphi) - 2aD^\epsilon(\varphi)_x - ac)u.\end{aligned}$$

Accordingly, for any $\lambda \in \mathbb{C}$ we define

$$\begin{aligned}\mathcal{J}_a^\epsilon(\lambda) &:= D^\epsilon(\varphi)^{-1}(\mathcal{L}_a^\epsilon - \lambda)u \\ &= u_{xx} + D^\epsilon(\varphi)^{-1}b_{1,a}^\epsilon(x)u_x + D^\epsilon(\varphi)^{-1}(b_{0,a}^\epsilon(x) - \lambda)u,\end{aligned} \tag{5.7.2}$$

where

$$\begin{aligned}b_{1,a}^\epsilon(x) &= 2D^\epsilon(\varphi)_x - 2aD^\epsilon(\varphi) + c, \\ b_{0,a}^\epsilon(x) &= D^\epsilon(\varphi)_{xx} + f'(\varphi) + a^2 D^\epsilon(\varphi) - 2aD^\epsilon(\varphi)_x - ac.\end{aligned} \tag{5.7.3}$$

We recast the spectral problem as a first order system of the form

$$W_x = \mathbb{A}_a^\epsilon(x, \lambda)W,$$

where

$$W = \begin{pmatrix} u \\ u_x \end{pmatrix} \in H^2(\mathbb{R}; \mathbb{C}^2), \;\; A_a^\epsilon(x; \lambda) = \begin{pmatrix} 0 & 1 \\ D^\epsilon(\varphi)^{-1}(\lambda - b_{0,a}^\epsilon(x)) & -D^\epsilon(\varphi)^{-1}b_{1,a}^\epsilon(x) \end{pmatrix}.$$

The constant asymptotic matrices are

$$\mathbb{A}_a^{\epsilon,\pm}(\lambda) := \lim_{x\to\pm\infty} \mathbb{A}_a^\epsilon(x; \lambda) = \begin{pmatrix} 0 & 1 \\ D^\epsilon(u_\pm)^{-1}(\lambda - b_{0,a}^{\epsilon,\pm}) & -D^\epsilon(u_\pm)^{-1}b_{1,a}^{\epsilon,\pm} \end{pmatrix}, \tag{5.7.4}$$

where

$$\begin{aligned}b_{1,a}^{\epsilon,\pm} &:= \lim_{x\to\pm\infty} b_{1,a}^\epsilon(x) = c - 2aD(u_\pm)^\epsilon, \\ b_{0,a}^{\epsilon,\pm} &:= \lim_{x\to\pm\infty} b_{0,a}^\epsilon(x) = f'(u_\pm) + a^2 D^\epsilon(u_\pm) - ac.\end{aligned}$$

To compute the matrix eigenvalues of $\mathbb{A}_a^{\epsilon,\pm}(\lambda)$, we introduce the characteristic polynomial

$$\pi_a^{\epsilon,\pm}(\lambda, \mu) = \det(\mathbb{A}_a^{\epsilon,\pm}(\lambda) - \mu I),$$

and for each $k \in \mathbb{R}$ we have the complex dispersion relation

$$\pi_a^{\epsilon,\pm}(\lambda, ik) = -k^2 + ikD^\epsilon(u_\pm)^{-1}b_{1,a}^{\epsilon,\pm} - D^\epsilon(u_\pm)^{-1}(\lambda - b_{0,a}^{\epsilon,\pm}).$$

The λ-roots of the complex dispersion relation define algebraic curves parametrized by the parameter $k \in \mathbb{R}$, the Fredholm curves, in the λ-complex plane of the form

$$\begin{aligned}\lambda_a^{\epsilon,\pm}(k) &= -D^\epsilon(u_\pm)k^2 + ikb_{1,a}^{\epsilon,\pm} + b_{0,a}^{\epsilon,\pm} \\ &= -D^\epsilon(u_\pm)k^2 + ik(c - 2aD^\epsilon(u_\pm)) + f'(u_\pm) + a^2D^\epsilon(u_\pm) - ac \\ &= D^\epsilon(u_\pm)(a^2 - k^2) - ac + f'(u_\pm) + ik(c - 2aD^\epsilon(u_\pm)).\end{aligned}$$

Observe that for each curve $\lambda_a^{\epsilon,\pm}(k)$, the point at rightmost position is found by evaluating at $k = 0$, this is,

$$\max_{k\in\mathbb{R}} \operatorname{Re}\lambda_a^{\epsilon,\pm}(k) = \lambda_a^{\epsilon,\pm}(0) = D^\epsilon(u_\pm)a^2 - ac + f'(u_\pm).$$

Thus, the region of consistent splitting is the set

$$\Omega(a,\epsilon) := \{\lambda \in \mathbb{C} : \operatorname{Re}\lambda > \max\{D^\epsilon(u_+)a^2 - ac + f'(u_+), D^\epsilon(u_-)a^2 - ac + f'(u_-)\}\}.$$

We denote, for each fixed $\lambda \in \mathbb{C}$, $\epsilon > 0$ and $a \geq 0$, $S_a^{\epsilon,\pm}(\lambda)$, $U_a^{\epsilon,\pm}(\lambda)$ as the stable and unstable eigenspaces of $\mathbb{A}_a^{\epsilon,\pm}(\lambda)$ in $\mathbb{C}^2$, respectively. Arguing as in Lemma 5.5.1 we recognize that for $\lambda \in \Omega(a,\epsilon)$ the matrices $\mathbb{A}_a^{\epsilon,\pm}(\lambda)$ have no center space, and $\dim S_a^{\epsilon,\pm}(\lambda) = \dim U_a^{\epsilon,\pm}(\lambda) = 1$.

Lemma 5.7.1. *Let φ be a monotone front and $\mathcal{L}_a$ the conjugated linear operator defined in* (5.7.1)*. Then*

$$\sigma_\delta(\mathcal{L}_a) \subset \mathbb{C} \setminus \Omega(a),$$

where $\Omega(a) := \Omega(a,0)$.

Proof. Let $\lambda \in \mathbb{C}$. If we keep $a \in \mathbb{R}$ constant, we may apply the same proof of Lemma 5.6.1 to conclude that $\mathcal{L}_a^\epsilon - \lambda$ converge in generalized sense to $\mathcal{L}_a - \lambda$ as $\epsilon \to 0^+$.

Now suppose that $\lambda \in \Omega(a,\epsilon)$. Following the lines of the proof of Lemma 5.5.2 we conclude that $\mathcal{L}_a^\epsilon - \lambda$ is Fredholm with index zero. We may apply Theorem 5.6.2 and argument as in Theorem5.6.3 to conclude that for $0 < \epsilon \ll 1$, the operators $\mathcal{L}_a^\epsilon - \lambda$ and $\mathcal{L}_a - \lambda$ have the same Fredholm properties.

Finally, we follow the arguments of Theorem 5.6.3. Let $\lambda \in \sigma_\delta(\mathcal{L}_a)$. Hence, by definition $\mathcal{L}_a - \lambda$ is semi-Fredholm with $\operatorname{ind}(\mathcal{L}_a - \lambda) \neq 0$. Arguing by contradiction, we suppose that $\lambda \in \sigma_\delta(\mathcal{L}_a) \cap \Omega(a,\epsilon)$, for $0 < \epsilon \ll 1$. Therefore, $\operatorname{ind}(\mathcal{L}_a - \lambda) = \operatorname{ind}(\mathcal{L}_a^\epsilon - \lambda) = 0$; and at the same time $\operatorname{ind}(\mathcal{L}_a - \lambda) \neq 0$. This is a contradiction, and hence for $0 < \epsilon \ll 1$ small enough we have that $\sigma_\delta(\mathcal{L}_a) \cap \Omega(a,\epsilon) = \emptyset$ and $\sigma_\delta(\mathcal{L}_a) \subset \mathbb{C} \setminus \Omega(a,\epsilon)$. By continuity, taking the limit $\epsilon \to 0^+$, we have

$$\sigma_\delta(\mathcal{L}_a) \subset \mathbb{C} \setminus \Omega(a).$$

□

Proposition 5.7.2. *Let φ be a monotone front and $\mathcal{L}$ the associated linearized operator in $\mathcal{L}^2$. Then, for any appropriate weight $a \geq 0$, we have:*

$$\sigma_{pt}(\mathcal{L}) = \sigma_{pt}(\mathcal{L}_a). \tag{5.7.5}$$

(Here, $\sigma_{pt}(\cdot)$ is computed with respect to the space $L^2(\mathbb{R};\mathbb{C})$.)

Proof. Let $\lambda \in \sigma_{pt}(\mathcal{L})$. Then, there exists $u(x) \in \mathcal{D}(\mathcal{L}) = H^2$ such that $\mathcal{L}u = \lambda u$. For any appropriate $a \geq 0$, suppose that

$$v(x) = e^{ax}u(x) \in H^2. \tag{5.7.6}$$

Hence, $u \in H^2_a$ if and only if $v \in H^2$.

We have that

$$\mathcal{L}_a v = e^{ax}(\mathcal{L}(e^{-ax}v)) = e^{ax}(\mathcal{L}u) = e^{ax}\lambda u = \lambda v,$$

and this implies that $\lambda \in \sigma_{pt}(\mathcal{L}_a)$, proving the result.

□

5.7.3 Choice of the weight $a \geq 0$.

The location of the region of consistent splitting $\Omega(a)$ depends on value of $f'(u_\pm)$. In addition, the stability of $\sigma_\delta(\mathcal{L}_a)$ depends on the sign of $f'(u_\pm)$, since it lies on the left of $\Omega(a)$. Thus, the appropriate weight a is the one that pushes the boundary between this two sets into the left stable semiplane.

For a non-linearity of Fisher-KPP type, $u_- = 1$ and $u_+ = 0$, $f'(0) > 0$ and $f'(1) < 0$, and the fronts travel with velocity $c > c_* > 0$. Then, the region of consistent splitting is

$$\Omega(a) = \{\lambda \in \mathbb{C} : \operatorname{Re}\lambda > \max\{f'(0) - a, D(1)a^2 - ac + f'(1)\}\},$$

for any $a \in \mathbb{R}$.

We must find $a \in \mathbb{R}$ such that $f'(0) - ac < 0$ and $p(a) := D(1)a^2 - ac + f'(1) < 0$ simultaneously. Observe that, $p(0) = f'(1) < 0$ and $p(a) < 0$ for $a \in [0, a_0)$, where

$$a_0(c) = (2D(1))^{-1}\left(c + \sqrt{c^2 - 4D(1)f'(1)}\right),$$

is the first positive root of $p(a) = 0$. Therefore, we have to find a such that

$$0 < \frac{f'(0)}{c} < a < a_0(c). \tag{5.7.7}$$

Hence, this condition imposes the restriction $f'(0)/c < a_0(c)$ on the speed c. This last condition implies

$$\sqrt{c^2 - 4D(1)f'(1)} > \frac{2f'(0)D(1)}{c} - c$$

Squaring both sides, we obtain

$$c^2 - 4D(1)f'(1) > \frac{4f'(0)^2D(1)^2}{c^2} - 4f'(0)D(1) + c^2,$$

thus,

$$4c^2D(1)(f'(0) - f'(1)) > 4f'(0)^2D(1)^2.$$

Finally, we arrive to

$$c^2 > \frac{D(1)f'(0)^2}{f'(0) - f'(1)}. \tag{5.7.8}$$

Therefore, if restriction (5.7.8) holds, then we can choose $a \in \mathbb{R}$ such that $0 < f'(0)/c < a < a_0(c)$. Thus, with this appropriate weight we have

$$\sigma_\delta(\mathcal{L}_a) \subset \mathbb{C} \setminus \Omega(a) \subset \{\lambda \in \mathbb{C} : \operatorname{Re}\lambda \leq 0\}.$$

Before we apply Proposition 5.7.2 we must verify that condition (5.7.6) holds for a defined by equations (5.7.7) and (5.7.8). To verify condition (5.7.6), we have to find the asymptotic behavior at $\pm\infty$ of solutions $u \in H^2$ to the spectral equation $\mathcal{L}u = \lambda u$.

At the non-degenerate side, as $x \to -\infty$, following Alexander *et al.* [4] we rewrite the spectral equation as the first order system of the form

$$W' = \mathbb{A}(x, \lambda)W, \tag{5.7.9}$$

where

$$W = \begin{pmatrix} u \\ u_x \end{pmatrix} \in H^2(\mathbb{R}; \mathbb{C}^2),$$

$$\mathbb{A}(x;\lambda) = \begin{pmatrix} 0 & 1 \\ D(\varphi)^{-1}(\lambda - D(\varphi)_{xx} - f'(\varphi)) & -D(\varphi)^{-1}(2D(\varphi)_x + c) \end{pmatrix}.$$

The asymptotic matrix is

$$\mathbb{A}_-(\lambda) := \lim_{x\to-\infty} \mathbb{A}(x,\lambda) = \begin{pmatrix} 0 & 1 \\ D(1)^{-1}(\lambda - f'(1)) & -D(1)^{-1}c \end{pmatrix}.$$

We invoke the Gap Lemma [167] to relate the solutions of the variable-coefficient system (5.7.9) to the solutions of its constant-coefficient asymptotic system

$$W' = \mathbb{A}_-(\lambda)W,$$

as $x \to -\infty$. To apply the Gap Lemma we need to verify that $\mathbb{A}(x,\lambda)$ approaches exponentially fast to its limit $\mathbb{A}_-(\lambda)$ as $x \to -\infty$.

We develop $D(\varphi)$ in Taylor series around $\varphi = 1$,

$$D(\varphi) = D(1) + D'(1)(\varphi - 1) + O((\varphi - 1)^2),$$

where by hypothesis $D(1), D'(1) > 0$. Then, we make Taylor expansions around $\varphi = 1$ of the form

$$\begin{aligned} \frac{1}{D(\varphi)} &= \frac{1}{D(1)} - \frac{D'(1)}{D(1)^2}(\varphi - 1) + O((\varphi - 1)^2), \\ D'(\varphi) &= D'(1) + O(\varphi - 1), \\ D''(\varphi) &= D''(1) + O(\varphi - 1), \\ f'(\varphi) &= f'(1) + O(\varphi - 1). \end{aligned} \tag{5.7.10}$$

By Lemma 5.2.2 the wave and its derivatives decay as $\partial_x^j(\varphi - 1) = O(e^{\eta x})$ as $x \to -\infty$, for $j = 0, 1, 2$, with $\eta > 0$.

Hence we find

$$\begin{aligned} D(\varphi)_x &= D'(\varphi)\varphi_x \\ &= (D'(1) + O(\varphi - 1))\varphi_x \\ &= D'(1)\varphi_x + \varphi_x\, O(\varphi - 1) \\ &= O(e^{\eta x}) + O(e^{2\eta x}) \\ &= O(e^{\eta x}) \end{aligned} \tag{5.7.11}$$

as $x \to -\infty$. In as similar fashion, we have

$$\begin{aligned} D(\varphi)_{xx} &= D'(\varphi)\varphi_{xx} + D''(\varphi)\varphi_x^2 \\ &= D'(1)\varphi_{xx} + O((\varphi - 1)^2) \\ &= O(e^{\eta x}) + O(e^{2\eta x}) \\ &= O(e^{\eta x}) \end{aligned} \tag{5.7.12}$$

as $x \to -\infty$.

Now, we look at the difference

$$\mathbb{A}(x,\lambda) - \mathbb{A}_-(\lambda) = \begin{pmatrix} 0 & 0 \\ D(\varphi)^{-1}(\lambda - D(\varphi)_{xx} - f'(\varphi)) - D(1)^{-1}(\lambda - f'(1)) & -D(\varphi)^{-1}(2D(\varphi)_x + c) + D(1)^{-1}c \end{pmatrix}.$$

Thus, substituting Taylor expansions (5.7.10) and (5.7.12), we have

$$\begin{aligned}\frac{\lambda - D(\varphi)_{xx} - f'(\varphi)}{D(\varphi)} - \frac{\lambda - f'(1)}{D(1)} &= (\lambda - D(\varphi)_{xx} - f'(\varphi)) \left(\frac{1}{D(1)} + O(\varphi - 1)\right) - \frac{\lambda - f'(1)}{D(1)} \\ &= -\frac{f'(1)}{D(1)} + O(\varphi - 1) + O((\varphi - 1)^2) + \frac{f'(1)}{D(1)} \\ &= O(\varphi - 1) \\ &= O(e^{\eta x})\end{aligned} \tag{5.7.13}$$

as $x \to -\infty$.

On the other hand, substituting Taylor expansions (5.7.10) and (5.7.11), we have

$$\begin{aligned}\frac{-2D(\varphi)_x - c}{D(\varphi)} + \frac{C}{D(1)} &= (-2D(\varphi)_x - c) \left(\frac{1}{D(1)} + O(\varphi - 1)\right) + \frac{C}{D(1)} \\ &= -\frac{2D(\varphi)_x}{D(1)} + D(\varphi)_x \, O(\varphi - 1) \\ &= O(\varphi - 1) + O((\varphi - 1)^2) \\ &= O(e^{\eta x})\end{aligned} \tag{5.7.14}$$

as $x \to -\infty$. Therefore,

$$\mathbb{A}(x, \lambda) - \mathbb{A}_-(\lambda) = O(e^{\eta x}), \quad \text{as } x \to -\infty.$$

It follows from the Gap Lemma that for all $\bar{\eta} < \eta$ and any $\lambda \in \sigma_{pt}(\mathcal{L})$, system (5.7.9) has solutions $W_j(x, \lambda)$, $j = 1, 2$, which satisfy

$$W_j(x, \lambda) = e^{\mu_j(\lambda)x}(V_j(\lambda) + O(e^{-\bar{\eta}|x|}|V_j(\lambda)|)), \quad x < 0, \tag{5.7.15}$$

where $\mu_j(\lambda)$ are the eigenvalues of $\mathbb{A}_-(\lambda)$ with associated eigenvectors $V_j(\lambda)$, $j = 1, 2$.

The eigenvalues of $\mathbb{A}_-(\lambda)$ are the μ-roots of the polynomial

$$\det(\mathbb{A}_-(\lambda) - \mu I) = D(1)\mu^2 + c\mu + f'(1) - \lambda = 0.$$

Hence,

$$\mu_{1,2}(\lambda) = \frac{-c \pm \sqrt{c^2 + 4D(1)(\lambda - f'(1))}}{2D(1)}, \tag{5.7.16}$$

and the corresponding eigenvectors are

$$V_{1,2}(\lambda) = \begin{pmatrix} 1 \\ \mu_{1,2}(\lambda) \end{pmatrix}. \tag{5.7.17}$$

For $\lambda \in \sigma_{pt}(\mathcal{L})$, a solution u to the spectral equation $\mathcal{L}u = \lambda u$, must decay to zero at $-\infty$, so we have $u \in H^2$. Then, we verify that at least one of $\mu_{1,2}(\lambda)$ has positive real part for $\lambda \in \sigma_{pt}(\mathcal{L})$. Observe that

$$\mu_1(\lambda) + \mu_2(\lambda) = -\frac{c}{D(1)} < 0, \tag{5.7.18}$$

and

$$\mu_1(\lambda) \cdot \mu_2(\lambda) = \frac{f'(1) - \lambda}{D(1)}. \tag{5.7.19}$$

Since $\lambda \in \sigma_{pt}(\mathcal{L}) \subset (-\infty, 0]$, then λ is real and negative. We look at different cases depending on the sign of equation (5.7.19).

If $f'(1) < \lambda \leq 0$, then $\mu_1(\lambda) \cdot \mu_2(\lambda) < 0$. Hence, the discriminant $\Delta = c^2 + 4D(1)(\lambda - f'(1)) > 0$, implying that both roots $\mu_1(\lambda), \mu_2(\lambda) \in \mathbb{R}$ and with opposite sign. We have $\mu_1(\lambda) > 0 > \mu_2(\lambda)$.

If $\lambda = f'(1)$, then $\mu_1(\lambda) = 0$ and $\mu_2(\lambda) = -c/D(1)$.

If $\lambda < f'(1)$, then $\mu_1(\lambda) \cdot \mu_2(\lambda) > 0$. In this case we have two alternatives, either μ_1 and μ_2 are both negative, since $\mu_1(\lambda) + \mu_2(\lambda) < 0$; or μ_1 and μ_2 are complex conjugates with negative real part.

We conclude that for $\lambda \in (f'(1), 0]$ the solution

$$W_1(x, \lambda) = e^{\mu_1(\lambda)x}(V_1(\lambda) + O(e^{-\bar{\eta}|x|}|V_1(\lambda)|)),$$

decays exponentially as $x \to -\infty$. Therefore, for $\lambda \in (f'(1), 0]$ the decaying solution u to the spectral equation $\mathcal{L}u = \lambda u$ behaves like

$$\begin{aligned} u(x) &\sim e^{\mu_1(\lambda)x}, \\ u(x)_x &\sim \mu_1(\lambda) e^{\mu_1(\lambda)x}, \end{aligned} \tag{5.7.20}$$

as $x \to -\infty$.

Finally, from the second equation of system (5.7.9) and using equations (5.7.13) and (5.7.14) we have

$$\begin{aligned} u_{xx} &= \frac{\lambda - D(\varphi)_{xx} - f'(\varphi)}{D(\varphi)} u + \frac{-2D(\varphi)_x - c}{D(\varphi)} u_x \\ &= \left(\frac{\lambda - f'(1)}{D(1)} + O(e^{\eta x}) \right) O(e^{\mu_1(\lambda)x}) + \left(\frac{-c}{D(1)} + O(e^{\eta x}) \right) O(e^{\mu_1(\lambda)x}) \\ &= O(e^{\mu_1(\lambda)x}) + O(e^{(\eta + \mu_1(\lambda))x}) \\ &= O(e^{\mu_1(\lambda)x}), \end{aligned} \tag{5.7.21}$$

as $x \to -\infty$.

For $x_0 > 0$ fixed and large enough, we verify that for $a \in \mathbb{R}$ such that $0 < f'(0)/c < a < a_0(c)$, $v(x) = e^{ax}u(x) \in H^2(-\infty, -x_0)$. It follows from (5.7.20) that there exists a uniform constant $C_1 > 0$ such that

$$|u(x)| \leq C_1 e^{\mu_1(\lambda)x}, \quad x < -x_0.$$

Thus,

$$\|v\|^2_{L^2(-\infty,-x_0)} = \int_{-\infty}^{-x_0} e^{2ax}|u(x)|^2 dx \leq C_1^2 \int_{-\infty}^{-x_0} e^{2(a+\mu_1(\lambda))x} dx < \infty,$$

because $a + \mu_1(\lambda) > f'(0)/c + \mu_1(\lambda) > 0$. Then $v \in L^2(-\infty, -x_0)$.

Notice that

$$\begin{aligned} v_x &= e^{ax}u_x + ae^{ax}u, \\ v_{xx} &= e^{ax}u_{xx} + 2ae^{ax}u_x + a^2e^{ax}u. \end{aligned} \tag{5.7.22}$$

Applying Minkowski inequality we have

$$\begin{aligned} \|v_x\|_{L^2(-\infty,-x_0)} &\leq \|e^{ax}u_x\|_{L^2(-\infty,-x_0)} + a\|e^{ax}u\|_{L^2(-\infty,-x_0)}, \\ \|v_{xx}\|_{L^2(-\infty,-x_0)} &\leq \|e^{ax}u_{xx}\|_{L^2(-\infty,-x_0)} + 2a\|e^{ax}u_x\|_{L^2(-\infty,-x_0)} + a^2\|e^{ax}u\|_{L^2(-\infty,-x_0)}. \end{aligned} \tag{5.7.23}$$

Thus, we verify that the norms $\|e^{ax}u_x\|_{L^2(-\infty,-x_0)}$ and $\|e^{ax}u_{xx}\|_{L^2(-\infty,-x_0)}$ are finite. From equation (5.7.20) we have $u_x = O(e^{\mu_1(\lambda)x})$ as $x \to -\infty$, then there exist an uniform constant $C_2 > 0$ such that

$$|u_x| \leq C_2 e^{\mu_1(\lambda)x}, \quad x < -x_0.$$

Hence,

$$\|e^{ax}u_x\|^2_{L^2(-\infty,-x_0)} = \int_{-\infty}^{-x_0} e^{2ax}|u_x|^2 dx \leq C_2^2 \int_{-\infty}^{-x_0} e^{2(a+\mu_1(\lambda))x} dx < \infty,$$

because $a + \mu_1(\lambda) > f'(0)/c + \mu_1(\lambda) > 0$. Thus, $e^{ax}u_x \in L^2(-\infty, -x_0)$.

In a similar fashion, it can be proved that $e^{ax}u_{xx} \in L^2(-\infty, -x_0)$, using the fact that $u_{xx} = O(e^{\mu_1(\lambda)x})$ as $x \to -\infty$.

The previous calculations and equation (5.7.23) imply that

$$\|v_x\|_{L^2(-\infty,-x_0)} < \infty, \quad \|v_{xx}\|_{L^2(-\infty,-x_0)} < \infty.$$

Therefore, we conclude that $v \in H^2(-\infty, -x_0)$.

At the degenerate side, as $x \to +\infty$, suppose that u is an H^2-solution to equation $\mathcal{L}u = \lambda u$. Thus, by Lemma 5.8.5 u is written as

$$u = C\widetilde{\Theta}(x)\zeta(x),$$

with $\widetilde{\Theta}(x) \in H^2(x_0, +\infty)$ an $\zeta(x) \in H^2(x_0, +\infty)$. We verify that $v = e^{ax}u \in H^2(x_0, +\infty)$, for all $a > f'(0)/c > 0$.

Observe that $e^{ax}u \in L^2(x_0 + \infty)$. To see this, recall that the behavior of u as $x \to +\infty$ is given by equation (5.8.80),

$$|u_1(x)| \sim |C| \exp(n_1 x) \exp\left(-\frac{c^2}{D'(0)f'(0)} e^{f'(0)x/c}\right) \to 0,$$

where

$$n_1 = \frac{k}{2} + \frac{c\hat{d}}{2} - \frac{B}{2A} = \frac{1}{c}(2f'(0) - \operatorname{Re}\lambda) + c\frac{D''(0)}{2D'(0)^2}.$$

Thus, due to the fast decaying term

$$\exp\left(-\frac{c^2}{D'(0)f'(0)} e^{f'(0)x/c}\right),$$

any possible diverging behavior at $+\infty$ provided by the term e^{ax} is controlled. Then, we have

$$|v| \sim |C| e^{ax} \exp(n_1 x) \exp\left(-\frac{c^2}{D'(0)f'(0)} e^{f'(0)x/c}\right) \to 0,$$

as $x \to +\infty$. Hence $v \in L^2(x_0 + \infty)$.

On the other hand, notice that from equation (5.8.81) we have

$$|e^{ax}u_x| \leq C_1 e^{ax} \exp((n_1 + k)x) \exp\left(-\frac{c^2}{D'(0)f'(0)} e^{f'(0)x/c}\right) \to 0,$$

for some uniform $C_1 > 0$, as $x \to +\infty$. Thus, $e^{ax}u_x \in L^2(x_0, +\infty)$. Therefore, applying Minkowski inequality to equation (5.7.22) we have

$$\|v_x\|_{L^2(x_0,+\infty)} \leq \|e^{ax}u_x\|_{L^2(x_0,+\infty)} + a\|e^{ax}u\|_{L^2(x_0,+\infty)} < \infty.$$

Hence, $v_x \in L^2(x_0, +\infty)$.

Finally, it follows from equation (5.8.82) that

$$|e^{ax}u_{xx}| \leq C_2 e^{ax} \exp(\hat{\eta}x) \exp\left(-\frac{c^2}{D'(0)f'(0)} e^{f'(0)x/c}\right) \to 0,$$

for some uniform $C_2 > 0$, as $x \to +\infty$. Thus, $e^{ax}u_{xx} \in L^2(x_0, +\infty)$. Therefore, applying Minkowski inequality to equation (5.7.22) we have

$$\|v_{xx}\|_{L^2(x_0,+\infty)} \leq \|e^{ax}u_{xx}\|_{L^2(x_0,+\infty)} + 2a\|e^{ax}u_x\|_{L^2(x_0,+\infty)} + a^2\|e^{ax}u\|_{L^2(x_0,+\infty)} < \infty.$$

Hence $v_{xx} \in L^2(x_0, +\infty)$. Therefore, $v(x) = e^{ax}u(x) \in H^2(x_0, +\infty)$, for any $a > f'(0)/c > 0$.

If $u \in H^2$, then for fixed $x_0 \in \mathbb{R}$, it is clear that $v(x) = e^{ax}u(x) \in H^2(-x_0, x_0)$. In conclusion $v(x) = e^{ax}u(x) \in H^2(\mathbb{R}; \mathbb{C})$, and condition (5.7.6) holds.

Remark 7. It is to be observed that the analysis of the asymptotic behavior at $-\infty$ of solutions $u \in H^2$ to the spectral equation $\mathcal{L}u = \lambda u$, imposes a restriction on the acceptable values of the associated eigenvalue λ, which must be in the interval $(f'(1), 0]$. We do not have an equivalent restriction in the analysis of the asymptotic behavior at $+\infty$ of the solutions of the spectral equation, however, we must consider this restriction on the degenerate side in order to construct the eigenfunction on the whole real line.

Therefore, for all $\lambda \in (f'(1), 0]$ the equation $\mathcal{L}u = \lambda u$ has a solution $u(x) \in H^2$ such that decay exponentially to zero as $x \to \pm\infty$. On the non-degenerate side, we choose $u(x)$ as the solution that behaves like equation (5.7.20) as $x \to -\infty$. At the degenerate side, as $x \to +\infty$, we choose $u(x)$ as the solution given by Lemma 5.8.5 and which behaves as equation (5.8.80).

We apply Proposition 5.7.2, Theorem 5.4.4 and the preceding Remark 7 to conclude that

$$\sigma_{pt}(\mathcal{L}_a) \subset (f'(1), 0].$$

In conclusion, we have proved that for any diffusion degenerate traveling front with speed c such that

$$c > \max\left\{c*, \frac{\sqrt{D(1)}f'(0)}{\sqrt{f'(0) - f'(1)}}\right\} > 0, \tag{5.7.24}$$

there exist $a \in \mathbb{R}$ satisfying (5.7.7), such that

$$\begin{aligned} \sigma_{pt}(\mathcal{L}) = \sigma_{pt}(\mathcal{L}_a) \subset (f'(1), 0] \subset \{\lambda \in \mathbb{C} : \operatorname{Re}\lambda \leq 0\}, \\ \sigma_{\delta}(\mathcal{L})_{L^2_a} = \sigma_{\delta}(\mathcal{L}_a) \subset \{\lambda \in \mathbb{C} : \operatorname{Re}\lambda \leq 0\}. \end{aligned} \tag{5.7.25}$$

5.8 Asymptotic decay of solutions of spectral equation

In this section we provide the analysis of the asymptotic behavior of solutions $u \in H^2$ to the spectral equation

$$(\mathcal{L} - \lambda)u = 0, \tag{5.8.1}$$

where $\lambda \in \mathbb{C}$ is fixed.

We consider the eigenproblem $(\mathcal{L} - \lambda)u = 0$, that is

$$D(\varphi)u_{xx} + (2D(\varphi)_x + c)u_x + (D(\varphi)_{xx} + f'(\varphi) - \lambda)u = 0.$$

Upon dividing by $D(\varphi)$ we arrive to

$$u_{xx} + \rho(x)u_x + q(x)u = 0, \tag{5.8.2}$$

where

$$\rho(x) = \frac{2D(\varphi)_x + c}{D(\varphi)}, \quad q(x) = \frac{D(\varphi)_{xx} + f'(\varphi) - \lambda}{D(\varphi)}. \tag{5.8.3}$$

Let us consider the change of variables

$$u(x) = \exp\left(-\frac{1}{2}\int_{x_0}^{x} \rho(s)ds\right) z(x). \tag{5.8.4}$$

We compute the first and second derivatives of (5.8.4) with respect to x,

$$u_x = \left(-\frac{1}{2}\rho z + z_x\right) \exp\left(-\frac{1}{2}\int_{x_0}^{x} \rho(s)ds\right),$$

and

$$u_{xx} = \left(z_{xx} - \rho z_x - \frac{1}{2}\rho_x z + \frac{1}{4}\rho^2 z\right) \exp\left(-\frac{1}{2}\int_{x_0}^{x} \rho(s)ds\right).$$

Substituting (5.8.4) and its derivatives in (5.8.2) we have

$$z_{xx} - \rho z_x - \frac{1}{2}\rho_x z + \frac{1}{4}\rho^2 z + \rho\left(-\frac{1}{2}\rho z + z_x\right) + q(x)z = 0, \tag{5.8.5}$$

which reduces to

$$z_{xx} - F(x,\lambda)z = 0, \tag{5.8.6}$$

where

$$F(x,\lambda) := \frac{1}{2}\rho_x + \frac{1}{4}\rho^2 - q(x). \tag{5.8.7}$$

We shall analyze the asymptotic behavior of solutions to equation (5.8.6) as $x \to +\infty$, and using (5.8.4) we shall find the corresponding behavior of solutions to equation (5.8.2). We notice that

$$\begin{aligned} -\frac{1}{2}\int_{x_0}^{x} \rho(s)ds &= -\frac{1}{2}\int_{x_0}^{x} \left(\frac{2D(\varphi)_x}{D(\varphi)} + \frac{c}{D(\varphi)}\right) ds \\ &= -\int_{x_0}^{x} \frac{d}{ds}\ln|D(\varphi)|ds - \frac{c}{2}\int_{x_0}^{x} \frac{ds}{D(\varphi)} \\ &= \ln|D(\varphi(x_0))| - \ln|D(\varphi)| - \frac{c}{2}\int_{x_0}^{x} \frac{ds}{D(\varphi)}. \end{aligned} \tag{5.8.8}$$

Thus,

$$\exp\left(-\frac{1}{2}\int_{x_0}^{x} \rho(s)ds\right) = \frac{C_0}{D(\varphi)} \exp\left(-\frac{c}{2}\int_{x_0}^{x} \frac{ds}{D(\varphi)}\right), \tag{5.8.9}$$

where $C_0 = D(\varphi(x_0)) > 0$. To simplify the notation, we denote

$$\widetilde{\Theta}(x) := \exp\left(-\frac{c}{2}\int_{x_0}^{x}\frac{ds}{D(\varphi)}\right).$$

Hence, substituting (5.8.9) in (5.8.4) we arrive to

$$\begin{aligned} u(x) &= \exp\left(-\frac{1}{2}\int_{x_0}^{x}\rho(s)ds\right)z(x) \\ &= C_0\zeta(x)\widetilde{\Theta}(x), \end{aligned} \tag{5.8.10}$$

where $\zeta = z/D(\varphi)$ and z is solution to (5.8.6).

In order to find the behavior of solutions to (5.8.6) we make direct application of a result in [46, Chp.2, p. 50], which for reader's convenience we state below:

Theorem 5.8.1. *Let $Q(x) \in \mathcal{C}^2(\mathbb{R}^+)$ be complex-valued satisfying*

$$Q(x) \neq 0 \quad \textit{and} \quad \operatorname{Re}\sqrt{Q(x)} \geq 0,$$

for $x \gg 1$. Denote

$$\alpha_1(x) = \frac{1}{8}\frac{Q''(x)}{Q(x)^{3/2}} - \frac{5}{32}\frac{Q'(x)^2}{Q(x)^{5/2}}.$$

If the integral

$$\int_x^{\infty}|\alpha_1(s)|ds < \infty, \tag{5.8.11}$$

then the homogeneous equation

$$z_{xx} - Q(x)z = 0,$$

has a fundamental system of solutions satisfying for $x \to \infty$

$$z(x) \sim Q(x)^{-1/4}\exp\left(\pm\int_{x_0}^{x}Q(s)^{1/2}ds\right). \tag{5.8.12}$$

If in addition

$$Q'(x)Q(x)^{-3/2} \to 0, \quad \textit{as} \quad x \to \infty,$$

then the asymptotic formula (5.8.12) *can be differentiated twice, that is*

$$z(x)^{(j)} \sim (\pm Q(x)^{1/2})^j Q(x)^{-1/4}\exp\left(\pm\int_{x_0}^{x}Q(s)^{1/2}ds\right), \tag{5.8.13}$$

as $x \to +\infty$, for $j = 1, 2$.

In the following subsections we describe the asymptotic behavior of the coefficient $F(x, \lambda)$ as $x \to +\infty$, in order to apply Theorem 5.8.1 to equation (5.8.6).

In Section 5.8.1 we find the behavior of coefficients involving $D(\varphi)$ and $f(\varphi)$. Afterwards, in Section 5.8.2 we describe the behavior of $F(x; \lambda)$ and its derivatives to estimate the integral (5.8.11) in Section 5.8.3. The detailed behavior of solutions to the spectral equation (5.8.1), as $x \to +\infty$, is contained in Section 5.8.4.

5.8.1 Asymptotic behavior of coefficients

We shall describe the asymptotic behavior of coefficients for $x \gg 1$ large enough. According to Lemma 5.2.2 the front $\varphi(x)$ satisfies the decay rate

$$\varphi(x) = O(e^{-kx}), \quad \text{as} \quad x \to +\infty,$$

where

$$k := \frac{f'(0)}{c} > 0,$$

since by hypothesis $f'(0) > 0$ and $c > c^* > 0$.

Additionally, since $\varphi_x \in H^2$ by Lemma 5.2.3, we may write

$$\begin{aligned} \varphi_x(x) &= -k\varphi + O(\varphi^2), \\ \varphi_{xx}(x) &= \mathcal{C}_2\varphi + O(\varphi^2), \\ \varphi_{xxx}(x) &= \mathcal{C}_3\varphi + O(\varphi^2), \end{aligned} \tag{5.8.14}$$

for φ near 0, as $x \to +\infty$.

For future reference, in the following we make Taylor expansions near $\varphi = 0$ of coefficients that involve $D(\varphi)$ and $f(\varphi)$. Observe that due to the exponential decay of the front φ at $x = +\infty$, these expansion are valid near $\varphi = 0$, as $x \to +\infty$.

Taylor expansions

The Taylor expansion of $D(\varphi)$ around $\varphi = 0$ is,

$$D(\varphi) = D'(0)\varphi + \frac{D''(0)}{2}\varphi^2 + O(\varphi^3),$$

where, by hypothesis, $D'(0) > 0$ and $D''(0) \neq 0$. Thus, we have

$$\frac{1}{D(\varphi)} = \frac{1}{D'(0)\varphi + d\varphi^2 + O(\varphi^3)} = \frac{1}{D'(0)\varphi} \cdot \frac{1}{(1 + d\varphi + O(\varphi^2))},$$

where $d = D''(0)/2D'(0)$. Hence, we have

$$\begin{aligned} \frac{1}{D(\varphi)} &= \frac{1}{D'(0)\varphi}(1 - d\varphi + O(\varphi^2)) \\ &= \frac{1}{D'(0)\varphi} - \hat{d} + O(\varphi), \end{aligned}$$

where

$$\hat{d} = \frac{d}{D'(0)} = \frac{D''(0)}{2D'(0)^2} \neq 0.$$

The sign of $\hat{d}$ depends on the sign of $D''(0)$. In the following, we will consider the approximation up to the constant term, i.e.,

$$\frac{1}{D(\varphi)} = \frac{1}{D'(0)\varphi} + O(1), \quad \text{as} \quad \varphi \to 0. \tag{5.8.15}$$

In addition, we may derive the expansion of $1/D(\varphi)^2$ as

$$\begin{aligned} \frac{1}{D(\varphi)^2} &= \left(\frac{1}{D'(0)\varphi} + O(1) \right)^2 \\ &= \frac{1}{D'(0)^2\varphi^2} + O(\varphi^{-1}). \end{aligned} \tag{5.8.16}$$

On the other hand, we have the expansions near $\varphi = 0$

$$\begin{aligned} D'(\varphi) &= D'(0) + O(\varphi), \\ f'(\varphi) &= f'(0) + O(\varphi), \\ D''(\varphi) &= D''(0) + O(\varphi). \end{aligned} \tag{5.8.17}$$

We may derive more Taylor expansion near $\varphi = 0$, using (5.8.14). For instance

$$\begin{aligned} D(\varphi)_x = D'(\varphi)\varphi_x &= (D'(0) + O(\varphi))(-k\varphi + O(\varphi^2)) \\ &= -D'(0)k\varphi + O(\varphi^2); \end{aligned} \tag{5.8.18}$$

furthermore, for the second derivative of $D(\varphi)$ we have

$$\begin{aligned} D(\varphi)_{xx} &= D'(\varphi)\varphi_{xx} + D''(\varphi)\varphi_x^2 \\ &= (D'(0) + O(\varphi))(\mathcal{C}_2\varphi + O(\varphi^2)) + (D''(0) + O(\varphi))(k^2\varphi^2 + O(\varphi^3)) \\ &= D'(0)\mathcal{C}_2\varphi + O(\varphi^2), \end{aligned} \tag{5.8.19}$$

and

$$\begin{aligned} f(\varphi)_x = f'(\varphi)\varphi_x &= (f'(0) + O(\varphi))(-k\varphi + O(\varphi^2)) \\ &= -f'(0)k\varphi + O(\varphi^2). \end{aligned} \tag{5.8.20}$$

5.8.2 Asymptotic behavior of $F(x;\lambda)$ and its derivatives

We shall describe the behavior of $F(x;\lambda)$, $F'(x;\lambda)$ and $F''(x;\lambda)$ as $x \to +\infty$, considering $\lambda \in \mathbb{C}$ arbitrary but fixed. The prime $'$ denotes differentiation with respect to x.

Behavior of $F(x;\lambda)$

Using expressions for $\rho(x)$ and $q(x)$ defined in (5.8.3), we observe that $F(x;\lambda)$ has the following form

$$\begin{aligned}
F(x;\lambda) &= \frac{1}{2}\rho_x + \frac{1}{4}\rho^2 - q(x) \\
&= \frac{2D(\varphi)_{xx}D(\varphi) - 2(D(\varphi)_x)^2 - cD(\varphi)_x}{2D(\varphi)^2} + \frac{4(D(\varphi)_x)^2 + 4cD(\varphi)_x + c^2}{4D(\varphi)^2} - \\
&\quad - \frac{D(\varphi)_{xx} + f'(\varphi) - \lambda}{D(\varphi)} \\
&= \frac{1}{D(\varphi)^2}\bigg(D(\varphi)_{xx}D(\varphi) - (D(\varphi)_x)^2 - \frac{c}{2}D(\varphi)_x + (D(\varphi)_x)^2 + cD(\varphi)_x + \\
&\quad + \frac{c^2}{4} - D(\varphi)D(\varphi)_{xx} + D(\varphi)(\lambda - f'(\varphi))\bigg) \\
&= \frac{c^2}{4D(\varphi)^2} + \frac{c}{2}\frac{D(\varphi)_x}{D(\varphi)^2} + \frac{\lambda - f'(\varphi)}{D(\varphi)}.
\end{aligned}$$

The function $F(x;\lambda)$ is complex-valued. We may write its real and imaginary parts separately, that is

$$F(x;\lambda) = \frac{c^2}{4D(\varphi)^2} + \frac{c}{2}\frac{D(\varphi)_x}{D(\varphi)^2} + \frac{\operatorname{Re}\lambda - f'(\varphi)}{D(\varphi)} + i\frac{\operatorname{Im}\lambda}{D(\varphi)}. \tag{5.8.21}$$

We may use the information of the Taylor expansion near $\varphi = 0$ found in Section 5.8.1 to find the behavior of the real and imaginary parts in equation (5.8.21). For instance, we use (5.8.16) to find

$$\frac{c^2}{4D(\varphi)^2} = \frac{c^2}{4D'(0)^2}\varphi^{-2} + O(\varphi^{-1}),$$

and substituting (5.8.16) and (5.8.18), we obtain

$$\begin{aligned}
\frac{c}{2}\frac{D(\varphi)_x}{D(\varphi)^2} &= \frac{c}{2}\left(-D'(0)k\varphi + O(\varphi^2)\right)\left(\frac{1}{D'(0)^2\varphi^2} + O(\varphi^{-1})\right) \\
&= -\frac{ck}{2D'(0)}\varphi^{-1} + O(1).
\end{aligned}$$

Using equations (5.8.17) and (5.8.15) we have

$$\begin{aligned}
\frac{\operatorname{Re}\lambda - f'(\varphi)}{D(\varphi)} &= (\operatorname{Re}\lambda - f'(0) + O(\varphi))(D'(0)^{-1}\varphi^{-1} + O(1)) \\
&= \frac{\operatorname{Re}\lambda - f'(0)}{D'(0)}\varphi^{-1} + O(1).
\end{aligned}$$

Therefore, the real part of $F(x;\lambda)$ has the behavior

$$\operatorname{Re} F(x;\lambda) = \frac{c^2}{4D'(0)^2}\varphi^{-2} + O(\varphi^{-1}). \tag{5.8.22}$$

Finally, the behavior imaginary part of $F(x;\lambda)$ is given by

$$\operatorname{Im} F(x;\lambda) = \frac{\operatorname{Im}\lambda}{D(\varphi)} = \frac{\operatorname{Im}\lambda}{D'(0)}\varphi^{-1} + O(1). \tag{5.8.23}$$

Behavior of $F'(x;\lambda)$

We compute the derivative of $F(x;\lambda)$ with respect x, by deriving termwise:

$$\begin{aligned}
\frac{d}{dx}\left(\frac{c^2}{4D(\varphi)^2}\right) &= -\frac{c^2}{2}\frac{D(\varphi)_x}{D(\varphi)^3},\\
\frac{d}{dx}\left(\frac{c}{2}\frac{D(\varphi)_x}{D(\varphi)^2}\right) &= \frac{c}{2}\left(\frac{D(\varphi)_{xx}}{D(\varphi)^2} - \frac{2(D(\varphi)_x)^2}{D(\varphi)^3}\right),\\
\frac{d}{dx}\left(\frac{\lambda - f'(\varphi)}{D(\varphi)}\right) &= -\frac{f'(\varphi)_x}{D(\varphi)} + \frac{(f'(\varphi)-\lambda)D(\varphi)_x}{D(\varphi)^2}.
\end{aligned}$$

Therefore,

$$\begin{aligned}
F'(x;\lambda) = &\underbrace{-\frac{1}{D(\varphi)^3}\left(\frac{c^2}{2}D(\varphi)_x + c(D(\varphi)_x)^2\right)}_{\text{(I)}} +\\
&+\underbrace{\frac{1}{D(\varphi)^2}\left(\frac{c}{2}D(\varphi)_{xx} + (f'(\varphi) - \operatorname{Re}\lambda)D(\varphi)_x\right)}_{\text{(II)}}\underbrace{-\frac{f'(\varphi)_x}{D(\varphi)}}_{\text{(III)}} -\\
&+ i\underbrace{\frac{-\operatorname{Im}\lambda D(\varphi)_x}{D(\varphi)^2}}_{\text{(IV)}}.
\end{aligned} \tag{5.8.24}$$

For the term (I) in equation (5.8.24) it follows from equation (5.8.18) that

$$\begin{aligned}
\frac{c^2}{2}D(\varphi)_x + c(D(\varphi)_x)^2 &= -\frac{c^2}{2}D'(0)k\varphi + O(\varphi^2) + cD'(0)^2k^2\varphi^2 + O(\varphi^3)\\
&= -\frac{c^2}{2}D'(0)k\varphi + O(\varphi^2).
\end{aligned}$$

Hence, we have

$$\begin{aligned}\textcircled{\text{I}} &= -\left(\frac{1}{D'(0)^3}\varphi^{-3} + O\left(\varphi^{-2}\right)\right)\left(-\frac{c^2}{2}D'(0)k\varphi + O(\varphi^2)\right) \\ &= \frac{c^2k}{2D'(0)}\varphi^{-2} + O(\varphi^{-1}).\end{aligned} \tag{5.8.25}$$

For the term $\textcircled{\text{II}}$ in (5.8.24) we observe that upon substitution of (5.8.19) and (5.8.18), the terms in the parenthesis behave as

$$\frac{c}{2}D(\varphi)_{xx} = \frac{c}{2}\mathcal{C}_2D'(0)\varphi + O(\varphi^2),$$

$$\begin{aligned}(f'(\varphi) - \operatorname{Re}\lambda)D(\varphi)_x &= (f'(0) - \operatorname{Re}\lambda + O(\varphi))(-D'(0)k\varphi + O(\varphi^2)) \\ &= (\operatorname{Re}\lambda - f'(0))D'(0)k\varphi + O(\varphi^2).\end{aligned}$$

Thus, we have

$$\begin{aligned}\textcircled{\text{II}} &= \left(\frac{1}{D'(0)^2}\varphi^{-2} + O\left(\varphi^{-1}\right)\right)\left(\left(\frac{c}{2}\mathcal{C}_2D'(0) + (\operatorname{Re}\lambda - f'(0))D'(0)k\right)\varphi + O(\varphi^2)\right) \\ &= \left(\frac{\mathcal{C}_2c}{2D'(0)} + \frac{(\operatorname{Re}\lambda - f'(0))k}{D'(0)}\right)\varphi^{-1} + O(1).\end{aligned} \tag{5.8.26}$$

Observe that,

$$f'(\varphi)_x = f''(\varphi)\varphi_x.$$

By the hypothesis (5.1.3) on f, we may assume that $f''(0) \neq 0$ and take

$$f''(\varphi) = f''(0) + O(\varphi),$$

hence we obtain

$$\begin{aligned}f'(\varphi)_x &= (f''(0) + O(\varphi))(-k\varphi + O(\varphi)) \\ &= -kf''(0)\varphi + O(\varphi^2)\end{aligned}$$

Thus, for the term $\textcircled{\text{III}}$ in (5.8.24) we have

$$\begin{aligned}\textcircled{\text{III}} &= -\left(\frac{1}{D'(0)}\varphi^{-1} + O(1)\right)(-kf''(0)\varphi + O(\varphi^2)) \\ &= \frac{kf''(0)}{D'(0)} + O(\varphi).\end{aligned} \tag{5.8.27}$$

Therefore, substituting equations (5.8.25), (5.8.26) and (5.8.27), the real part of $F'(x;\lambda)$ has the behavior

$$\operatorname{Re}F'(x;\lambda) = \textcircled{\text{I}} + \textcircled{\text{II}} + \textcircled{\text{III}} = \frac{c^2k}{2D'(0)}\varphi^{-2} + O(\varphi^{-1}) \tag{5.8.28}$$

On the other hand, for the imaginary part of $F'(x;\lambda)$ the only the term contributing is (IV) in (5.8.24). Substituting Taylor expansion for $D(\varphi)_x$ defined in (5.8.18) we have

$$\begin{aligned}\operatorname{Im} F'(x;\lambda) &= -\operatorname{Im}\lambda\left(\frac{1}{D'(0)^2}\varphi^{-2} + O\left(\varphi^{-1}\right)\right)\left(-D'(0)k\varphi + O(\varphi^2)\right) \\ &= \frac{\operatorname{Im}\lambda}{D'(0)}k\varphi^{-1} + O(1).\end{aligned} \tag{5.8.29}$$

Behavior of $F''(x;\lambda)$

We compute the second derivative of $F(x;\lambda)$ with respect to x. Deriving (5.8.24) termwise, we have

$$\begin{aligned}
\frac{d}{dx}\left(-\frac{c^2}{2}\frac{D(\varphi)_x}{D(\varphi)^3}\right) &= -\frac{c^2}{2}\left(\frac{D(\varphi)_{xx}}{D(\varphi)^3} - \frac{(D(\varphi)_x)^2}{D(\varphi)^4}\right), \\
\frac{d}{dx}\left(-c\frac{(D(\varphi)_x)^2}{D(\varphi)^3}\right) &= -c\left(\frac{2D(\varphi)_xD(\varphi)_{xx}}{D(\varphi)^3} - \frac{3(D(\varphi)_x)^3}{D(\varphi)^4}\right), \\
\frac{d}{dx}\left(\frac{c}{2}\frac{D(\varphi)_{xx}}{D(\varphi)^2}\right) &= \frac{c}{2}\left(\frac{D(\varphi)_{xxx}}{D(\varphi)^2} - \frac{2D(\varphi)_xD(\varphi)_{xx}}{D(\varphi)^3}\right), \\
\frac{d}{dx}\left(\frac{f'(\varphi)D(\varphi)_x}{D(\varphi)^2}\right) &= \frac{f'(\varphi)_xD(\varphi)_x + f'(\varphi)D(\varphi)_{xx}}{D(\varphi)^2} - \frac{2f'(\varphi)(D(\varphi)_x)^2}{D(\varphi)^3}, \\
\frac{d}{dx}\left(-\lambda\frac{D(\varphi)_x}{D(\varphi)^2}\right) &= -\lambda\left(\frac{D(\varphi)_{xx}}{D(\varphi)^2} - \frac{2(D(\varphi)_x)^2}{D(\varphi)^3}\right), \\
\frac{d}{dx}\left(-\frac{f'(\varphi)_x}{D(\varphi)}\right) &= \frac{f'(\varphi)_xD(\varphi)_x}{D(\varphi)^2} - \frac{f'(\varphi)_{xx}}{D(\varphi)}.
\end{aligned}$$

Therefore,

$$
\begin{aligned}
F''(x;\lambda) = &\underbrace{\frac{1}{D(\varphi)^4}\left(\frac{3c^2}{2}(D(\varphi)_x)^2 + 3c(D(\varphi)_x)^3\right)}_{\text{(I)}} + \\
&+ \underbrace{\frac{1}{D(\varphi)^3}\left(-\frac{c^2}{2}D(\varphi)_{xx} - 3cD(\varphi)_x D(\varphi)_{xx} + 2(\operatorname{Re}\lambda - f'(\varphi))(D(\varphi)_x)^2\right)}_{\text{(II)}} + \\
&+ \underbrace{\frac{1}{D(\varphi)^2}\left(\frac{c}{2}D(\varphi)_{xxx} + 2f'(\varphi)_x D(\varphi)_x + (f'(\varphi) - \operatorname{Re}\lambda)D(\varphi)_{xx}\right)}_{\text{(III)}} - \\
&\underbrace{+\frac{1}{D(\varphi)}(-f'(\varphi)_{xx})}_{\text{(IV)}} + i\Bigg(\underbrace{\frac{2\operatorname{Im}\lambda(D(\varphi)_x)^2}{D(\varphi)^3}}_{\text{(V)}} \underbrace{-\frac{\operatorname{Im}\lambda D(\varphi)_{xx}}{D(\varphi)^2}}_{\text{(VI)}}\Bigg)
\end{aligned}
\tag{5.8.30}
$$

For (I) in equation (5.8.30), observe that for the terms in the parenthesis $(D(\varphi)_x)^3$ is smaller than $(D(\varphi)_x)^2$, for φ near 0. Hence, the behavior of (I) in equation (5.8.30) is

$$
\begin{aligned}
\text{(I)} &= \left(\frac{1}{D'(0)^4}\varphi^{-4} + O(\varphi^{-3})\right)\left(\frac{3}{2}c^2 D'(0)^2 k^2\varphi^2 + O(\varphi^3)\right) \\
&= \frac{3}{2}\frac{c^2k^2}{D'(0)^2}\varphi^{-2} + O(\varphi^{-1}).
\end{aligned}
\tag{5.8.31}
$$

For each term in the parenthesis of term (II) in equation (5.8.30), we have

$$
\begin{aligned}
-\frac{c^2}{2}D(\varphi)_{xx} &= -\frac{c^2\mathcal{C}_2 D'(0)}{2}\varphi + O(\varphi^2), \\
-3cD(\varphi)_{xx}D(\varphi)_x &= -3c(\mathcal{C}_2 D'(0)\varphi + O(\varphi^2))(-D'(0)k\varphi + O(\varphi^2)) \\
&= 3c\mathcal{C}_2 D'(0)^2 k\varphi^2 + O(\varphi^3),
\end{aligned}
$$

and,

$$
2(\operatorname{Re}\lambda - f'(\varphi))(D(\varphi)_x)^2 = 2(\operatorname{Re}\lambda - f'(0))D'(0)^2k^2\varphi^2 + O(\varphi^3).
$$

Hence,

$$
\begin{aligned}
\text{(II)} &= \left(\frac{1}{D'(0)^3}\varphi^{-3} + O(\varphi^2)\right)\left(-\frac{c^2\mathcal{C}_2 D'(0)}{2}\varphi + O(\varphi^2)\right) \\
&= -\frac{c^2\mathcal{C}_2}{2D'(0)^2}\varphi^{-2} + O(\varphi^{-1}).
\end{aligned}
\tag{5.8.32}
$$

The next term in (5.8.30) is (III). For the first term in the parenthesis we observe that

$$D(\varphi)_{xxx} = D'(\varphi)\varphi_{xxx} + 3D''(\varphi)\varphi_{xx}\varphi_x + D'''(\varphi)\varphi_x^3,$$

and notice that the dominant term is $D'(\varphi)\varphi_{xxx}$, since near $\varphi = 0$,

$$\varphi_{xxx} = O(\varphi), \quad \varphi_{xx}\varphi_x = O(\varphi^2), \quad \varphi_x^3 = O(\varphi^3).$$

Thus we have

$$\frac{c}{2}D(\varphi)_{xxx} = \frac{c}{2}D'(0)\mathcal{C}_3\varphi + O(\varphi^2).$$

The remaining terms in the parenthesis are

$$\begin{aligned} 2f'(\varphi)_x D(\varphi)_x &= 2f''(\varphi)\varphi_x D(\varphi)_x \\ &= 2(f''(0) + O(\varphi))(-k\varphi + O(\varphi^2))(-D'(0)k\varphi + O(\varphi^2)) \\ &= 2f''(0)D'(0)k^2\varphi^2 + O(\varphi^3), \end{aligned}$$

and

$$\begin{aligned} (f'(\varphi) - \operatorname{Re}\lambda)D(\varphi)_{xx} &= ((f'(0) - \operatorname{Re}\lambda) + O(\varphi))(D'(0)\mathcal{C}_2\varphi + O(\varphi^2)) \\ &= (f'(0) - \operatorname{Re}\lambda)D'(0)\mathcal{C}_2\varphi + O(\varphi^2). \end{aligned}$$

Thus, we have

$$\begin{aligned} \text{(III)} &= \left(\frac{1}{D'(0)^2}\varphi^{-2} + O(\varphi^{-1})\right)\left(\left(\frac{c}{2}D'(0)\mathcal{C}_3 + (f'(0) - \operatorname{Re}\lambda)D'(0)\mathcal{C}_2\right)\varphi + O(\varphi^2)\right) \\ &= \left(\frac{c}{2}\frac{\mathcal{C}_3}{D'(0)} + \frac{f'(0) - \operatorname{Re}\lambda}{D'(0)}\mathcal{C}_2\right)\varphi^{-1} + O(1). \end{aligned} \tag{5.8.33}$$

Last term on equation (5.8.30) contributing to the real part is (IV). Observe that

$$f'(\varphi)_{xx} = f''(\varphi)\varphi_{xx} + f'''(\varphi)\varphi_x^2,$$

and in this case the dominant term is $f''(\varphi)\varphi_{xx}$, since near $\varphi = 0$,

$$\varphi_{xx} = O(\varphi), \quad \varphi_x^2 = O(\varphi^2).$$

We have

$$\begin{aligned} \text{(IV)} &= \frac{-f'(\varphi)_{xx}}{D(\varphi)} = \left(\frac{1}{D'(0)}\varphi^{-1} + O(1)\right)(-\mathcal{C}_2 f''(0)\varphi + O(\varphi^2)) \\ &= \frac{\mathcal{C}_2 f''(0)}{D'(0)} + O(\varphi). \end{aligned} \tag{5.8.34}$$

Therefore, substituting equations (5.8.31), (5.8.32), (5.8.33) and (5.8.34), the real part of $F''(x;\lambda)$ has the behavior

$$\begin{aligned}\operatorname{Re} F''(x;\lambda) &= \textcircled{I} + \textcircled{II} + \textcircled{III} + \textcircled{IV} \\ &= \left(\frac{3}{2}\frac{c^2k^2}{D'(0)^2} - \frac{c^2\mathcal{C}_2}{2D'(0)}\right)\varphi^{-2} + O(\varphi^{-1}).\end{aligned} \tag{5.8.35}$$

The contributions to the imaginary part of $F''(x,\lambda)$ are from terms $\textcircled{V}$ and $\textcircled{VI}$ in equation (5.8.30). We then have

$$2\mathrm{Im}\,\lambda(D(\varphi)_x)^2 = 2\mathrm{Im}\,\lambda D'(0)^2k^2\varphi^2 + O(\varphi^3);$$

hence

$$\begin{aligned}\textcircled{V} = \frac{2\mathrm{Im}\,\lambda(D(\varphi)_x)^2}{D(\varphi)^3} &= \left(\frac{1}{D'(0)^3}\varphi^{-3} + O(\varphi^{-2})\right)2\mathrm{Im}\,\lambda D'(0)^2k^2\varphi^2 + O(\varphi^3) \\ &= 2\mathrm{Im}\,\lambda\frac{k^2}{D'(0)}\varphi^{-1} + O(1).\end{aligned}$$

Finally, upon substitution of (5.8.19) we obtain for the last term

$$\begin{aligned}\textcircled{VI} = -\frac{\mathrm{Im}\,\lambda D(\varphi)_{xx}}{D(\varphi)^2} &= -\left(\frac{1}{D'(0)^2}\varphi^{-2} + O(\varphi^{-1})\right)(\mathrm{Im}\,\lambda D'(0)\mathcal{C}_2\varphi + O(\varphi^2)) \\ &= -\frac{\mathrm{Im}\,\lambda}{D'(0)}\mathcal{C}_2\varphi^{-1} + O(1).\end{aligned}$$

Finally, the behavior imaginary part of $F''(x;\lambda)$ is given by

$$\mathrm{Im}\,F''(x,\lambda) = \textcircled{V} + \textcircled{VI} = \mathrm{Im}\,\lambda\left(\frac{2k^2}{D'(0)} - \frac{\mathcal{C}_2}{D'(0)}\right)\varphi^{-1} + O(1). \tag{5.8.36}$$

5.8.3 Asymptotic behavior of $\alpha_1(x)$

Now we analyze the asymptotic behavior of $\alpha_1(x)$. Recall that

$$\alpha_1(x) = \frac{1}{8}\frac{Q''(x)}{Q(x)^{3/2}} - \frac{5}{32}\frac{Q'(x)^2}{Q(x)^{5/2}}.$$

Hence

$$|\alpha_1(x)| \le \frac{1}{8}|Q''(x)||Q(x)^{-3/2}| + \frac{5}{32}|Q'(x)^2||Q(x)^{-5/2}|.$$

Using equations (5.8.22) and (5.8.23) we compute the modulus of $F(x;\lambda)$:

$$\begin{aligned}
|F(x;\lambda)| &= \left((\operatorname{Re} F(x;\lambda))^2 + (\operatorname{Im} F(x;\lambda))^2\right)^{1/2} \\
&= \left(\left(\frac{c^2}{4D'(0)}\right)^2 \varphi^{-4} + O(\varphi^{-3}) + \left(\frac{\operatorname{Im}\lambda}{D'(0)}\right)^2 \varphi^{-2} + O(\varphi^{-1})\right)^{1/2} \\
&= \left(\left(\frac{c^2}{4D'(0)}\right)^2 \varphi^{-4} + O(\varphi^{-3})\right)^{1/2} \\
&= \frac{c^2}{4D'(0)}\varphi^{-2}(1+O(\varphi))^{1/2}.
\end{aligned}$$

To simplify last expression we use the Taylor series around $\varphi = 0$ of the term $(1+O(\varphi))^{1/2}$, hence we have

$$\begin{aligned}
|F(x;\lambda)| &= \frac{c^2}{4D'(0)}\varphi^{-2}(1+O(\varphi))^{1/2} \\
&= \frac{c^2}{4D'(0)}\varphi^{-2}(1+\frac{1}{2}\,O(\varphi)+O(O(\varphi)^2)) \\
&= \frac{c^2}{4D'(0)^2}\varphi^{-2}(1+O(\varphi)).
\end{aligned} \tag{5.8.37}$$

Last expression holds because, $O(\varphi)^2 = O(\varphi^2)$ and $O(O(\cdot)) = O(\cdot)$. In a similar way, upon substitution of (5.8.35) and (5.8.36), we compute

$$\begin{aligned}
|F''(x;\lambda)| &= \left(\gamma_1^2\varphi^{-4} + O(\varphi^{-3}) + \gamma_2^2\varphi^{-2} + O(\varphi^{-1})\right)^{1/2} \\
&= \left(\gamma_1^2\varphi^{-4} + O(\varphi^{-3})\right)^{1/2} \\
&= (\gamma_1^2\varphi^{-4})^{1/2}(1+O(\varphi))^{1/2} \\
&= \gamma_1\varphi^{-2}(1+O(\varphi)),
\end{aligned} \tag{5.8.38}$$

where

$$\gamma_1 = \frac{3}{2}\frac{c^2k^2}{D'(0)^2} - \frac{c^2\mathcal{C}_2}{2D'(0)}.$$

It follows from equation (5.8.37) that

$$\begin{aligned}
|F(x;\lambda)|^{-3/2} &= \left(\frac{c^2}{4D'(0)^2}\varphi^{-2}\right)^{-3/2}(1+O(\varphi))^{-3/2} \\
&= \left(\frac{c}{2D'(0)}\right)^{-3}\varphi^3(1+O(\varphi)),
\end{aligned} \tag{5.8.39}$$

and

$$\begin{aligned} |F(x;\lambda)|^{-5/2} &= \left(\frac{c^2}{4D'(0)^2}\varphi^{-2}\right)^{-5/2}(1+O(\varphi))^{-5/2} \\ &= \left(\frac{c}{2D'(0)}\right)^{-5}\varphi^5(1+O(\varphi)). \end{aligned} \tag{5.8.40}$$

On the other hand, it follows from equations (5.8.28) and (5.8.29) that

$$\begin{aligned} |F'(x;\lambda)|^2 &= \eta_1^2\varphi^{-4}+O(\varphi^{-3})+\eta_1\varphi^2+O(\varphi^{-1}) \\ &= \eta_1^2\varphi^{-4}+O(\varphi^{-3}), \end{aligned} \tag{5.8.41}$$

where

$$\eta_1 = \frac{c^2k}{2D'(0)^2}.$$

Hence, equations (5.8.38) and (5.8.39) yield

$$\begin{aligned} \frac{1}{8}|F''(x;\lambda)||F(x;\lambda)|^{-3/2} &= \frac{1}{8}(\gamma_1\varphi^{-2}+O(\varphi^{-1}))\left(\left(\frac{c}{2D'(0)}\right)^{-3}\varphi^3+O(\varphi^4)\right) \\ &= \frac{1}{8}\gamma_1\left(\frac{c}{2D'(0)}\right)^{-3}\varphi+O(\varphi^2), \end{aligned} \tag{5.8.42}$$

and equations (5.8.41) and (5.8.40) give

$$\begin{aligned} \frac{5}{32}|F'(x;\lambda)|^2|F(x;\lambda)|^{-5/2} &= \frac{5}{32}(\eta_1\varphi^{-4}+O(\varphi^{-3}))\left(\left(\frac{c}{2D'(0)}\right)^{-5}\varphi^5+O(\varphi^6)\right) \\ &= \frac{5}{32}\eta_1\left(\frac{c}{2D'(0)}\right)^{-5}\varphi+O(\varphi^2). \end{aligned} \tag{5.8.43}$$

Therefore, upon substitution of (5.8.42) and (5.8.43) we arrive at

$$|\alpha_1(s)| \le \left(\frac{1}{8}\gamma_1\left(\frac{c}{2D'(0)}\right)^{-3}+\frac{5}{32}\eta_1\left(\frac{c}{2D'(0)}\right)^{-5}\right)\varphi+O(\varphi^2).$$

Due to the exponential decay of $\varphi(s)=O(e^{-ks})$, as $s\to+\infty$, higher order terms $O(\varphi^2)$ decay faster and we estimate for $s\gg 1$ large enough

$$|\alpha_1(s)| \le \widetilde{C}_1\varphi(s) \le \widetilde{C}_2e^{-ks},$$

for some uniform $\widetilde{C}_1,\widetilde{C}_2>0$.

Therefore,

$$\int_x^\infty |\alpha_1(s)|ds \leq \widetilde{C}_2 \int_x^\infty e^{-ks}ds < \infty.$$

Furthermore, there holds that

$$\lim_{x\to\infty} F'(x;\lambda)F(x;\lambda)^{-3/2} = 0.$$

To see this, observe that follows from equations (5.8.41) and (5.8.39) that

$$\begin{aligned} |F'(x;\lambda)||F(x;\lambda)|^{-3/2} &= \left(\left(\frac{c^2k}{2D'(0)^2}\right)\varphi^{-2} + O(\varphi^{-1})\right)\left(\left(\frac{c}{2D'(0)}\right)^{-3}\varphi^3 + O(\varphi^4)\right) \\ &= \left(\frac{c^2k}{2D'(0)^2}\right)\left(\frac{c}{2D'(0)}\right)^{-3}\varphi + O(\varphi^2) \to 0, \end{aligned} \tag{5.8.44}$$

as $x \to +\infty$.

Therefore, by Theorem 5.8.1 the homogeneous equation

$$z_{xx} - F(x;\lambda)z = 0,$$

has two linearly independent solutions $z_1(x)$ and $z_2(x)$ decaying and diverging at $+\infty$, respectively, as (5.8.12). Moreover, their derivatives $z_1^{(j)}$ and $z_2^{(j)}$ $(j = 1, 2)$ decay and diverge at $+\infty$ as (5.8.13).

It is to be noted that for fixed $\lambda \in \mathbb{C}$, the leading term of $\alpha_1(x)$ is independent of λ, because the contribution of λ to the asymptotic behavior of $\alpha_1(x)$ enters at a lower order. In other words, the existence of solutions to the homogeneous equation (5.8.6) given by Theorem 5.8.1 is granted for arbitrary $\lambda \in \mathbb{C}$. Nevertheless, in the next section we shall write detailed expression for solutions z_1 and z_2; not only considering leading terms, but also the next lower term where λ appears .

5.8.4 Detailed behavior of solutions to the homogeneous equation

We consider the expansion for $D(\varphi)^{-1}$ found in Section 5.8.1

$$\frac{1}{D(\varphi)} = \frac{1}{D'(0)}\varphi^{-1} - \hat{d} + O(\varphi), \tag{5.8.45}$$

as $\varphi \to 0$, with $\hat{d} = D''(0)/2D'(0)^2$. We shall obtain an expression for $F(x;\lambda)$ in powers of φ to $O(1)$. Recall that

$$F(x;\lambda) = \frac{c^2}{4D(\varphi)^2} + \frac{c}{2}\frac{D(\varphi)_x}{D(\varphi)^2} + \frac{\operatorname{Re}\lambda - f'(\varphi)}{D(\varphi)} + i\frac{\operatorname{Im}\lambda}{D(\varphi)}.$$

For each term of $F(x;\lambda)$, using the expansion (5.8.45) we have

$$\frac{c^2}{4D(\varphi)^2} = \frac{c^2}{4}\left(\frac{1}{D'(0)^2}\varphi^{-2} - \frac{2\hat{d}}{D'(0)}\varphi^{-1} + O(1)\right).$$

$$\begin{aligned}\frac{cD(\varphi)_x}{2D(\varphi)^2} &= \left(\frac{-D'(0)f'(0)}{2}\varphi + O(\varphi^2)\right)\left(\frac{1}{D'(0)^2}\varphi^{-2} - \frac{2\hat{d}}{D'(0)}\varphi^{-1} + O(1)\right)\\ &= -\frac{f'(0)}{2D'(0)}\varphi^{-1} + O(1).\end{aligned}$$

The third term is

$$\frac{\operatorname{Re}\lambda - f'(\varphi)}{D(\varphi)} = \frac{\operatorname{Re}\lambda - f'(0)}{D'(0)}\varphi^{-1} + O(1).$$

Therefore, near $\varphi = 0$ the real part of $F(x;\lambda)$ is

$$\operatorname{Re} F(x;\lambda) = \frac{c^2}{4D'(0)^2}\varphi^{-2} + \left(\frac{\operatorname{Re}\lambda - f'(0)}{D'(0)} - \frac{c^2\hat{d}}{2D'(0)} - \frac{f'(0)}{2D'(0)}\right)\varphi^{-1} + O(1),$$

and the imaginary part of $F(x;\lambda)$ is

$$\operatorname{Im} F(x;\lambda) = \frac{\operatorname{Im}\lambda}{D'(0)}\varphi^{-1} + O(1).$$

For notation simplicity, we denote the constants in $\operatorname{Re} F(x;\lambda)$ and $\operatorname{Im} F(x;\lambda)$ as

$$A = \frac{c}{2D'(0)}, \quad B = \frac{\operatorname{Re}\lambda - f'(0)}{D'(0)} - \frac{c^2\hat{d}}{2D'(0)} - \frac{f'(0)}{2D'(0)}, \quad I = \frac{\operatorname{Im}\lambda}{D'(0)}. \tag{5.8.46}$$

Thus,

$$F(x;\lambda) = A^2\varphi^{-2} + B\varphi^{-1} + O(1) + i\left(I\varphi^{-1} + O(1)\right),$$

as $\varphi \to 0^+$.

Upon taking the modulus of $F(x;\lambda)$ we arrive to

$$\begin{aligned}|F(x;\lambda)| &= \left(A^4\varphi^{-4} + 2A^2B\varphi^{-3} + O(\varphi^{-2})\right)^{1/2}\\ &= (A^4\varphi^{-4})^{1/2}\left(1 + \frac{2B}{A^2}\varphi + O(\varphi^2)\right)^{1/2}.\end{aligned}$$

Observe that

$$\begin{aligned}\left(1 + \frac{2B}{A^2}\varphi + O(\varphi^2)\right)^{1/2} &= 1 + \frac{1}{2}\left(\frac{2B}{A^2}\varphi + O(\varphi^2)\right) + O\left(\left(\frac{2B}{A^2}\varphi + O(\varphi^2)\right)^2\right)\\ &= 1 + \frac{B}{A^2}\varphi + O(\varphi^2),\end{aligned}$$

as $\varphi \to 0^+$. This implies that

$$\begin{aligned} |F(x;\lambda)| =& A^2\varphi^{-2}\left(1+\frac{B}{A^2}\varphi+O(\varphi^2)\right) \\ =& A^2\varphi^{-2}+B\varphi^{-1}+O(1), \end{aligned} \tag{5.8.47}$$

as $\varphi \to 0^+$.

In order to calculate $\sqrt{F(x;\lambda)}$, we write

$$F(x;\lambda) = |F(x;\lambda)|e^{i\theta(x)},$$

where $\theta(x) = \arctan(\operatorname{Im} F(x;\lambda)/\operatorname{Re} F(x;\lambda))$. Hence

$$\sqrt{F(x;\lambda)} = |F(x;\lambda)|^{1/2}e^{i\frac{\theta(x)}{2}}.$$

First, we compute $|F(x;\lambda)|^{1/2}$. We proceed as in the previous calculations:

$$\begin{aligned} |F(x;\lambda)|^{1/2} &= \left(A^2\varphi^{-2}+B\varphi^{-1}+O(1)\right)^{1/2} \\ &= (A^2\varphi^{-2})^{1/2}\left(1+\frac{B}{A^2}\varphi+O(\varphi^2)\right)^{1/2} \\ &= A\varphi^{-1}\left(1+\frac{B}{2A^2}\varphi+O(\varphi^2)\right) \\ &= A\varphi^{-1}+\frac{B}{2A}+O(\varphi), \end{aligned} \tag{5.8.48}$$

as $\varphi \to 0^+$.

For the argument of $F(x;\lambda)$ we have

$$\begin{aligned} \frac{\operatorname{Im} F(x;\lambda)}{\operatorname{Re} F(x;\lambda)} &= \frac{I\varphi^{-1}+O(1)}{A^2\varphi^{-2}+B\varphi^{-1}+O(1)} \\ &= \frac{I\varphi^{-1}(1+O(\varphi))}{A^2\varphi^{-2}(1+\frac{B}{A^2}\varphi+O(\varphi^2))} \\ &= \frac{I}{A^2}\varphi\,(1+O(\varphi))\left(1-\frac{B}{A^2}\varphi+O(\varphi^2))\right) \\ &= \frac{I}{A^2}\varphi+O(\varphi^2). \end{aligned}$$

Using the Taylor expansion around $y=0$, $\arctan(y) = y+O(y^3)$, we have

$$\theta(x) = \arctan\left(\frac{I}{A^2}\varphi+O(\varphi^2)\right) = \frac{I}{A^2}\varphi+O(\varphi^2), \tag{5.8.49}$$

as $\varphi \to 0^+$.

Hence,

$$\begin{aligned} e^{i\frac{\theta(x)}{2}} &= \cos\left(\frac{\theta(x)}{2}\right) + i\sin\left(\frac{\theta(x)}{2}\right) \\ &= 1 + O(\varphi^2) + i\left(\frac{I}{2A^2}\varphi + O(\varphi^2)\right). \end{aligned} \tag{5.8.50}$$

Therefore, upon substitution of (5.8.48) and (5.8.50) we reckon

$$\begin{aligned} \sqrt{F(x;\lambda)} &= |F(x;\lambda)|^{1/2} e^{i\frac{\theta(x)}{2}} \\ &= \left(A\varphi^{-1} + \frac{B}{2A} + O(\varphi)\right)\left(1 + O(\varphi^2) + i\left(\frac{I}{2A^2}\varphi + O(\varphi^2)\right)\right) \\ &= A\varphi^{-1} + \frac{B}{2A} + O(\varphi) + i\left(\frac{I}{2A} + O(\varphi)\right). \end{aligned} \tag{5.8.51}$$

On the other hand, we may compute

$$F(x;\lambda)^{-1/4} = |F(x;\lambda)|^{-1/4} e^{-i\frac{\theta(x)}{4}}.$$

Substituting (5.8.47), we find

$$\begin{aligned} |F(x;\lambda)|^{-1/4} &= \left(A^2\varphi^{-2} + B\varphi^{-1} + O(1)\right)^{-1/4} \\ &= (A^2\varphi^{-2})^{-1/4}\left(1 + \frac{B}{A^2}\varphi + O(\varphi^2)\right)^{-1/4} \\ &= A^{-1/2}\varphi^{1/2}\left(1 - \frac{B}{4A^2}\varphi + O(\varphi^2)\right) \\ &= A^{-1/2}\varphi^{1/2} - \frac{B}{4A^{5/2}}\varphi^{3/2} + O(\varphi^{5/2}). \end{aligned}$$

Hence,

$$|F(x;\lambda)|^{-1/4} \sim A^{-1/2}e^{-kx/2}, \quad x \to +\infty. \tag{5.8.52}$$

Similarly,

$$\begin{aligned} e^{-i\frac{\theta(x)}{4}} &= \cos\left(\frac{\theta(x)}{4}\right) - i\sin\left(\frac{\theta(x)}{4}\right) \\ &= 1 + O(\varphi^2) - i\left(\frac{I}{4A^2}\varphi + O(\varphi^2)\right). \end{aligned} \tag{5.8.53}$$

Therefore, we have

$$\begin{aligned} F(x;\lambda)^{-1/4} &= \left(A^{-1/2}\varphi^{1/2} + O(\varphi^{3/2})\right)\left(1 + O(\varphi^2) - i\left(\frac{I}{4A^2}\varphi + O(\varphi^2)\right)\right) \\ &= A^{-1/2}\varphi^{1/2} + O(\varphi^{3/2}) - i\left(\frac{I}{4A^{5/2}}\varphi^{3/2} + O(\varphi^{5/2})\right). \end{aligned} \tag{5.8.54}$$

Now, we are in position to compute the detailed behavior of solutions to the homogeneous equation (5.8.3). According to Theorem 5.8.1 the decaying solution $z_1(x)$ behave as

$$z_1(x) \sim F(x;\lambda)^{-1/4} \exp\left(- \int_{x_0}^{x} F(s;\lambda)^{1/2} ds \right). \tag{5.8.55}$$

Observe that

$$\int_{x_0}^{x} F(s;\lambda)^{1/2} ds = \int_{x_0}^{x} \operatorname{Re} F(s;\lambda)^{1/2} ds + i \int_{x_0}^{x} \operatorname{Im} F(s;\lambda)^{1/2} ds.$$

Then substituting (5.8.51) we have

$$\begin{aligned} \int_{x_0}^{x} \operatorname{Re} F(s;\lambda)^{1/2} ds &= \int_{x_0}^{x} \left(A\varphi(s)^{-1} + \frac{B}{2A} + O(\varphi(s)) \right) ds \\ &= \int_{x_0}^{x} \left(Ae^{ks} + \frac{B}{2A} + O(e^{-ks}) \right) ds \\ &= \frac{A}{k}(e^{kx} - e^{kx_0}) + \frac{B}{2A}(x - x_0) + O(e^{-kx}), \end{aligned} \tag{5.8.56}$$

for $x > x_0 \gg 1$ sufficiently large. Hence,

$$\begin{aligned} \exp\left(- \int_{x_0}^{x} \operatorname{Re} F(s;\lambda)^{1/2} ds \right) &= \exp\left(-\frac{A}{k}(e^{kx} - e^{kx_0}) - \frac{B}{2A}(x - x_0) + O(e^{-kx}) \right) \\ &= m_1 \exp\left(-\frac{A}{k} e^{kx} - \frac{B}{2A} x \right) \exp(O(e^{-kx})) \\ &= m_1 \exp\left(-\frac{A}{k} e^{kx} - \frac{B}{2A} x \right) (1 + o(1)), \end{aligned} \tag{5.8.57}$$

as $x \to +\infty$, with

$$m_1 = \exp\left(\frac{A}{k} e^{kx_0} + \frac{B}{2A} x_0 \right). \tag{5.8.58}$$

In a similar way, we have

$$\begin{aligned} \int_{x_0}^{x} \operatorname{Im} F(s;\lambda)^{1/2} ds &= \int_{x_0}^{x} \left(\frac{I}{2A} + O(\varphi(s)) \right) ds \\ &= \frac{I}{2A}(x - x_0) + O(e^{-kx}), \end{aligned} \tag{5.8.59}$$

for $x > x_0 \gg 1$ sufficiently large. Hence we have

$$\begin{aligned}\exp\left(-i\int_{x_0}^{x}\operatorname{Im}F(s;\lambda)^{1/2}ds\right) &= \exp\left(-i\frac{I}{2A}(x-x_0)+O(e^{-kx})\right)\\ &= \widetilde{m}_1\exp\left(-i\frac{I}{2A}x\right)(1+o(1)),\end{aligned} \tag{5.8.60}$$

as $x \to +\infty$, with

$$\widetilde{m}_1 = \exp\left(i\frac{I}{2A}x_0\right).$$

Therefore, substituting equations (5.8.52), (5.8.57) and (5.8.60) in (5.8.55) we obtain

$$\begin{aligned}z_1(x) &\sim |F(x;\lambda)|^{-1/4}\exp\left(-\int_{x_0}^{x}\operatorname{Re}F(s;\lambda)^{1/2}ds\right)e^{-i\frac{\theta(x)}{4}}\exp\left(-i\int_{x_0}^{x}\operatorname{Im}F(s;\lambda)^{1/2}ds\right)\\ &\sim m_1\widetilde{m}_1A^{-1/2}e^{-kx/2}\exp\left(-\frac{A}{k}e^{kx}-\frac{B}{2A}x\right)e^{-i\frac{\theta(x)}{4}}\exp\left(-i\frac{I}{2A}x\right),\end{aligned} \tag{5.8.61}$$

as $x \to +\infty$. Since

$$\frac{A}{k} = \frac{c^2}{2D'(0)f'(0)} > 0,$$

$z_1(x)$ decays as

$$|z_1(x)| \sim M_1e^{-kx/2}\exp\left(-\frac{A}{k}e^{kx}-\frac{B}{2A}x\right) \to 0, \tag{5.8.62}$$

as $x \to +\infty$. Here $M_1 = |m_1\widetilde{m}_1A^{-1/2}| = m_1(2D'(0)/c)^{1/2}$.

On the other hand, we compute the behavior for the diverging solution $z_2(x)$ to the homogeneous equation. By Theorem 5.8.1 the diverging solution $z_2(x)$ behave as

$$z_2(x) \sim F(x;\lambda)^{-1/4}\exp\left(\int_{x_0}^{x}F(s;\lambda)^{1/2}ds\right).$$

Substituting equations (5.8.52), (5.8.56) and (5.8.59) we reckon

$$\begin{aligned}z_2(x) &\sim |F(x;\lambda)|^{-1/4}\exp\left(\int_{x_0}^{x}\operatorname{Re}F(s;\lambda)^{1/2}ds\right)e^{i\frac{\theta(x)}{4}}\exp\left(i\int_{x_0}^{x}\operatorname{Im}F(s;\lambda)^{1/2}ds\right)\\ &\sim m_2\widetilde{m}_2A^{-1/2}e^{-kx/2}\exp\left(\frac{A}{k}e^{kx}+\frac{B}{2A}x\right)\exp\left(i\frac{I}{2A}x\right)e^{i\frac{\theta(x)}{4}},\end{aligned}$$

as $x \to +\infty$, and where $m_2 = m_1^{-1}$ and $\widetilde{m}_2 = \widetilde{m}_1^{-1}$. Thus, $z_2(x)$ diverges as

$$|z_2(x)| \sim M_2e^{-kx/2}\exp\left(\frac{A}{k}e^{kx}+\frac{B}{2A}x\right) \to \infty, \tag{5.8.63}$$

as $x \to +\infty$. Here $M_2 = |m_2 \widetilde{m}_2 A^{-1/2}| = m_2 (2D'(0)/c)^{1/2}$.

To complete the information about the decaying solution $z_1(x)$, now we estimate the behavior of its derivatives $\partial_x z_1$ and $\partial_{xx} z_1$. By Theorem 5.8.1 the derivatives of z_1 behave like

$$\partial_x z_1 \sim -F(x;\lambda)^{1/4} \exp\left(-\int_{x_0}^{x} F(s;\lambda)^{1/2} ds \right),$$
$$\partial_{xx} z_1 \sim F(x;\lambda)^{3/4} \exp\left(-\int_{x_0}^{x} F(s;\lambda)^{1/2} ds \right),$$

as $x \to +\infty$. We write

$$F(x;\lambda)^{1/4} = |F(x;\lambda)|^{1/4} e^{i\theta(x)/4}.$$

Substituting equation (5.8.47) we have

$$\begin{aligned} |F(x;\lambda)|^{1/4} &= \left(A^2 \varphi^{-2} + B\varphi^{-1} + O(1) \right)^{1/4} \\ &= A^{1/2} \varphi^{-1/2} \left(1 + \frac{B}{4A^2} \varphi + O(\varphi^2) \right) \\ &= A^{1/2} \varphi^{-1/2} + \frac{B}{4A^{3/2}} \varphi^{1/2} + O(\varphi^{3/2}). \end{aligned}$$

Thus $|F(x;\lambda)|^{1/4}$ diverges like

$$|F(x;\lambda)|^{1/4} \sim A^{1/2} e^{kx/2}, \quad x \to +\infty. \tag{5.8.64}$$

Therefore, substituting equations (5.8.57), (5.8.60) and (5.8.64) we obtain

$$\partial_x z_1 \sim -m_1 \widetilde{m}_1 A^{1/2} e^{kx/2} \exp\left(-\frac{A}{k} e^{kx} - \frac{B}{2A} x \right) \exp\left(-i \frac{I}{2A} x \right) e^{i\theta(x)/4}, \tag{5.8.65}$$

as $x \to +\infty$. Thus, $\partial_x z_1$ decays like

$$|\partial_x z_1| \sim M_{11} e^{kx/2} \exp\left(-\frac{A}{k} e^{kx} - \frac{B}{2A} x \right) \to 0, \tag{5.8.66}$$

as $x \to +\infty$. Here $M_{11} = |m_1 \widetilde{m}_1 A^{1/2}|$.

In a similar fashion, we estimate

$$\begin{aligned} |F(x;\lambda)|^{3/4} &= \left(A^2 \varphi^{-2} + B\varphi^{-1} + O(1) \right)^{3/4} \\ &= A^{3/2} \varphi^{-3/2} \left(1 + \frac{3B}{4A^2} \varphi + O(\varphi^2) \right) \\ &= A^{3/2} \varphi^{-3/2} + \frac{3B}{4A^{1/2}} \varphi^{-1/2} + O(\varphi^{1/2}). \end{aligned}$$

Thus $|F(x;\lambda)|^{3/4}$ diverges like

$$|F(x;\lambda)|^{3/4} \sim A^{3/2} e^{3kx/2}, \quad x \to +\infty.$$

Therefore,

$$\partial_{xx} z_1 \sim m_1 \widetilde{m}_1 A^{3/2} e^{3kx/2} \exp\left(-\frac{A}{k} e^{kx} - \frac{B}{2A} x\right) \exp\left(-i \frac{I}{2A} x\right) e^{i3\theta(x)/4}.$$

Hence,

$$|\partial_{xx} z_1| \sim M_{12} e^{3kx/2} \exp\left(-\frac{A}{k} e^{kx} - \frac{B}{2A} x\right) \to 0, \tag{5.8.67}$$

as $x \to +\infty$. Here $M_{12} = |m_1 \widetilde{m}_1 A^{3/2}|$.

Therefore, we summarize the proceeding calculations in the following

Lemma 5.8.2. *Let $\lambda \in \mathbb{C}$ be fixed and $x_0 \in \mathbb{R}$ fixed, $x_0 \gg 1$ sufficiently large. Then the homogeneous equation*

$$z_{xx} - F(x;\lambda) z = 0, \tag{5.8.68}$$

with $F(x;\lambda)$ given by (5.8.21) has a solution $z_1(x) \in H^2(x_0, +\infty)$, defined in equation (5.8.61) and decaying to zero as $x \to +\infty$ like

$$|z_1(x)| \sim M_1 e^{-f'(0)x/2c} \exp\left(-\frac{c^2}{2D'(0)f'(0)} e^{f'(0)x/c}\right) \exp\left(-\frac{B}{2A} x\right),$$

where $M_1 > 0$ is constant and

$$\frac{B}{2A} = \frac{1}{c}\left(\operatorname{Re}\lambda - \frac{3}{2} f'(0) - \frac{c^2 D''(0)}{4D'(0)^2}\right).$$

The decaying solution to the homogeneous equation (5.8.2) satisfy (5.8.10), that is

$$u_1(x) = C_0 \zeta(x) \widetilde{\Theta}(x) = C_0 \frac{z_1(x)}{D(\varphi)} \widetilde{\Theta}(x),$$

where z_1 is solution to (5.8.6) given by Lemma 5.8.2. Before analyzing the decaying behavior of $u_1(x)$ as $x \to +\infty$, we have two lemmas on the behavior of $\widetilde{\Theta}(x)$ and $\zeta(x)$.

Lemma 5.8.3. *For $x_0 \in \mathbb{R}$ fixed, $x_0 \gg 1$ sufficiently large, the function*

$$\widetilde{\Theta}(x) = \exp\left(-\frac{c}{2} \int_{x_0}^{x} \frac{ds}{D(\varphi(s))}\right),$$

belongs to $H^2(x_0, +\infty)$*, and satisfies*

$$\widetilde{\Theta}(x) \sim \widetilde{C}_0 \exp\left(-\frac{c}{2kD'(0)}e^{kx} + \frac{c\hat{d}}{2}x\right), \tag{5.8.69}$$

as $x \to +\infty$*, for some constant* $\widetilde{C}_0 > 0$*.*

Proof. We substitute the expansion (5.8.45) of $D(\varphi)^{-1}$ to estimate

$$\begin{aligned}\int_{x_0}^{x} \frac{ds}{D(\varphi(s))} &= \int_{x_0}^{x} \left(\frac{e^{ks}}{D'(0)} - \hat{d} + O(e^{-ks})\right) ds \\ &= \frac{1}{kD'(0)}(e^{kx} - e^{kx_0}) - \hat{d}(x - x_0) + O(e^{-kx}),\end{aligned} \tag{5.8.70}$$

for $x > x_0 \gg 1$, sufficiently large. Therefore,

$$\begin{aligned}\widetilde{\Theta}(x) &= \exp\left(-\frac{c}{2kD'(0)}(e^{kx} - e^{kx_0}) + \frac{c\hat{d}}{2}(x - x_0) + O(e^{-kx})\right) \\ &= \widetilde{C}_0 \exp\left(-\frac{c}{2kD'(0)}e^{kx} + \frac{c\hat{d}}{2}x\right)(1 + o(1)),\end{aligned} \tag{5.8.71}$$

where $\hat{d} = D''(0)/2D'(0)^2$, and

$$\widetilde{C}_0 = \exp\left(\frac{c}{2kD'(0)}e^{kx_0} - \frac{c\hat{d}}{2}x_0\right) > 0. \tag{5.8.72}$$

Hence, equation (5.8.69) holds with $\widetilde{C}_0$ defined in (5.8.72). Regardless of the sign of $\hat{d}$, observe that $\widetilde{\Theta}(x)$ decay to zero as $x \to +\infty$. This implies that $\widetilde{\Theta}(x) \in L^2(x_0, +\infty)$. Furthermore, for $x_0 \gg 1$ large enough, due to the fast exponential decay of $\widetilde{\Theta}(x)$ at $+\infty$, we have that

$$\begin{aligned}\partial_x(\widetilde{\Theta}(x)) &= -\frac{c}{2}\frac{1}{D(\varphi(x))}\widetilde{\Theta}(x) \\ &\sim -\frac{\widetilde{C}_0 c}{2D'(0)}e^{kx}\exp\left(-\frac{c}{2kD'(0)}e^{kx} + \frac{c\hat{d}}{2}x\right) \to 0,\end{aligned} \tag{5.8.73}$$

as $x \to +\infty$. Therefore, $\partial_x(\widetilde{\Theta}(x)) \in L^2(x_0, +\infty)$.

And for the second derivative we have

$$\partial_{xx}(\widetilde{\Theta}(x)) = \left(\frac{c^2}{4}\frac{1}{D(\varphi)^2} + \frac{c}{2}\frac{D(\varphi)_x}{D(\varphi)^2}\right)\widetilde{\Theta}(x).$$

Observe that

$$\frac{1}{D(\varphi)^2}\left(\frac{c^2}{4}+\frac{c}{2}D(\varphi)_x\right)=\left(\frac{1}{D'(0)^2}\varphi^{-2}+O(\varphi^{-1})\right)\left(\frac{c^2}{4}-\frac{c}{2}D'(0)k\varphi+O(\varphi^2)\right)$$
$$=\frac{c^2}{4D'(0)^2}\varphi^{-2}+O(\varphi^{-1}),$$

as $\varphi\to 0$. Hence we have

$$\frac{1}{D(\varphi)^2}\left(\frac{c^2}{4}+\frac{c}{2}D(\varphi)_x\right)\sim\frac{c^2}{4D'(0)^2}e^{2kx},\quad x\to+\infty.$$

Therefore,

$$\partial_{xx}(\widetilde{\Theta}(x))\sim\frac{c^2\widetilde{C}_0}{4D'(0)^2}e^{2kx}\exp\left(-\frac{c}{2kD'(0)}e^{kx}+\frac{c\hat{d}}{2}x\right)\to 0, \tag{5.8.74}$$

as $x\to+\infty$. Hence $\partial_{xx}(\widetilde{\Theta}(x))\in L^2(x_0,+\infty)$. We conclude that $\widetilde{\Theta}(x)\in H^2(x_0,+\infty)$, and the proof is complete. □

Lemma 5.8.4. *For $x_0\in\mathbb{R}$ fixed, $x_0\gg 1$ sufficiently large, the function*

$$\zeta(x)=\frac{z_1(x)}{D(\varphi(x))},$$

where $z_1(x)$ is the decaying solution to equation (5.8.68) *given in Lemma 5.8.2 belongs to $H^2(x_0,+\infty)$, and satisfies*

$$|\zeta(x)|\sim\widetilde{M}_1e^{f'(0)x/2c}\exp\left(-\frac{c^2}{2D'(0)f'(0)}e^{f'(0)x/c}\right)e^{-Bx/2A}, \tag{5.8.75}$$

as $x\to+\infty$, for some constant $\widetilde{M}_1>0$.

Proof. By Lemma 5.8.2 we observe that

$$\begin{aligned}|\zeta(x)|&=\frac{|z_1(x)|}{D(\varphi)}\\&\sim\frac{M_1}{D'(0)}e^{f'(0)x/2c}\exp\left(-\frac{c^2}{2D'(0)f'(0)}e^{f'(0)x/c}\right)e^{-Bx/2A}\to 0,\end{aligned} \tag{5.8.76}$$

as $x\to+\infty$. The constant $\widetilde{M}_1=M_1/D'(0)>0$, where $M_1>0$ is given by equation (5.8.62). Thus, $\zeta\in L^2(x_0,+\infty)$.

We estimate the derivatives $\partial_x\zeta$ and $\partial_{xx}\zeta$. We observe that

$$\partial_x\zeta = \frac{\partial_x z_1}{D(\varphi)} - \frac{D(\varphi)_x z_1}{D(\varphi)^2}.$$

Thus,

$$|\partial_x\zeta| \leq \frac{|\partial_x z_1|}{|D(\varphi)|} + \frac{|D(\varphi)_x|}{|D(\varphi)^2|}|z_1|.$$

Substituting equations (5.8.66) and (5.8.62) we have

$$\begin{aligned} |\partial_x\zeta| &\leq \widehat{C}_1(e^{3kx/2} + e^{kx/2}) \exp\left(-\frac{A}{k}e^{kx} - \frac{B}{2A}x\right) \\ &\leq \widehat{C}_1 e^{3kx/2} \exp\left(-\frac{A}{k}e^{kx} - \frac{B}{2A}x\right) \to 0, \end{aligned} \tag{5.8.77}$$

as $x \to +\infty$, for some uniform $\widehat{C}_1 > 0$. Thus, $\partial_x\zeta \in L^2(x_0, +\infty)$.

On the other hand, we observe that

$$\partial_{xx}\zeta = \frac{\partial_{xx} z_1}{D(\varphi)} - 2\partial_x z_1 \frac{D(\varphi)_x}{D(\varphi)^2} - z_1\left(\frac{D(\varphi)_{xx}}{D(\varphi)^2} - 2\frac{(D(\varphi)_x)^2}{D(\varphi)^2}\right),$$

hence

$$|\partial_{xx}\zeta| \leq \frac{|\partial_{xx} z_1|}{|D(\varphi)|} + 2|\partial_x z_1|\frac{|D(\varphi)_x|}{|D(\varphi)^2|} + |z_1|\frac{|D(\varphi)_{xx}|}{|D(\varphi)^2|} + 2|z_1|\frac{|(D(\varphi)_x)^2|}{|D(\varphi)^2|}.$$

Substituting equations (5.8.62), (5.8.66) and (5.8.67) we notice that

$$\begin{aligned} |\partial_{xx}\zeta| &\leq \widehat{C}_2\left(e^{kx}e^{3kx/2} + e^{kx}e^{kx/2} + e^{kx}e^{-kx/2} + e^{-kx/2}\right) \exp\left(-\frac{A}{k}e^{kx} - \frac{B}{2A}x\right) \\ &\leq \widehat{C}_2 e^{5kx/2} \exp\left(-\frac{A}{k}e^{kx} - \frac{B}{2A}x\right) \to 0, \end{aligned} \tag{5.8.78}$$

as $x \to +\infty$, for some uniform $\widehat{C}_2 > 0$. Hence $\partial_{xx}\zeta \in L^2(x_0, +\infty)$. We conclude that $\zeta(x) \in H^2(x_0, +\infty)$. □

Finally, we substitute equations (5.8.61) and (5.8.71) to find the detailed asymptotic behavior of $u_1(x)$. We have

$$\begin{aligned} u_1(x) &= C_0\frac{z_1(x)}{D(\varphi)}\widetilde{\Theta}(x) \\ &\sim Ce^{-kx/2}e^{kx} \exp\left(-\frac{A}{k}e^{kx} - \frac{B}{2A}x\right) e^{-i\frac{\theta(x)}{4}} \exp\left(-i\frac{I}{2A}x\right) \exp\left(-\frac{c}{2kD'(0)}e^{kx} + \frac{c\hat{d}}{2}x\right) \\ &= C \exp\left(\left(\frac{k}{2} + \frac{c\hat{d}}{2} - \frac{B}{2A}\right)x\right) \exp\left(-\frac{c^2}{D'(0)f'(0)}e^{kx}\right) e^{-i\theta(x)/4}e^{-iIx/2A}, \end{aligned} \tag{5.8.79}$$

as $x \to +\infty$ and where the constant $C = C_0\widetilde{C}_0 m_1 \widetilde{m}_1 A^{-1/2} D'(0)^{-1}$.

Thus, $u_1(x)$ decays like

$$|u_1(x)| \sim |C| \exp\left(\left(\frac{k}{2} + \frac{c\hat{d}}{2} - \frac{B}{2A}\right)x\right) \exp\left(-\frac{c^2}{D'(0)f'(0)} e^{f'(0)x/c}\right) \to 0, \tag{5.8.80}$$

as $x \to +\infty$. Hence $u_1(x) \in L^2(x_0, +\infty)$. Moreover, we may use the decaying behavior of $\zeta(x), \widetilde{\Theta}(x)$ and their derivatives to prove that $u_1(x) \in H^2(x_0, +\infty)$. Notice that

$$\partial_x u_1 = C_0 \left(\partial_x \zeta \widetilde{\Theta} + \zeta \partial_x \widetilde{\Theta}\right).$$

Upon substitution of equations (5.8.71), (5.8.73), (5.8.76) and (5.8.77) we arrive at

$$\begin{aligned} |\partial_x u_1| &\leq C_0 \left(|\partial_x \zeta \widetilde{\Theta}| + |\zeta \partial_x \widetilde{\Theta}|\right) \\ &\leq C_1 \exp\left(\left(\frac{3k}{2} + \frac{c\hat{d}}{2} - \frac{B}{2A}\right)x\right) \exp\left(-\frac{c^2}{D'(0)f'(0)} e^{f'(0)x/c}\right) \to 0, \end{aligned} \tag{5.8.81}$$

as $x \to +\infty$, for some uniform $C_1 > 0$. Thus, $\partial_x u_1(x) \in L^2(x_0, +\infty)$.

We compute the second derivative of u_1 with respect to x, we have

$$\partial_{xx} u_1 = C_0 \left(\partial_{xx} \zeta \widetilde{\Theta} + 2\partial_x \zeta \partial_x \widetilde{\Theta} + \zeta \partial_{xx} \widetilde{\Theta}\right).$$

Hence, substituting equations (5.8.71), (5.8.73), (5.8.74), (5.8.76), (5.8.77) and (5.8.78), we arrive at

$$\begin{aligned} |\partial_{xx} u_1| &\leq C_0 \left(|\partial_{xx} \zeta \widetilde{\Theta}| + 2|\partial_x \zeta \partial_x \widetilde{\Theta}| + |\zeta \partial_{xx} \widetilde{\Theta}|\right) \\ &\leq C_2 e^{\hat{\eta} x} \exp\left(-\frac{c^2}{D'(0)f'(0)} e^{f'(0)x/c}\right) \to 0, \end{aligned} \tag{5.8.82}$$

as $x \to +\infty$, for some uniform $C_2 > 0$. Here, $\hat{\eta}$ is a constant depending on $c, A, B, \hat{d}$ and k. Thus, $\partial_{xx} u_1(x) \in L^2(x_0, +\infty)$.

We summarize the results of this section into the following

Lemma 5.8.5. *Suppose that φ is a Fisher-KPP diffusion-degenerate front. Then, for any fixed $\lambda \in \mathbb{C}$, any H^2-solution u to the spectral equation $(\mathcal{L} - \lambda)u = 0$ can be written as*

$$u(x) = C \exp\left(-\frac{c}{2} \int_{x_0}^{x} \frac{ds}{D(\varphi)}\right) \zeta(x)$$

for $x > x_0$, $x_0 \in \mathbb{R}$ fixed, $x_0 \gg 1$ sufficiently large, with some constant $C \in \mathbb{C}$, and where $\zeta(x) \in H^2(x_0, +\infty)$ decay to zero as $x \to +\infty$ like

$$\zeta(x) \sim e^{f'(0)x/2c} \exp\left(-\frac{c^2}{2D'(0)f'(0)} e^{f'(0)x/c}\right) e^{-Bx/2A}, \tag{5.8.83}$$

and

$$\frac{B}{2A} = \frac{1}{c}\left(\operatorname{Re}\lambda - \frac{3}{2}f'(0) - \frac{c^2 D''(0)}{4D'(0)^2}\right).$$

On the other hand, for completeness we write down the behavior of the diverging solution $u_2(x)$ to equation (5.8.2), which is of the form

$$u_2(x) = C_0 \widetilde{\Theta}(x) \frac{z_2(x)}{D(\varphi)}, \tag{5.8.84}$$

where $z_2(x)$ is the diverging solution of (5.8.6). Substituting (5.8.71) and (5.8.63)

$$\begin{aligned} |u_2(x)| &\sim \exp\left(-\frac{c^2}{2D'(0)f'(0)} e^{kx} + \frac{c\hat{d}}{2}x\right) e^{kx/2} \exp\left(\frac{c^2}{2D'(0)f'(0)} e^{kx} + \frac{B}{2A}x\right) \\ &= \exp\left(\left(\frac{c\hat{d}}{2} + \frac{k}{2} + \frac{B}{2A}\right)x\right), \end{aligned}$$

as $x \to +\infty$. Observe that

$$\begin{aligned} \frac{c\hat{d}}{2} + \frac{k}{2} + \frac{B}{2A} &= \frac{c\hat{d}}{2} + \frac{f'(0)}{2c} + \frac{D'(0)}{c}\left(\frac{\operatorname{Re}\lambda - f'(0)}{D'(0)} - \frac{c^2\hat{d}}{2D'(0)} - \frac{f'(0)}{2D'(0)}\right) \\ &= \frac{c\hat{d}}{2} + \frac{f'(0)}{2c} + \frac{1}{c}\left(\operatorname{Re}\lambda - f'(0) - \frac{c^2\hat{d}}{2} - \frac{f'(0)}{2}\right) \\ &= \frac{\operatorname{Re}\lambda - f'(0)}{c}. \end{aligned}$$

Therefore, $u_2(x)$ diverges for $\operatorname{Re}\lambda > f'(0)$, as $x \to +\infty$.

5.9 Discussion

In this chapter we have studied the spectral stability of the linearized differential operator around any diffusion-degenerate Fisher-KPP traveling front. We have shown that, according to the partition of the spectrum given in Definition 2, the subsets σ_{pt} and σ_δ are stable when they are computed with respect to an appropriate exponentially weighted L^2-space. More precisely, if the velocity of the front satisfies (5.7.24), it is possible to find a weighted space where the set σ_{pt} and σ_δ

are localized in the stable complex semi-plane, $\{\lambda \in \mathbb{C} : \operatorname{Re}\lambda \leq 0\}$ (see equation (5.7.25)).

In particular, we have shown that the point spectrum $\sigma_{pt}(\mathcal{L})$ is stable using energy estimates (see Proposition 5.4.3). It is to be observed that the monotonicity of the traveling front was crucial to achieve such an estimate, since it motivated the appropriate change of variables (see equation (5.4.3)) that allowed us to close the energy estimate. In order to justify the change of variables, we performed a detailed asymptotic analysis of the decay of solutions to the spectral equation (see Section 5.8).

We introduced a regularization technique to circumvent the degeneration of the diffusion and locate the subset σ_δ of the compression spectrum. We proved that regularized operators converge in generalized sense to the original degenerate operator as $\epsilon \to 0^+$. The independence of regularization parameter ϵ of the Fredholm properties of the regularized operators in conjunction with the generalized convergence, allowed us to exploit the robustness of Fredholm properties under small perturbations. Therefore, we related the Fredholm properties of the regularized operators to those of the original degenerate operator.

It is to be highlighted that the regularization technique is not useful to control the whole of the Weyl essential spectrum $\sigma_{ess}(\mathcal{L})$, because the reduced minimum modulus of the perturbed operator $\gamma(\mathcal{L}^\epsilon - \lambda)$ might go to zero as $\epsilon \to 0^+$. Therefore, it is vital to sort out the points where the operator $\mathcal{L} - \lambda$ has a closed range. It is at these points where Fredholm properties can be defined. This is the main reason behind the proposed partition of the spectrum in Definition 2, $\sigma = \sigma_{pt} \cup \sigma_\delta \cup \sigma_\pi$. We notice that with this partition the point spectrum $\sigma_{pt}(\mathcal{L})$ is not necessarily composed of isolated eigenvalues (see Remark 2.2.4 in [128]).

On the other hand, we point out that the technique of energy estimates we applied in Section 5.4.1 is limited by the change of variables (5.4.3). To be more specific, the restriction comes from the justification of the change of variables, as we need $w \in H^2$ whenever $u \in H^2$ (see Lemma 5.4.1).

In addition, we remark that we have not proved the existence of a "spectral gap", that is, $\sigma \subset \{\operatorname{Re}\lambda \leq -\varpi < 0\} \cup \{0\}$, for some $\varpi > 0$. The existence of an spectral gap is important because it allows to study the non-linear orbital stability using the standard semigroup theory (see [41, 61, 71, 122, 128]). The contents of this chapter have been reported in [87].

Chapter 6

Conclusions

In Chapter 3 we introduced a model of reaction-diffusion-chemotaxis for bacterial aggregation patterns which is based on the system originally proposed by Kawasaki *et al.* [73]. Motivated by the experimental observations of Ben-Jacob *et al.* [20, 55] we incorporated a nutrient chemotaxist term into system (3.2.1) that is compatible with the non-linear diffusion.

We explored the effects of the new chemotactic term on the aggregation patterns by performing high-resolution numerical simulations of system (3.4.1) for various values of the parameters (see table 3.1), including the case without chemotaxis in order to compare with those simulations with the chemotactic signal switched on. Hence, we reproduce the numerical results obtained by Kawasaki et al. in [73].

Our numerical simulations show that the main qualitative effect of nutrient chemotaxis on the bacterial patterns is the enhancement of the growth velocity of the colony when the chemotactic term is present. This can be observed in Figures 3.6 to 3.10 of section 3.6. When the chemotaxis signal is present, the bacterial movement is greatly increased in the outward direction and, hence increasing the propagation of the envelope front of the colony.

Another qualitative effect of nutrient chemotaxis is the change of morphology in the regime of soft agar, poor nutrient. Compare figures 3.8 and 3.9 of section 3.6.2, where it is observed that chemotaxis induces a homogenization of the patterns as the chemotaxis strength is increased. There is a morphological transition between branching patterns of region E to homogeneously spreading disks pertaining to region D, of the morphological diagram.

In Chapter 4 we explored the effects of the chemotactic term has on the propagation velocity of the envelope front of the colony. We numerically solved a one-dimensional version of system (4.1.1) in order to estimate the propagation velocity of the front. Subsequently, by doing asymptotic calculations we found the velocity of the front as a function of both the nutrient concentration and the chemotaxis strength. Under the assumption of mass conservation (see equation

(4.2.2)) we found an approximated scalar equation for the bacterial density (Eq. (4.2.6)). Then, applying a result from Malaguti and Marcelli [92] we proved that the normal velocity is greater than the speed associated to the sharp front when there is no chemotaxis. Hence, the colony envelope will propagate faster when the chemotaxis signal is present, as expected from the numerical simulations from Chapter 3. Moreover, the asymptotic approximation to the front velocity is increased when the chemotaxis signal is present. These observations provide support to the claim of Ben-Jacob and co-workers [20, 55], that food chemotaxis is a basic mechanism involved in the development of bacterial colonies that increase the growth velocity, maintaining and even decreasing the degree of ramification of the patterns.

The theoretical speed thresholds, derived for the scalar equation (4.2.5) and defined in equations (4.2.20) and (4.2.21), were compared with the numerical estimations (see Fig. 4.2). This comparison reveals two facts: (1) the velocity of propagation is increased when the nutrient chemotaxis signal is present, and (2) it shows a good match between both, theoretical and numerical, estimations of the velocity. This implies that the conservation-like equation (4.2.2) is a good approximation to solutions of system (4.1.1). Our results for the case without chemotaxis (Fig. 4.2(a)) are comparable to those found by Kawasaki *et al.* [73], we note however, that in our calculations we used a more accurate approximation to the bacterial density.

In Chapter 5 we have studied the stability of subsets of the spectrum of the linearized differential operator around any smooth-monotone-degenerate Fisher-KPP traveling front supported by the scalar reaction-diffusion equation (5.1.1). The existence of such fronts has been studied by the Sánchez-Garduño and Maini [126, 127].

In order to circumvent the difficulties posed by the degeneracy of the diffusion, we introduced an alternative partition of the spectrum of the linearized operator in the form $\sigma = \sigma_{pt} \cup \sigma_{\delta} \cup \sigma_{\pi}$ (see Definition 2, Chapter 5). We have shown that the subsets σ_{pt} and σ_{δ} are stable when are computed with respect to an appropriated exponentially weighted L^2-space.

Using energy estimates we have shown that the point spectrum is stable (see Theorem 5.4.4). Moreover, we were able to close the energy estimates thanks to an appropriate change of variables that was motivated by the monotonicity of the fronts. In order to justify the change of variables, in Section 5.8 we made a detailed analysis of the asymptotic behavior of eigenfunctions on the degenerate side.

The degeneracy of the diffusion coefficient at one of the equilibrium points of the reaction function precludes a direct application of the standard methods to localize the essential spectrum. Those methods are based on the hyperbolicity of the asymptotic matrices associated to the spectral problem recast as a first

order differential system. For the degenerate linearized differential operator this hyperbolicity is lost on the degenerate side.

Thus, to locate the subset σ_δ of the compression spectrum we introduced a regularization technique. This approach is based on the robustness of the Fredholm properties under small perturbations. We showed that the family of regularized operators converge in a generalized sense to the original degenerate operator. In turn, this convergence allowed us to relate the Fredholm properties of the regularized operators to those of the degenerate operator, and finally locate σ_δ (see Theorem 5.6.3).

The location of σ_δ is determined by the Fredholm borders which turned to be unstable when computed with respect to L^2 (see Remark 6). Hence, since Fredholm borders are sensitive to changes at spatial infinity, we introduced exponentially weighted spaces where the stability of σ_δ holds. To be more specific, we proved that if the velocity of the front satisfies (5.7.24), it is possible to find a weighted space where the set σ_{pt} and σ_δ are localized in the stable complex semi-plane, $\{\lambda \in \mathbb{C} : \operatorname{Re}\lambda \leq 0\}$ (see equation (5.7.25)).

Chapter 7

Bibliography

[1] Adler, J. Chemotaxis in bacteria. *Science*, **153**(3737), pp. 708–716, 1966.

[2] Adler, J. Chemoreceptors in bacteria. *Science*, **166**(3913), pp. 1588–1597, 1969.

[3] Ahrens, J., Geveci, B., and Law, C. Paraview: An end-user tool for large data visualization. In Hansen, C. D. and Johnson, C. R., editors, *Visualization Handbook*. Elsevier, 2005.

[4] Alexander, J., Gardner, R., and Jones, C. K. R. T. A topological invariant arising in the stability analysis of travelling waves. *Journal für die Reine und Angewandte Mathematik*, **410**, pp. 167–212, 1990.

[5] Allee, W. C. Animal agregations. *The Quarterly Review of Biology*, **2**, pp. 367–398, 1927.

[6] Alt, W. Biased random walk models for chemotaxis and related diffusion approximations. *Journal of Mathematical Biology*, **9**(2), pp. 147–177, 1980.

[7] Alt, W. and Lauffenburger, D. A. Transient behavior of a chemotaxis system modelling certain types of tissue inflammation. *Journal of mathematical biology*, **24**(6), pp. 691–722, 1987.

[8] Amar, M. B. Collective chemotaxis and segregation of active bacterial colonies. *Scientific reports*, **6**, 2016.

[9] Anderson, A. R. A. and Chaplain, M. A. J. Continuous and discrete mathematical models of tumor-induced angiogenesis. *Bulletin of mathematical biology*, **60**(5), pp. 857–900, 1998.

[10] Andronov, A. A., Leontovich, E. A., Gordon, I. I., and Maier, A. G. *Qualitative theory of second-order dynamic systems.* Halsted Press, Israel Program for Scientific Translations, 1973.

[11] Aronson, D. G. Density-dependent interaction-diffusion systems. In Stewart, W. E., Ray, W. H., and Conley, C. C., editors, *Dynamics and modelling of reactive systems (Proc. Adv. Sem., Math. Res. Center, Univ. Wisconsin, Madison, Wis., 1979)*, volume 44 of *Publ. Math. Res. Center Univ. Wisconsin*, pp. 161–176. Academic Press, New York-London, 1980.

[12] Aronson, D. G. The role of diffusion in mathematical population biology: Skellam revisited. In *Mathematics in biology and medicine*, pp. 2–6. Springer, 1985.

[13] Aronson, D. G. The porous medium equation. In *Nonlinear diffusion problems*, pp. 1–46. Springer, 1986.

[14] Aronson, D. G. and Weinberger, H. F. Nonlinear diffusion in population genetics, combustion, and nerve pulse propagation. In Goldstein, J. A., editor, *Partial differential equations and related topics*, pp. 5–49. Springer, 1975.

[15] Arouh, S. and Levine, H. Nutrient chemotaxis suppression of a diffusive instability in bacterial colony dynamics. *Physical Review E*, **62**(1), pp. 1444–1447, 2000.

[16] Bellomo, N., Bellouquid, A., Tao, Y., and Winkler, M. Toward a mathematical theory of Keller–Segel models of pattern formation in biological tissues. *Mathematical Models and Methods in Applied Sciences*, **25**(9), pp. 1663–1763, 2015.

[17] Ben-Jacob, E. From snowflake formation to the growth of bacterial colonies II: Cooperative formation of complex colonial patterns. *Contemporary Physics*, **38**(3), pp. 205–241, 1997.

[18] Ben-Jacob, E. Bacterial self-organization: co-enhancement of complexification and adaptability in a dynamic environment. *The Royal Society of London. Philosophical Transactions. Series A. Mathematical, Physical and Engineering Sciences*, **361**(1807), pp. 1283–1312, 2003. Self-organization: the quest for the origin and evolution of structure (Stockholm, 2002).

[19] Ben-Jacob, E., Cohen, I., Golding, I., Gutnick, D. L., Tcherpakov, M., Helbing, D., and Ron, I. G. Bacterial cooperative organization under antibiotic stress. *Physica A*, **282**(1-2), pp. 247–282, 2000.

[20] Ben-Jacob, E., Cohen, I., and Levine, H. Cooperative self-organization of microorganisms. *Advances in Physics*, **49**(4), pp. 395–554, 2000.

[21] Ben-Jacob, E. and Garik, P. The formation of patterns in non-equilibrium growth. *Nature*, **343**(6258), pp. 523–530, 1990.

[22] Ben-Jacob, E. and Levine, H. Self-engineering capabilities of bacteria. *Journal of The Royal Society Interface*, **3**(6), pp. 197–214, 2006.

[23] Ben-Jacob, E., Schochet, O., Tenenbaum, A., Cohen, I., Czirók, A., and Vicsek, T. Generic modelling of cooperative growth patterns in bacterial colonies. *Nature*, **368**, pp. 46–49, 1994.

[24] Ben-Jacob, E., Shmueli, H., Shochet, O., and Tenenbaum, A. Adaptive self-organization during growth of bacterial colonies. *Physica A*, **187**(3), pp. 378–424, 1992.

[25] Ben-Jacob, E., Shochet, O., Tenenbaum, A., Cohen, I., Czirok, A., and Vicsek, T. Communication, regulation and control during complex patterning of bacterial colonies. *Fractals*, **2**(1), pp. 15–44, 1994.

[26] Ben-Jacob, E., Tenenbaum, A., Shochet, O., and Avidan, O. Holotransformations of bacterial colonies and genome cybernetics. *Physica A*, **202**(1), pp. 1–47, 1994.

[27] Biró, Z. Stability of travelling waves for degenerate reaction-diffusion equations of KPP-type. *Advanced Nonlinear Studies*, **2**(4), pp. 357–371, 2002.

[28] Bonachela, J. A., Nadell, C. D., Xavier, J. B., and Levin, S. A. Universality in bacterial colonies. *Journal of Statistical Physics*, **144**(2), pp. 303–315, 2011.

[29] Budrene, E. O. and Berg, H. C. Complex patterns formed by motile cells of *Escherichia coli*. *Nature*, **349**(6310), p. 630, 1991.

[30] Carl, E. A. Population control in arctic ground squirrels. *Ecology*, **52**(3), pp. 395–413, 1971.

[31] Carr, J. *Applications of centre manifold theory*, volume 35 of *Applied Mathematical Sciences*. Springer-Verlag, New York, 1982.

[32] Carslaw, H. S. and Jaeger, J. C. *Conduction of heat in solids*. Clarendon Press, Oxford, second edition, 1959.

[33] Ciprandi, G., Scordamaglia, A., Venuti, D., Caria, M., and Canonica, G. W. In vitro effects of *Bacillus subtilis* on the immune response. *Chemioterapia : International Journal of the Mediterranean Society of Chemotherapy*, **5**(6), pp. 404–7, 1986.

[34] Cohen, I., Czirók, A., and Ben-Jacob, E. Chemotactic-based adaptive self organization during colonial development. *Physica A*, **233**(3–4), pp. 678–698, 1996.

[35] Costerton, J. W., Lewandowski, Z., DeBeer, D., Caldwell, D., Korber, D., and James, G. Biofilms, the customized microniche. *Journal of bacteriology*, **176**(8), p. 2137, 1994.

[36] Cvitkovitch, D. G. Genetic exchange in biofilms. In Ghannoum, M. and O'Toole, G., editors, *Microbial biofilms*, pp. 192–205. ASM Press, Washington, DC., 2004.

[37] Dahlquist, F. W., Lovely, P., and Koshland, D. E. Quantitative analysis of bacterial migration in chemotaxis. *Nature: New biology*, **236**(65), pp. 120–123, 1972.

[38] Devroye, L. *Nonuniform random variate generation*. Springer-Verlag, New York, 1986.

[39] Edmunds, D. E. and Evans, W. D. *Spectral Theory and Differential Operators*. Oxford University Press, USA, 1987.

[40] Eisenbach, M. Bacterial chemotaxis. *eLS*, 2011.

[41] Engel, K. J. and Nagel, R. *One-parameter semigroups for linear evolution equations*, volume 194 of *Graduate Texts in Mathematics*. Springer, New York, 2000.

[42] Engelmann, T. W. Neue methode zur untersuchung der sauerstoffausscheidung pflanzlicher und thierischer organismen. *Pflügers Archiv European Journal of Physiology*, **25**(1), pp. 285–292, 1881.

[43] Erban, R. and Othmer, H. G. From individual to collective behavior in bacterial chemotaxis. *SIAM Journal on Applied Mathematics*, **65**(2), pp. 361–391, 2004.

[44] Erban, R. and Othmer, H. G. From signal transduction to spatial pattern formation in *E. coli*: a paradigm for multiscale modeling in biology. *Multiscale Modeling & Simulation*, **3**(2), pp. 362–394, 2005.

[45] Faull, R. J., Stanley, J. M., Fraser, S., Power, D. A., and Leavesley, D. I. Hb-egf is produced in the peritoneal cavity and enhances mesothelial cell adhesion and migration. *Kidney international*, **59**(2), pp. 614–624, 2001.

[46] Fedoryuk, M. V. *Asymptotic analysis*. Springer-Verlag, Berlin, 1993.

[47] Feng, P. and Zhou, Z. Finite traveling wave solutions in a degenerate cross-diffusion model for bacterial colony. *Communications on Pure and Applied Analysis*, **6**(4), p. 1145, 2007.

[48] Fife, P. C. *Mathematical aspects of reacting and diffusing systems*. Springer-Verlag, 1979.

[49] Fife, P. C. and McLeod, J. B. The approach of solutions of nonlinear diffusion equations to travelling front solutions. *Archive for Rational Mechanics and Analysis*, **65**(4), pp. 335–361, 1977.

[50] Fisher., R. A. The wave of advance of advantageous genes. *Annals of Eugenics*, **7**, pp. 335–369, 1937.

[51] Ford, R.M. and Lauffenburger, D.A. Measurement of bacterial random motility and chemotaxis coefficients: II. Application of single-cell-based mathematical model. *Biotechnology and Bioengineering*, **37**(7), pp. 661–672, 1991.

[52] Fujikawa, H. Periodic growth of *Bacillus subtilis* colonies on agar plates. *Physica A*, **189**(1), pp. 15–21, 1992.

[53] Gilding, B. H. and Kersner, R. *Travelling waves in nonlinear diffusion-convection reaction*, volume 60 of *Progress in Nonlinear Differential Equations and Their Applications*. Birkhäuser, 2004.

[54] Goldberg, S. *Unbounded linear operators: Theory and applications*. Courier Corporation, 2006.

[55] Golding, I., Kozlovsky, Y., Cohen, I., and Ben-Jacob, E. Studies of bacterial branching growth using reaction-diffusion models for colonial development. *Physica A*, **260**(3), pp. 510–554, 1998.

[56] Goldman, D. J. and Ordal, G. W. Sensory adaptation and deadaptation by *Bacillus subtilis*. *Journal of Bacteriology*, **147**(1), pp. 267–70, 1981.

[57] Grindrod, P. *Patterns and waves: The theory and applications of reaction-diffusion equations*. Oxford University Press, USA, 1991.

[58] Gurney, W. S. C. and Nisbet, R. M. The regulation of inhomogeneous populations. *Journal of Theoretical Biology*, **52**(2), pp. 441–457, 1975.

[59] Gurney, W. S. C. and Nisbet, R. M. A note on non-linear population transport. *Journal of Theoretical Biology*, **56**(1), pp. 249–251, 1976.

[60] Gurtin, M. E. and MacCamy, R. C. On the diffusion of biological populations. *Mathematical Biosciences*, **33**(1), pp. 35–49, 1977.

[61] Henry, D. *Geometrical Theory of Semilinear Parabolic Equations*. Number 840 in Lecture Notes in Math. Springer-Verlag, New York, 1981.

[62] Hillen, T. and Othmer, H. G. The diffusion limit of transport equations derived from velocity-jump processes. *SIAM Journal on Applied Mathematics*, pp. 751–775, 2000.

[63] Hillen, T. and Painter, K. J. A user's guide to PDE models for chemotaxis. *Journal of Mathematical Biology*, **58**(1), pp. 183–217, 2009.

[64] Holmes, E. E. Are diffusion models too simple? A comparison with telegraph models of invasion. *The American Naturalist*, **142**(5), pp. 779–795, 1993.

[65] Horger, T., Kuttler, C., Wohlmuth, B., and Zhigun, A. Analysis of a bacterial model with nutrient-dependent degenerate diffusion. *Mathematical Methods in the Applied Sciences*, **38**(17), pp. 3851–3865, 2015.

[66] Horstmann, D. From 1970 until present: the Keller-Segel model in chemotaxis and its consequences I. *Jahresberichte der DMV*, **105**(3), pp. 103–165, 2004.

[67] Hosono, Y. Traveling wave solutions for some density dependent diffusion equations. *Japan Journal of Applied Mathematics*, **3**(1), pp. 163–196, 1986.

[68] Ingalls, B. P. *Mathematical modeling in systems biology*. MIT Press Harvard, MA, 2013.

[69] Iserles, A. *A first course in the numerical analysis of differential equations*. 44. Cambridge University Press, 2009.

[70] Janeway Jr., C. A., Travers, P., Walport, M., and Shlomchik, M. J. *Immunobiology: The Immune System in Health and Disease*. New York: Garland Science, fifth edition, 2001.

[71] Kapitula, T. and Promislow, K. *Spectral and dynamical stability of nonlinear waves*, volume 185 of *Applied Mathematical Sciences*. Springer, New York, 2013.

[72] Kato, T. *Perturbation Theory for Linear Operators*. Classics in Mathematics. Springer-Verlag, New York, Second edition, 1980.

[73] Kawasaki, K., Mochizuki, A., Matsushita, M., Umeda, T., and Shigesada, N. Modeling spatio-temporal patterns generated by *Bacillus subtilis*. *Journal of Theoretical Biology*, **188**(2), pp. 177 – 185, 1997.

[74] Keller, E. F. Assessing the Keller-Segel model: how has it fared? In Jäger, W., Rost, H., and Tautu, P., editors, *Biological growth and spread*, pp. 379–387. Springer-Verlag, 1980.

[75] Keller, E. F. and Segel, L. A. Initiation of slime mold aggregation viewed as an instability. *Journal of Theoretical Biology*, **26**(3), pp. 399 – 415, 1970.

[76] Keller, E. F. and Segel, L. A. Model for chemotaxis. *Journal of Theoretical Biology*, **30**(2), pp. 225 – 234, 1971.

[77] Keller, E. F. and Segel, L. A. Traveling bands of chemotactic bacteria: A theoretical analysis. *Journal of Theoretical Biology*, **30**(2), pp. 235 – 248, 1971.

[78] Kessler, D. A. and Levine, H. Fluctuation-induced diffusive instabilities. *Nature*, **394**, pp. 556–558, 1998.

[79] Kirk, D. B. and Hwu, W. W. *Programming Massively Parallel Processors: A Hands-on Approach*. Morgan Kaufmann Publishers Inc., San Francisco, CA, USA, first edition, 2010.

[80] Kitsunezaki, S. Interface dynamics for bacterial colony formation. *Journal of the Physical Society of Japan*, **66**(5), pp. 1544–1550, 1997.

[81] Kolmogorov, A. N., Petrovsky, I. G., and Piskunov., N. S. Étude de l'équation de la diffusion avec croissance de la quantité de matière et son application à un problème biologique. *Bulletin de l'Université d'État de Moscou, Série Internationale A*, **1**, pp. 1–26, 1937.

[82] Krembel, A. K., Neumann, S., and Sourjik, V. Universal response-adaptation relation in bacterial chemotaxis. *Journal of Bacteriology*, **197**(2), pp. 307–313, 2015.

[83] Lapidus, R. I. and Schiller, R. Model for the chemotactic response of a bacterial population. *Biophysical Journal*, **16**(7), pp. 779–789, 1976.

[84] Lazova, M. D., Ahmed, T., Bellomo, D., Stocker, R., and Shimizu, T. S. Response rescaling in bacterial chemotaxis. *Proceedings of the National Academy of Sciences of the United States of America*, **108**(33), pp. 13870–5, 2011.

[85] Levine, H. and Ben-Jacob, E. Physical schemata underlying biological pattern formation–examples, issues and strategies. *Physical Biology*, **1**(2), p. P14, 2004.

[86] Leyva, J. F., Málaga, C., and Plaza, R. G. The effects of nutrient chemotaxis on bacterial aggregation patterns with non-linear degenerate cross diffusion. *Physica A*, **392**(22), pp. 5644–5662, 2013.

[87] Leyva, J. F. and Plaza, R. G. Spectral stability of traveling fronts for reaction diffusion-degenerate Fisher-KPP equations. *arXiv:1606.04831v2. Submitted to Journal of Dynamics and Differential Equations*, 2017.

[88] Luster, A. D., Alon, R., and von Andrian, U. H. Immune cell migration in inflammation: present and future therapeutic targets. *Nature immunology*, **6**(12), pp. 1182–1190, 2005.

[89] Luther, R. Räumliche fortpflanzung chemischer reaktionen. *Zeitschrift für Elektrochemie und angewandter physikalische Chemie*, **12**(32), pp. 596–600, 1906.

[90] Lynch, A. S. and Robertson, G. T. Bacterial and fungal biofilm infections. *Annual Review of Medicine*, **59**, pp. 415–428, 2008.

[91] Macnab, R. M. and Koshland, D. E. The gradient-sensing mechanism in bacterial chemotaxis. *Proceedings of the National Academy of Sciences*, **69**(9), pp. 2509–2512, 1972.

[92] Malaguti, L. and Marcelli, C. Sharp profiles in degenerate and doubly degenerate Fisher-KPP equations. *Journal of Differential Equations*, **195**(2), pp. 471–496, 2003.

[93] Matsushita, M. and Fujikawa, H. Diffusion-limited growth in bacterial colony formation. *Physica A*, **168**, pp. 498–506, 1990.

[94] Matsushita, M., Hiramatsu, F., Kobayashi, N., Ozawa, T., Yamazaki, Y., and Matsuyama, T. Colony formation in bacteria: experiments and modeling. *Biofilms*, **1**(4), pp. 305–317, 2004.

[95] Matsushita, M., Wakita, J., Itoh, H., Rafols, I., Matsuyama, T., Sakaguchi, H., and Mimura, M. Interface growth and pattern formation in bacterial colonies. *Physica A*, **249**(1), pp. 517–524, 1998.

[96] Meakin, P. *Fractals, scaling and growth far from equilibrium*, volume 5 of *Cambridge Nonlinear Science Series*. Cambridge University Press, Cambridge, 1998.

[97] Medvedev, G. S., Ono, K., and Holmes, P. J. Travelling wave solutions of the degenerate Kolmogorov–Petrovski–Piskunov equation. *European Journal of Applied Mathematics*, **14**(3), pp. 343–367, 2003.

[98] Mesibov, R., Ordal, G. W., and Adler, J. The range of attractant concentrations for bacterial chemotaxis and the threshold and size of response over this range. *Journal of General Physiology*, **62**(2), pp. 203–223, 1973.

[99] Meyries, M., Rademacher, J. D. M., and Siero, E. Quasi-linear parabolic reaction-diffusion systems: a user's guide to well-posedness, spectra, and stability of travelling waves. *SIAM Journal on Applied Dynamical Systems*, **13**(1), pp. 249–275, 2014.

[100] Mimura, M., Sakaguchi, H., and Matsushita, M. Reaction–diffusion modelling of bacterial colony patterns. *Physica A*, **282**(1), pp. 283–303, 2000.

[101] Morisita, M. Dispersal and population density of a water-strider, *Gerris lacustris L. Contribution to Physiology and Ecology Kyoto University*, **65**, pp. 1–149, 1950.

[102] Moses, S., Sinner, T., Zaprasis, A., Stöveken, N., Hoffman, T., Belitsky, B. R., Sonenshein, A. L., and Bremer, E. Proline utilization of *Bacillus subtilis*: Uptake and catabolism. *Journal Bacteriology*, **194**(4), pp. 745–758, 2012.

[103] Moukarzel, C. Laplacian growth on a random lattice. *Physica A*, **190**(1), pp. 13–23, 1992.

[104] Müller, J., Schiel, S., Ordal, G. W., and Saxild, H. H. Functional and genetic characterization of *mcpc*, which encodes a third methyl-accepting chemotaxis protein in *Bacillus subtilis*. *Microbiology*, **143**(10), pp. 3231–3240, 1997.

[105] Murray, J. D. *Mathematical biology I. An introduction*, volume 17 of *Interdisciplinary Applied Mathematics*. Springer-Verlag, New York, third edition, 2002.

[106] Murray, J. D. *Mathematical biology II. Spatial models and biomedical applications*, volume 18 of *Interdisciplinary Applied Mathematics*. Springer-Verlag, New York, third edition, 2003.

[107] Newman, W. I. Some exact solutions to a nonlinear diffusion problem in population genetics and combustion. *Journal of Theoretical Biology*, **85**(2), pp. 325–334, 1980.

[108] Newman, W. I. The long-time behavior of the solution to a nonlinear diffusion problem in population genetics and combustion. *Journal of Theoretical Biology*, **104**(4), pp. 473–484, 1983.

[109] NVIDIA. *NVIDIA CUDA C Programming Guide 4.0*. NVIDIA Corporation, 2011.

[110] NVIDIA. *CUDA Toolkit 4.0 CURAND Guide*. NVIDIA Corporation, 2012.

[111] Ohgiwari, M., Matsushita, M., and Matsuyama, T. Morphological changes in growth phenomena of bacterial colony patterns. *Journal of the Mathematical Society of Japan*, **61**(3), pp. 816–822, 1992.

[112] Okubo, A. and Levin, S. A. *Diffusion and ecological problems: modern perspectives*, volume 14. Springer, second edition, 2001.

[113] O'Neill, J. Tackling drug-resistant infections globally: final report and recommendations. *London: Wellcome Trust & HM Government*, 2016.

[114] Ordal, G. W. and Goldman, D. J. Chemotaxis away from uncouplers of oxidative phosphorylation in *Bacillus subtilis*. *Science*, **189**(4205), pp. 802–805, 1975.

[115] Ordal, G. W., Márquez-Magaña, L. M., and Chamberlin, M. J. Motility and chemotaxis in *Bacillus subtilis*. In Sonenshein, A., Losick, R., and Hoch, J., editors, *Bacillus subtilis and Other Gram Positive Bacteria*, Biochemistry, Physiology, and Molecular Genetics, pp. 765–784. American Society of Microbiology, Washington, D.C., 1993.

[116] Organization, World Health. Antimicrobial resistance global report on surveillance: 2014 summary. 2014.

[117] Othmer, H. G., Dunbar, S. R., and Alt, W. Models of dispersal in biological systems. *Journal of mathematical biology*, **26**(3), pp. 263–298, 1988.

[118] Othmer, H. G. and Hillen, T. The diffusion limit of transport equations II: Chemotaxis equations. *SIAM Journal on Applied Mathematics*, **62**(4), pp. 1222–1250, 2002.

[119] Othmer, H. G. and Stevens, A. Aggregation, blowup, and collapse: the ABCs of taxis in reinforced random walks. *SIAM Journal on Applied Mathematics*, **57**(4), pp. 1044–1081, 1997.

[120] Othmer, H. G. and Xue, C. The mathematical analysis of biological aggregation and dispersal: progress, problems and perspectives. In Lewis, A. M., Maini, K. P., and Petrovskii, V. S., editors, *Dispersal, Individual Movement and Spatial Ecology*, pp. 79–127. Springer Berlin Heidelberg, Berlin, 2013.

[121] Patlak, C. S. Random walk with persistence and external bias. *The Bulletin of mathematical biophysics*, **15**(3), pp. 311–338, 1953.

[122] Pego, R. L. and Weinstein, M. I. Asymptotic stability of solitary waves. *Communications in Mathematical Physics*, **164**(2), pp. 305–349, 1994.

[123] Pfeffer, W. Lokomotorische richtungsbewegungen durch chemische reize. *Untersuch. aus d. Botan. Inst. Tübingen*, **1**, pp. 363–482, 1884.

[124] Pfeffer, W. *Untersuch. aus d. Botan. Inst. Tübingen*, **2**, pp. 582–661, 1888.

[125] Renardy, M. and Rogers, R. C. *An introduction to partial differential equations*, volume 13 of *Texts in Applied Mathematics*. Springer-Verlag, New York, second edition, 2004.

[126] Sánchez-Garduño, F. and Maini, P. K. Existence and uniqueness of a sharp travelling wave in degenerate non-linear diffusion Fisher-KPP equations. *Journal of Mathematical Biology*, **33**(2), pp. 163–192, 1994.

[127] Sánchez-Garduño, F. and Maini, P. K. Travelling wave phenomena in some degenerate reaction-diffusion equations. *Journal of Differential Equations*, **117**(2), pp. 281–319, 1995.

[128] Sandstede, B. Stability of travelling waves. In Fiedler, B., editor, *Handbook of Dynamical Systems*, volume 2, pp. 983–1055. North-Holland, Amsterdan, 2002.

[129] Satnoianu, R. A., Maini, P. K., Garduno, F. S., and Armitage, J. P. Travelling waves in a nonlinear degenerate diffusion model for bacterial pattern formation. *Discrete and Continuous Dynamical Systems. Series B.*, **1**(3), pp. 339–362, 2001.

[130] Satnoianu, R. A., Maini, P. K., Garduno, F. S., and Armitage, J. P. Travelling waves in a nonlinear degenerate diffusion model for bacterial pattern formation. *Discrete and Continuous Dynamical Systems. Series B.*, **1**(3), pp. 339–362, 2001.

[131] Sattinger, D. H. On the stability of waves of nonlinear parabolic systems. *Advances in Mathematics*, **22**(3), pp. 312–355, 1976.

[132] Schwarcz, D., Levine, H., Ben-Jacob, E., and Ariel, G. Uniform modeling of bacterial colony patterns with varying nutrient and substrate. *Physica D: Nonlinear Phenomena*, **318**, pp. 91–99, 2016.

[133] Scianna, M., Bell, C.G., and Preziosi, L. A review of mathematical models for the formation of vascular networks. *Journal of Theoretical Biology*, **333**, pp. 174–209, 2013.

[134] Segel, L. A. Incorporation of receptor kinetics into a model for bacterial chemotaxis. *Journal of Theoretical Biology*, **57**(1), pp. 23–42, 1976.

[135] Segel, L. A. A theoretical study of receptor mechanisms in bacterial chemotaxis. *SIAM Journal on Applied Mahematics*, **32**(3), pp. 653–665, 1977.

[136] Segel, L. A. and Jackson, J. L. Theoretical analysis of chemotactic movement in bacteria. *Journal of mechanochemistry & cell motility*, **2**(1), pp. 25–34, 1973.

[137] Shapiro, J. A. Bacteria as multicellular organisms. *Scientific American*, **258**(6), pp. 82–89, 1988.

[138] Shapiro, J. A. Thinking about bacterial populations as multicellular organisms. *Annual Reviews in Microbiology*, **52**(1), pp. 81–104, 1998.

[139] Sherratt, J. A. and Marchant, B. P. Nonsharp travelling wave fronts in the Fisher equation with degenerate nonlinear diffusion. *Applied Mathematics Letters*, **9**(5), pp. 33–38, 1996.

[140] Shigesada, N. Spatial distribution of dispersing animals. *Journal of mathematical biology*, **9**(1), pp. 85–96, 1980.

[141] Shigesada, N. and Kawasaki, K. *Biological Invasions: Theory and Practice*. Oxford University Press, UK, 1997.

[142] Showalter, K. and Tyson, J. J. Luther's 1906 discovery and analysis of chemical waves. *Journal of Chemical Education*, **64**(9), pp. 742–744, 1987.

[143] Shylakhovenko, V. A., Olishevsky, S. V., Kozak, V. V., Yanish, Y. V., and Rybalko, S. L. Anticancer and immunostimulatory effects of nucleoprotein fraction of *Bacillus subtilis*. *Experimental Oncology*, **25**, pp. 119–123, 2003.

[144] Skellam, J. G. Random dispersal in theoretical populations. *Biometrika*, **38**, pp. 196–218, 1951.

[145] Skellam, J. G. The formulation and interpretation of mathematical models of diffusionary processes in population biology. In Barlett, M. S. and Hiorns, R. W., editors, *The mathematical theory of the dynamics of biological populations*, pp. 63–85. Academic Press, New York, 1973.

[146] Smoller, J. *Shock waves and reaction-diffusion equations*, volume 258. Springer-Verlag, second edition, 1994.

[147] Sonenshein, A. L., Hoch, J. A., Losick, R., *et al. Bacillus subtilis and its closest relatives: from genes to cells*. Asm Press, 2002.

[148] Stevens, A. The derivation of chemotaxis equations as limit dynamics of moderately interacting stochastic many-particle systems. *SIAM Journal on Applied Mathematics*, **61**(1), pp. 183–212, 2000.

[149] Tindall, M. J., Maini, P. K., Porter, S. L., and Armitage, J. P. Overview of mathematical approaches used to model bacterial chemotaxis. II. Bacterial populations. *Bulletin of Mathematical Biology*, **70**(6), pp. 1570–1607, 2008.

[150] Tindall, M. J., Porter, S. L., Maini, P. K., Gaglia, G., and Armitage, J. P. Overview of mathematical approaches used to model bacterial chemotaxis I: the single cell. *Bulletin of mathematical biology*, **70**(6), pp. 1525–1569, 2008.

[151] Turing, A. M. The chemical basis of morphogenesis. *Philosophical Transactions of the Royal Society of London B: Biological Sciences*, **237**(641), pp. 37–72, 1952.

[152] Vázquez, J. L. *The porous medium equation: mathematical theory*. Oxford University Press, 2007.

[153] Verhulst, P. F. Notice sur la loi que la population suit dans son accroissement. *Correspondence mathematique et physique*, **10**, pp. 113–121, 1838.

[154] Vicsek, T. *Fractal growth phenomena*, volume 2. World Scientific, 1992.

[155] Vicsek, T., Cserző, M., and Horváth, V. K. Self-affine growth of bacterial colonies. *Physica A*, **167**(2), pp. 315–321, 1990.

[156] Vladimirov, N. and Sourjik, V. Chemotaxis: How bacteria use memory. *Biological Chemistry*, **390**(11), pp. 1097–1104, 2009.

[157] Wadhams, G. H. and Armitage, J. P. Making sense of it all: bacterial chemotaxis. *Nature Reviews Molecular Cell Biology*, **5**(12), pp. 1024–1037, 2004.

[158] Wakita, J., Shimada, H., Itoh, H., Matsuyama, T., and Matsushita, M. Periodic colony formation by bacterial species *Bacillus subtilis*. *Journal of the Physical Society of Japan*, **70**(3), pp. 911–919, 2001.

[159] Wakita, J.-I., Komatsu, K., Nakahara, A., Matsuyama, T., and Matsushita, M. Experimental investigation on the validity of population dynamics approach to bacterial colony formation. *Journal of the Physical Society of Japan*, **63**(3), pp. 1205–1211, 1994.

[160] Wang, Z. A. Mathematics of traveling waves in chemotaxis–review paper. *Discrete and Continuous Dynamical Systems Series B*, **13**, pp. 601–641, 2013.

[161] Weigel, L. M., Donlan, R. M., Shin, D. H., Jensen, B., Clark, N. C., McDougal, L. K., Zhu, W., Musser, K. A., Thompson, J., Kohlerschmidt, D., *et al.* High-level vancomycin-resistant *Staphylococcus aureus* isolates associated with a polymicrobial biofilm. *Antimicrobial agents and chemotherapy*, **51**(1), pp. 231–238, 2007.

[162] Weyl, H. Über gewöhnliche differentialgleichungen mit singularitäten und die zugehörigen entwicklungen willkürlicher funktionen. *Mathematische Annalen*, **68**(2), pp. 220–269, 1910.

[163] Woodward, D. E., Tyson, R., Myerscough, M. R., Murray, J. D., Budrene, E. O., and Berg, H. C. Spatio-temporal patterns generated by *Salmonella typhimurium*. *Biophysical journal*, **68**(5), p. 2181, 1995.

[164] Wu, M., Zou, X.-W., and Jin, Z.-Z. Morphological diagram of bacterial colony pattern simulated using a revised Mimura-Sakaguchi-Matsushita model. *Journal of the Physical Society of Japan*, **74**(8), pp. 2379–2380, 2005.

[165] Xue, C. Macroscopic equations for bacterial chemotaxis: integration of detailed biochemistry of cell signaling. *Journal of Mathematical Biology*, **70**(1), pp. 1–44, 2015.

[166] Xue, C. and Othmer, H. G. Multiscale models of taxis-driven patterning in bacterial populations. *SIAM Journal on Applied Mathematics*, **70**(1), pp. 133–167, 2009.

[167] Zumbrun, K. Stability of large-amplitude shock waves of compressible navier–stokes equations. *Handbook of Mathematical Fluid Dynamics*, **3**, pp. 311–533, 2005.